

**The Rho-kinase Signaling Pathway in  
Tenon's Capsule Fibroblasts and Retinal Ganglion Cells:  
A novel pharmacological target for improving the outcomes of filtration  
surgery and promoting retinal cell survival in glaucoma**

**DISSERTATION**

zur Erlangerung des Grades eines Doktors  
der Naturwissenschaften

der Fakultät für Biologie  
und  
der Medizinischen Fakultät  
der Eberhard-Karls-Universität Tübingen

vorgelegt  
von

**AYŞEGÜL TURA**

aus Istanbul, Türkei

**2007**

Tag der mündlichen Prüfung: 13. 6. 2007

Dekan der Fakultät für Biologie: Prof. Dr. F. Schöffl

Dekan der Medizinischen Fakultät: Prof. Dr. I. B. Autenrieth

1. Berichterstatter: Prof. Dr. S. Grisanti

Dr. S. Henke-Fahle

2. Berichterstatter: Prof. Dr. H. J. Wagner

Prüfungskommission: Prof. Dr. R. Feil

Prof. Dr. K. Kohler

Prof. Dr. H. Wolburg

## Erklärungen

Ich erkläre hiermit,

1. dass ich bisher keine Promotions- oder entsprechende Prüfungsverfahren abgebrochen oder abgeschlossen habe.
2. dass die vorgelegte Dissertation noch nie ganz oder teilweise als Dissertation oder sonstige Prüfungsarbeit eingereicht worden ist und bereits teilweise in „*Investigative Ophthalmology & Visual Science*“ veröffentlicht wurde.
3. dass ich die zur Promotion eingereichte Arbeit mit dem Titel: „*The Rho-kinase Signaling Pathway in Tenon’s Capsule Fibroblasts and Retinal Ganglion Cells: A new pharmacological target for improving the outcomes of filtration surgery and promoting retinal cell survival in glaucoma*“ selbstständig verfasst, nur die angegebenen Quellen und Hilfsmittel benutzt und wörtlich oder inhaltlich übernommene Stellen als solche gekennzeichnet habe. Ich versichere an Eides statt, dass diese Angaben wahr sind und dass ich nichts verschwiegen habe. Mir ist bekannt, dass die falsche Abgabe einer Versicherung an Eides statt mit Freiheitsstrafe bis zu drei Jahren oder mit Geldstrafe bestraft wird.
4. dass ich bisher weder strafrechtlich verurteilt, noch Disziplinarmaßnahmen und anhängigen Straf- und Disziplinarverfahren unterzogen worden bin.

Tübingen, den 13.6.2007

.....

(Unterschrift)



## **Acknowledgements**

I would like to thank Dr. Sigrid Henke-Fahle for providing me the opportunity to conduct this comprehensive project. I also appreciate her valuable suggestions and friendly support.

I am grateful to Prof. Salvatore Grisanti for his constructive advices and continuous motivation throughout my work. I also thank Dr. Frank Schüttauf for the productive collaboration.

I feel indebted to Prof. Karl Ulrich Bartz-Schmidt for allowing me the opportunity to conduct my research further at the University Eye Hospital, Tübingen. I would like to thank Prof. Ulrich Schraermeyer for his kind support, as well.

I should not forget to mention the readiness of Prof. Horst Herbert to help along whenever I encountered difficulties and the considerate efforts of the late Prof. Werner J. Schmidt. I am also indebted to Prof. Hans-Joachim Wagner, Prof. Hartwig Wolburg, Prof. Konrad Kohler and Prof. Robert Feil who kindly spared their time to evaluate my work.

My particular gratitude goes to Prof. Philippe P. Monnier for not only the inspiring discussions but also for his patience and genuine friendship.

I also express my thanks to PD Dr. Bernhard K. Müller and Dr. Sabine Hirsch for their friendly encouragement.

I owe Dr. Peter Szurman special thanks for his immeasurable support at difficult times.

I am also grateful to my colleagues at the Breuninger Labor for the pleasant working atmosphere, particularly to Dr. Ana Sierra for always being a “comadre” and to Dr. Martin Spitzer, Claudia Riedinger, Monika Wild, Sigrid Schultheiss, Helga Möller, Christel Fischer-Lamprecht, Dr. Qi Zhu, Dr. Peter Heiduschka, Antje Biesemeier, Sven Schnichels, Kai Januschowski, Judith Birch, Sabine Hofmeister, and Monika Rittgarn for their sincere friendship.

Finally I would like to thank all the members of my family for their endless support.



<b>1. INTRODUCTION</b> .....	<b>1</b>
1.1. Glaucoma and the major risk factors .....	1
1.2. Possible mechanisms of retinal ganglion cell death in glaucoma.....	3
1.2.1. Neurotrophic factor deprivation.....	4
1.2.2. Ischemia of the anterior optic nerve.....	4
1.2.3. Glutamate excitotoxicity.....	5
1.2.4. Oxidative stress.....	5
1.2.5. Glial cell activation.....	7
1.2.6. Apoptosis of retinal ganglion cells.....	10
1.3. Current approaches of glaucoma treatment and their limitations.....	11
1.3.1. Pharmacological treatment of glaucoma.....	11
1.3.2. Surgical treatment of glaucoma.....	11
1.3.3. Postoperative wound healing – an initially protective attempt resulting in the failure of glaucoma filtration surgery.....	12
1.4. The possible role of the Rho-kinase/ROCK signalling pathway in postoperative wound healing and retinal cell damage.....	13
1.5. The aim of the study.....	17
<b>2. MATERIALS AND METHODS</b> .....	<b>19</b>
2.1. Chemicals, culture reagents, assay kits, and other materials.....	19
2.1.1. Chemicals and solutions.....	19
2.1.2. Cell and tissue culture reagents.....	21
2.1.3. Assay kits.....	21
2.1.4. Other materials.....	21
2.2. Buffers and solutions.....	22
2.3. Cell culture.....	28
2.3.1. Culture of human Tenon’s capsule fibroblasts.....	28
2.3.2. Growing fibroblasts on collagen-coated coverslips.....	28
2.3.3. Culture of RGC-5 cells.....	29
2.3.4. Trypsinization of the cells.....	29
2.4. Tissue culture.....	30
2.4.1. Retinal flat mounts.....	30
2.4.2. Incubation of retinal flat mounts in the conditioned medium of retina or optic nerve.....	30
2.4.3. Incubation of retinal flat mounts with reduced glutathione (GSH).....	30
2.4.4. Determining the level of total glutathione in retina.....	31
2.5. Analyzing the wound healing activities of human Tenon’s capsule fibroblasts.....	33
2.5.1. MTT Test.....	33
2.5.2. Bromodeoxyuridine (BrdU)-incorporation.....	33
2.5.3. Migration of fibroblasts on collagen gels.....	34

2.5.4. Scratch (wound) Assay.....	34
2.5.5. Contraction assay.....	35
2.6. Cytotoxicity assays.....	36
2.6.1. Ethidium homodimer-1 (EthD-1) staining.....	36
2.6.2. Lactate dehydrogenase (LDH) assay.....	36
2.7. Staining of cultured cells and retinae.....	38
2.7.1. Alexa488-Phalloidin Staining.....	38
2.7.2. DAPI staining of fibroblasts embedded in collagen gels.....	38
2.7.3. Immunofluorescence staining of fibroblasts and RGC-5 cells.....	38
2.7.4. Preparing cryosections of collagen gels and flat mounted retinae.....	39
2.7.5. Immunohistochemistry (IHC) on the sections of retinae and collagen gels.....	39
2.7.6. IHC on flat-mounted retina.....	39
2.8. Protein purification.....	42
2.8.1. Protein extraction from cells.....	42
2.8.2. Protein extraction from retinae.....	42
2.8.3. Determining the protein concentration by Bradford assay.....	42
2.8.4. Determining the protein concentration by bichinchoninic acid (BCA) assay.....	43
2.9. SDS-Polyacrylamide gel electrophoresis (PAGE) and Western blot.....	44
2.9.1. SDS-PAGE.....	44
2.9.2. Non-denaturing gel electrophoresis.....	44
2.9.3. Silver staining of gels.....	45
2.9.4. Transfer of proteins onto nitrocellulose membranes .....	46
2.9.5. PonceauS staining.....	47
2.9.6. Western blot.....	47
2.9.7. Signal detection by NBT/BCIP.....	47
2.9.8. Signal detection by 4-chloro-1-naphthol.....	48
2.9.9. Signal detection by enhanced chemiluminescence (ECL).....	48
2.10. Cytokine arrays.....	50
2.10.1. Membrane-based mouse cytokine array.....	50
2.10.2. Bio-Plex flow cytometric cytokine assay.....	50
2.11. Protein database search and sequence analysis.....	51
2.12. In vivo effects of H-1152P after optic nerve crush.....	52
2.13. Statistical analysis.....	52
<b>3. RESULTS.....</b>	<b>53</b>
3.1. Effect of ROCK Inhibition on the wound healing activities of human Tenon’s capsule fibroblasts.....	53
3.1.1. Optimal concentration of the ROCK inhibitor H-1152P.....	53
3.1.2. Anti-proliferative effect of H-1152P.....	55
3.1.3. Short-term application of H-1152P.....	56
3.1.4. Rearrangement of the actin cytoskeleton in response to H-1152P.....	58
3.1.5. Fibroblast migration in response to H-1152P.....	60
3.1.6. Effect of H-1152P on collagen gel contraction.....	63
3.1.7. Specificity of H-1152P action.....	65



<b>3.2. Effect of ROCK inhibition on retinal cell survival.....</b>	<b>67</b>
<b>3.2.1. Time course of cell damage in retinae under serum deprivation..</b>	<b>67</b>
<b>3.2.2. Neuroprotective effect of H-1152P on the ganglion cell layer.....</b>	<b>68</b>
<b>3.2.3. Reduced caspase-3 activation in response to H-1152P.....</b>	<b>70</b>
<b>3.2.4. Specificity of H-1152P action in mouse retinal cells.....</b>	<b>72</b>
<b>3.2.5. Decrease in astrocyte reactivity in response to ROCK inhibition..</b>	<b>75</b>
<b>3.2.6. H-1152P induced changes in the levels of proteins released         from the retina and the optic nerve.....</b>	<b>80</b>
<b>3.2.7. Reduction in the toxicity of the conditioned media of retina and         optic nerve incubated with H-1152P.....</b>	<b>81</b>
<b>3.2.8. Characterization of the secreted proteins.....</b>	<b>85</b>
<b>3.2.9. Changes in the cytokine profile of the conditioned medium of the         retina and optic nerve in response to ROCK-Inhibition.....</b>	<b>89</b>
<b>3.2.10. Effect of H-1152P in the presence of exogenous         glutathione.....</b>	<b>92</b>
<b>3.2.11. Effect of H-1152P on the level of total glutathione after         24 hours of serum deprivation.....</b>	<b>93</b>
<b>3.3. Effect of ROCK-inhibition on RGC-5 cells.....</b>	<b>94</b>
<b>3.3.1. Concentration dependent effects of H-1152P on the survival of         serum starved RGC-5 cells.....</b>	<b>94</b>
<b>3.3.2. Reduced caspase-3 activation in serum starved RGC-5 cells         treated with H-1152P.....</b>	<b>96</b>
<b>3.3.3. Specificity of H-1152P action in RGC-5 cells.....</b>	<b>96</b>
<b>3.4. Effect of ROCK-inhibition on retinal ganglion cell survival after optic nerve crush.....</b>	<b>100</b>
<b>4. DISCUSSION.....</b>	<b>102</b>
<b>4.1. Influence of ROCK-signalling on the wound healing activities of human         Tenon’s capsule fibroblasts.....</b>	<b>102</b>
<b>4.2. Influence of ROCK-signalling on retinal cell survival.....</b>	<b>106</b>
<b>4.2.1. Effect of ROCK inhibition on retinal cell survival in isolated             mouse retinae under serum deprivation.....</b>	<b>106</b>
<b>4.2.2. The concentration dependent effects of ROCK inhibition on the             survival of RGC-5 cells.....</b>	<b>113</b>
<b>4.2.3. Effect of ROCK inhibition on retinal ganglion cell survival after             optic nerve crush.....</b>	<b>120</b>
<b>5. SUMMARY.....</b>	<b>123</b>
<b>6. ABBREVIATIONS.....</b>	<b>127</b>
<b>7. REFERENCES.....</b>	<b>132</b>
<b>PUBLICATIONS.....</b>	<b>156</b>
<b>LEBENS LAUF.....</b>	<b>157</b>



# 1. INTRODUCTION

## 1.1. Glaucoma and the major risk factors

Glaucoma represents a group of optic neuropathies characterized by the progressive loss of retinal ganglion cells and their axons comprising the optic nerve. Degeneration of the ganglion cell axons impedes the transmission of visual information from the eye to the brain and results in the atrophy of the optic nerve. This in turn gives rise to irreversible visual field defects leading to blindness when left untreated.<sup>1-3</sup> According to the estimates of World Health Organisation in 1997, 105 million people were affected by glaucoma worldwide, with 5 million of them being legally blind.<sup>4</sup> Currently, this ocular neurodegenerative disease remains to be a leading cause of blindness particularly in industrialized countries.<sup>5, 6</sup>

The major risk factors identified for glaucoma include advancing age, family history of glaucoma, history of ocular trauma, African descent, vasospastic disorders, and most frequently, elevated intraocular pressure (IOP).<sup>5-7</sup> Elevated IOP arises when aqueous humor, the fluid providing structural and nutritional support to the anterior chamber of the eye, accumulates due to excess production by the ciliary body or insufficient drainage through the trabecular meshwork and uveoscleral pathways.<sup>8</sup> Depending on the degree of aqueous humor accumulation in the anterior chamber, the IOP may rise to levels that compromise the survival of retinal ganglion cells or their axons particularly at the level of the lamina cribrosa, the connective tissue in the optic nerve head through which the retinal ganglion cell axons and central retinal vessels pass (Figure 1).<sup>9, 10</sup> Yet, elevated IOP appears unlikely to be the sole initiator of glaucomatous optic nerve damage since approximately one-sixth of the patients suffer from glaucoma despite IOP levels in the normal range.<sup>11</sup> Moreover, a significant proportion of the patients experience ongoing vision loss even after the pharmacological or surgical reduction of IOP, suggesting the presence of other factors impeding the survival of the ganglion cells rescued from the primary damage. Therefore, considerable attention was directed to the characterization of the mechanisms underlying retinal ganglion cell death for developing alternative

therapeutic strategies aiming to prevent further visual field loss by maintaining the remaining retinal ganglion cells and their axons alive and functional.<sup>12</sup>

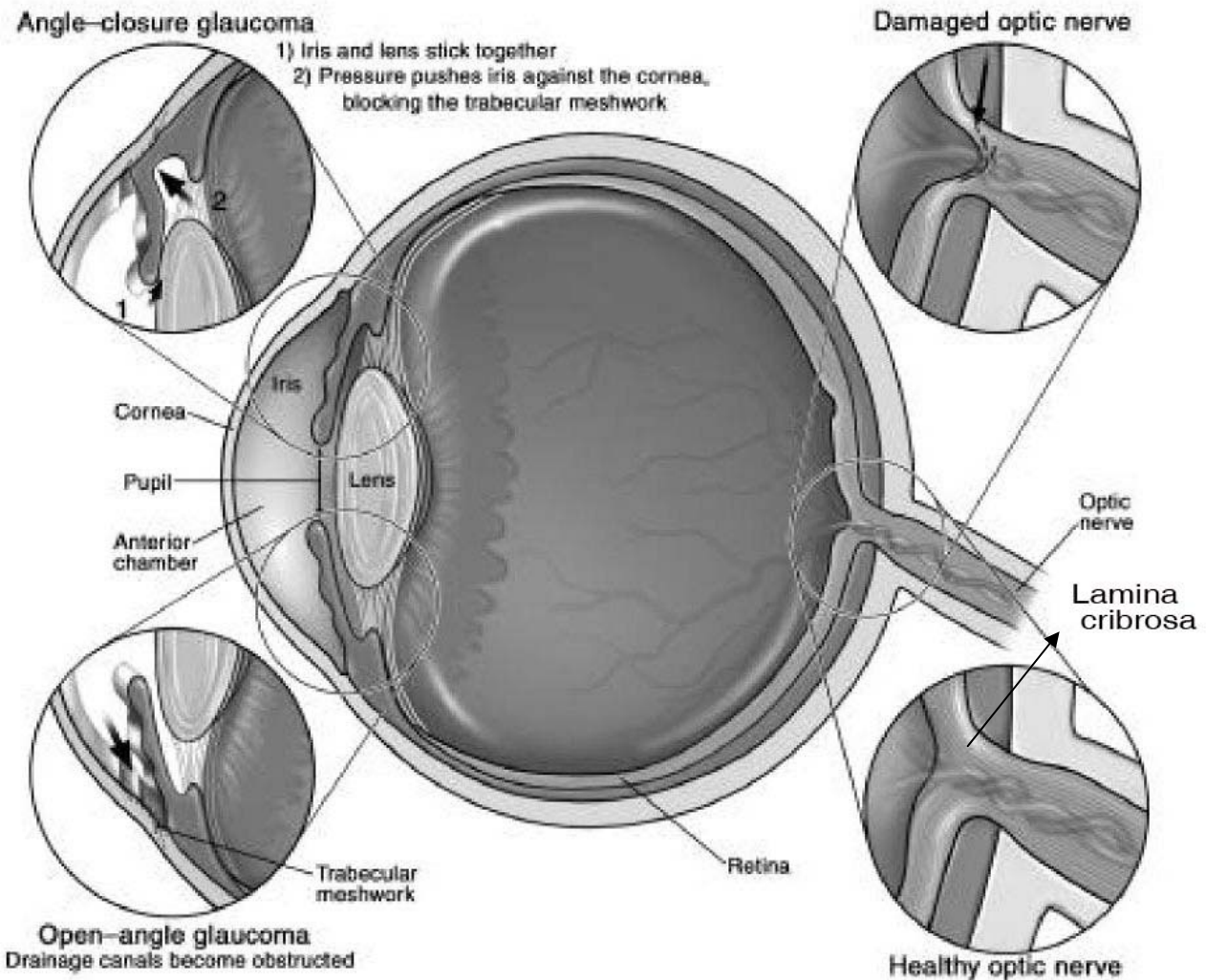


**Figure 1.** Mechanisms of IOP elevation accounting for the loss of retinal ganglion cells in two distinct types of glaucoma. Elevated IOP may cause the compression of the optic nerve head and impede the survival of retinal ganglion cells. The degeneration of the ganglion cell axons in turn results in the collapse and posterior bowing of the optic nerve head, referred to as the “cupping” of the optic nerve head, the most characteristic clinical feature of glaucoma.<sup>10</sup> However, the glaucomatous damage to the retinal ganglion cells and their axons can also occur or proceed in the absence of elevated IOP suggesting the involvement of additional risk factors (modified from the illustration available from Research to Prevent Blindness Organization, [www.rpbusa.org/library\\_content.php?document\\_id=56](http://www.rpbusa.org/library_content.php?document_id=56)).

## 1.2. Possible mechanisms of retinal ganglion cell death in glaucoma

Experiments on isolated cells as well as on animal models of glaucoma allowed for the identification of several mechanisms that may be simultaneously responsible for the ganglion cell death in glaucoma. These mechanisms can be summarised as neurotrophic factor deprivation, ischemia of the anterior optic nerve, glutamate induced excitotoxicity, oxidative stress, and glial cell activation. Evidence also indicates that these diverse mechanisms converge on a final common apoptotic pathway accounting for the removal of damaged retinal ganglion cells (Figure 2).<sup>13, 14</sup>

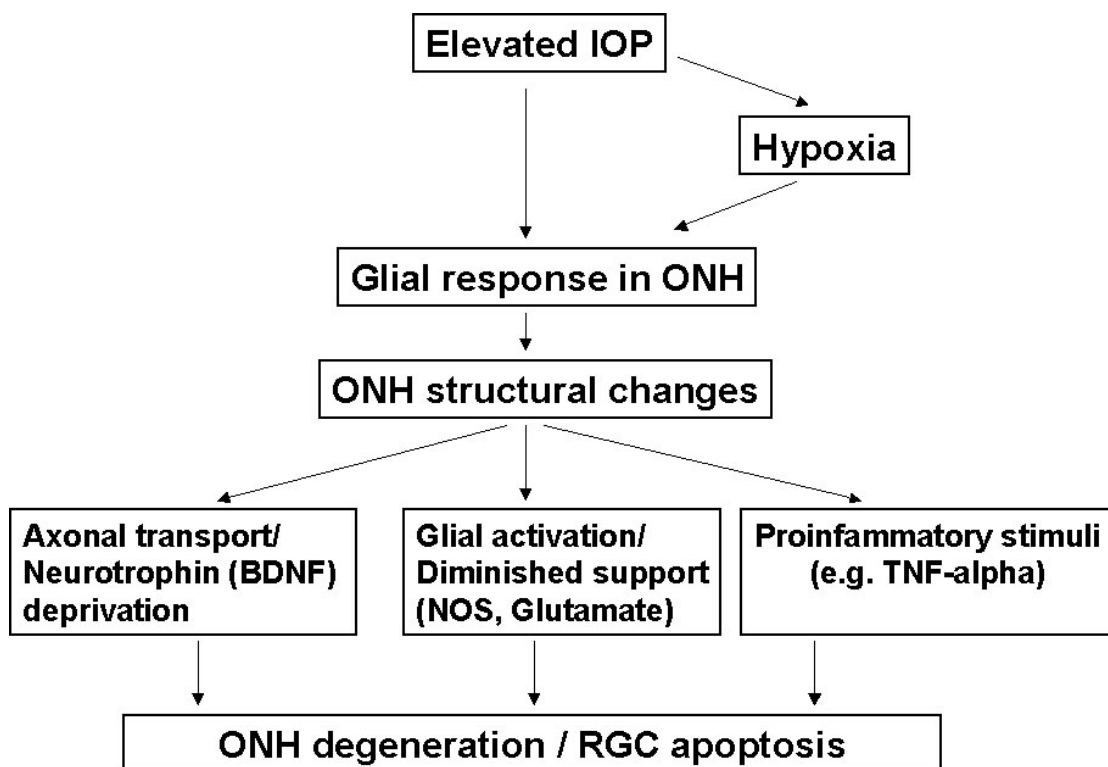


**Figure 2.** Proposed mechanism leading to retinal ganglion cell death in glaucoma. ONH: optic nerve head, BDNF: brain derived neurotrophic factor; NOS: nitric oxide synthase, RGC: retinal ganglion cell (modified from Kuehn et al., 2005).<sup>13</sup>

### **1.2.1. Neurotrophic factor deprivation**

The neurotrophic hypothesis suggests that the growth and maintenance of mammalian neurons depend on the retrograde transport of neurotrophins released from the target organ of a neuron.<sup>15</sup> Neurotrophins are small proteins that, upon binding to their receptors initiate events regulating cellular metabolism, homeostasis, proliferation, differentiation, and survival.<sup>16</sup> The survival of retinal ganglion cells was reported to be particularly dependent on the availability of the brain-derived neurotrophin factor (BDNF) secreted by the superior colliculus.<sup>17, 18</sup> Evidence from experimental studies indicate that elevated IOP causes the compression of the cribriform plates as observed in the human glaucomatous eyes<sup>19</sup> and blocks the axonal transport of labelled BDNF,<sup>20</sup> suggesting the impairment in the retrograde transport of neurotrophic factors as a possible mechanism threatening retinal ganglion cell survival.

### **1.2.2. Ischemia of the anterior optic nerve**

Blood flow to the anterior optic nerve depends on the perfusion pressure which is expressed as the difference between arterial blood pressure and IOP.<sup>21</sup> Elevation of IOP may therefore result in the obstruction of blood flow, i.e. ischemia, to the optic nerve.<sup>13</sup> Ischemia threatens cell survival not only due to the shortage of oxygen and metabolites, but also by inducing the production of oxygen free radicals and other reactive oxygen species, which react with and damage a number of cellular and extracellular elements.<sup>22, 23</sup>

The hypoperfusion theory of glaucomatous damage gains further support from the clinical association of vascular disorders such as migraine and Raynaud's syndrome with normal-tension glaucoma.<sup>13</sup> Moreover, the exogenous application of the vasoconstrictor peptide endothelin-1 was shown to reduce optic nerve blood flow and induce ganglion cell death in animal models in the absence of elevated IOP,<sup>24, 25</sup> suggesting the possible involvement of ischemic factors in the generation of ganglion cell damage regardless of the level of IOP.

### 1.2.3. Glutamate excitotoxicity

Glutamate is an essential amino acid functioning as the major excitatory neurotransmitter in the central nervous system (CNS). Glutamate excitotoxicity arises when the extracellular levels of glutamate are elevated either due to increased release or reduced uptake from the synapse. Though glutamate activates several types of cell receptors, its toxic effects are attributed mainly to the N-methyl-D-aspartate (NMDA) receptors which allow the influx of excessive amounts of calcium in response to high levels of glutamate. Calcium present in abnormally high intracellular concentrations activates nucleases, proteases, and lipases that attack cell constituents, resulting in the generation of highly reactive free radicals and nitric oxide which eventually activate the apoptotic programme.<sup>1, 13, 26</sup>

Retinal ganglion cells express a wide range of glutamate receptors including the NMDA-subtype<sup>27</sup> and are highly vulnerable to glutamate excitotoxicity in culture as well as in animal models.<sup>28, 29</sup> In addition, the intraocular injection of glutamate causes the excavation of the optic nerve as observed in glaucomatous eyes in neonatal mice.<sup>30</sup> The strongest support for the possible role of glutamate excitotoxicity in glaucoma emanated from an earlier study demonstrating a two-fold increase in the vitreal levels of this amino acid in human glaucoma patients as compared to controls.<sup>31</sup> Yet, the inability to confirm this finding in human glaucomatous eyes<sup>32</sup> as well as in an experimental model of glaucoma in subsequent studies<sup>33</sup> gave rise to a certain degree of controversy.<sup>34</sup> Nevertheless, current findings demonstrating the significant reduction in the levels of glutamate transporters and the neuroprotective effects of certain glutamate receptor antagonists in animal models of glaucoma underscore the need for further investigations in this field.

### 1.2.4. Oxidative stress

Reactive oxygen species (ROS) are partially reduced metabolites of oxygen generated as by-products of normal oxygen metabolism in the mitochondria and as second messengers in various signal transduction pathways.<sup>35</sup> These unstable intermediates include free radicals containing highly reactive unpaired electrons,

such as superoxide ( $O_2^{\cdot-}$ ), nitric oxide ( $NO\cdot$ ) and hydroxyl radical ( $OH\cdot$ ) as well as other molecular species like hydrogen peroxide ( $H_2O_2$ ) and peroxynitrite ( $ONOO^-$ ).<sup>36</sup> The strong tendency of ROS to interact with macromolecular cellular constituents to achieve a more stable configuration can result in the oxidative modification of proteins, lipid peroxidation of membranes, and nucleic acid breakdown, with detrimental effects on cell integrity and function.

All cells utilize complex systems of antioxidants like glutathione (GSH), and the vitamins E and C as well as the enzymes superoxide dismutase, catalase, glutathione peroxidase, glutathione reductase, and glutathione-s-transferase to maintain a reducing environment.<sup>35, 37, 38</sup> However, the levels of ROS can prevail the antioxidant capacity especially when the cells are in an energetically low state, resulting in oxidative stress implicated in a large number of pathological conditions including neurodegenerative disorders like glaucoma.<sup>35</sup> Experimental evidence from animal models of IOP elevation and retinal ischemia indeed demonstrated a significant decrease in retinal antioxidants and a parallel increase in the levels of ROS.<sup>39, 40</sup> This imbalance in the redox state of retinal cells was also associated with lipid peroxidation and the oxidative modification of proteins particularly in the inner retinal layers and ganglion cells,<sup>41-43</sup> suggesting the possible role of oxidative stress in glaucomatous damage.

Recently, light falling on the retina was proposed as an additional risk factor in glaucoma based on the demonstration of light-induced ROS release from mitochondria and the apoptosis of cultured, transformed retinal ganglion cells in response to excessive light exposure under serum deprivation.<sup>44</sup> This hypothesis was further supported by the energy requirements of the ganglion cell axons in the nerve fiber layer. The ganglion cell axons become myelinated from the level posterior to the lamina cribrosa onwards whereas in the nerve fiber layer they remain unmyelinated.<sup>45, 46</sup> Since the transmission of neural information in unmyelinated axons requires higher energy to operate efficiently, the ganglion cell axons in the nerve fiber layer are richly provided with mitochondria<sup>47-50</sup> and are therefore likely to be more susceptible to oxidative stress particularly after prolonged light exposure.



### 1.2.5. Glial cell activation

In the CNS, each neuron is outnumbered by approximately 10 glial cells which are specialized for performing activities essential for neuronal function and homeostasis. The major types of glial cells in the CNS include oligodendrocytes forming the myelin sheath that insulates the axons electrically, microglia representing the phagocytic immune cells of the CNS, and astrocytes, star-shaped or elongated cells performing various functions like the regulation of the extracellular ionic environment and pH, synthesis of growth factors, metabolites, and glutathione, release and removal of glutamate, modulation of synaptic transmission, and maintenance of the blood-brain-barrier. Oligodendrocytes, microglia, and astrocytes constitute the glial cells of the optic nerve<sup>45, 51, 52</sup> whereas the Müller cells, radial glia spanning the entire width of the retina with their end-feet forming the inner and outer limiting membranes, represent the most abundant type of glial cells in the retina. Being closely associated with all the retinal neurons, the Müller cells execute vital functions like the maintenance of the retinal extracellular milieu in homeostasis, release of neurotrophic factors, uptake and degradation of glutamate, and the secretion of the antioxidant glutathione.<sup>53</sup> In addition to Müller cells, astrocytes distributed along with the ganglion cell axons throughout the nerve fiber layer (except for the nonvascular areas) and microglia are also present in the retina.<sup>54, 55</sup>

The transition of quiescent astrocytes to the activated phenotype represents one of the earliest and most remarkable responses of the CNS to mechanical, ischemic, and various other types of insults. Though this reactivity may be initiated as an effort to maintain homeostasis and normal neuronal function under stress conditions,<sup>56</sup> activated astrocytes can also participate in the pathologic course of neuronal damage.<sup>57-59</sup> Astrocyte reactivity after CNS injury is characterized by the upregulation of glial fibrillary acidic protein (GFAP), an intermediate filament which confers stability to and allows the hypertrophy of astrocytic processes.<sup>60</sup> This event, presumably required for the formation of a glial network for sensing and responding to diverse disturbances, is also observed particularly in the Müller cells and optic nerve head astrocytes in human glaucomatous eyes<sup>61, 62</sup> and experimental models of glaucoma.<sup>63-65</sup>

Activation of astrocytes in the optic nerve head appears to persist during the chronic course of neurodegeneration in glaucoma and is associated with the upregulation of certain extracellular matrix molecules such as collagen, proteoglycans, and adhesion molecules.<sup>66-70</sup> However, the expression of matrix metalloproteinases, proteolytic enzymes degrading almost all the components of extracellular matrix, is also significantly increased in the ONH astrocytes, indicating extensive tissue remodelling that may allow for the migration of astrocytes to the injury area.<sup>71, 72</sup> This remodelling can eventually alter the biomechanical properties of the optic nerve head and increase the vulnerability of the remaining tissue to forces induced by elevated IOP.<sup>56, 73</sup>

Likewise, the reactivity of the Müller cells can also lead to the dysregulation of the supportive functions executed by these cells under normal conditions, resulting in the disturbance of the retinal glutamate metabolism and ion homeostasis.<sup>53</sup> Activation of the Müller cells as well as the optic nerve head and retinal astrocytes by simulated ischemia or elevated hydrostatic pressure also results in the secretion of nitric oxide.<sup>74-77</sup> Though the release of this vasodilator molecule might represent an attempt to counteract ischemia,<sup>78, 79</sup> higher concentrations of nitric oxide can give rise to the formation of free nitrogen radicals and other ROS that facilitate the apoptotic death of retinal ganglion cells.<sup>80</sup> In addition, reactive astrocytes release various proinflammatory cytokines, such as tumor necrosis factor(TNF)-alpha, interleukin(IL)-1 beta, IL-6, and interferon(IFN)-gamma that can initiate a neurodegenerative inflammatory response.<sup>81-82</sup> TNF-alpha also exerts direct toxicity on retinal ganglion cells by promoting nitric oxide generation.<sup>76</sup> A previous immunohistochemical study demonstrating the expression of TNF-alpha protein and mRNA predominantly in the retinal glial cells with an accompanying expression of the TNF-alpha receptor in the retinal ganglion cells of human glaucomatous eyes<sup>83</sup> provided further support for the possible role of TNF-alpha in the damage of retinal ganglion cells in glaucoma.

A noteworthy observation particularly in glaucoma patients having normal IOP is the presence of serum autoantibodies directed against retinal antigens.<sup>84, 85</sup> The autoantigens identified so far include proteins contributing to cellular defence mechanisms, such as the heat shock proteins<sup>86, 87</sup> which stabilize the actin cytoskeleton under environmental stress<sup>88</sup> and glutathione-s-transferase,<sup>89</sup> a

detoxification enzyme neutralizing free radicals.<sup>90, 91</sup> Autoantibodies to the proteoglycans in the optic nerve head and cell walls of blood vessels, which may weaken the extracellular matrix supporting the lamina cribrosa or its vasculature, have also been reported in the sera of certain glaucoma patients.<sup>13, 85</sup> Owing to their ability to release cytokines and function as antigen presenting cells, reactive astrocytes and microglia are implicated in the generation of this abnormal immune response which may contribute to the initiation and/or progression of neurodegeneration in glaucoma.<sup>92-94</sup> Activated astrocytes and Müller cells also proliferate to establish a glial scar possibly to occupy the spaces left by damaged neurons.<sup>95, 96</sup> However, the expression of various repulsive axon guidance cues on the surface of this glial scar constitutes a serious obstacle to axon regeneration after injury.<sup>97, 98</sup> The extent of glial cell reactivity therefore appears to be a critical determinant in the transformation of an initially protective attempt to a severe response facilitating the spread of secondary degeneration even after the removal of the primary cause of neural damage in glaucoma (Figure 3).

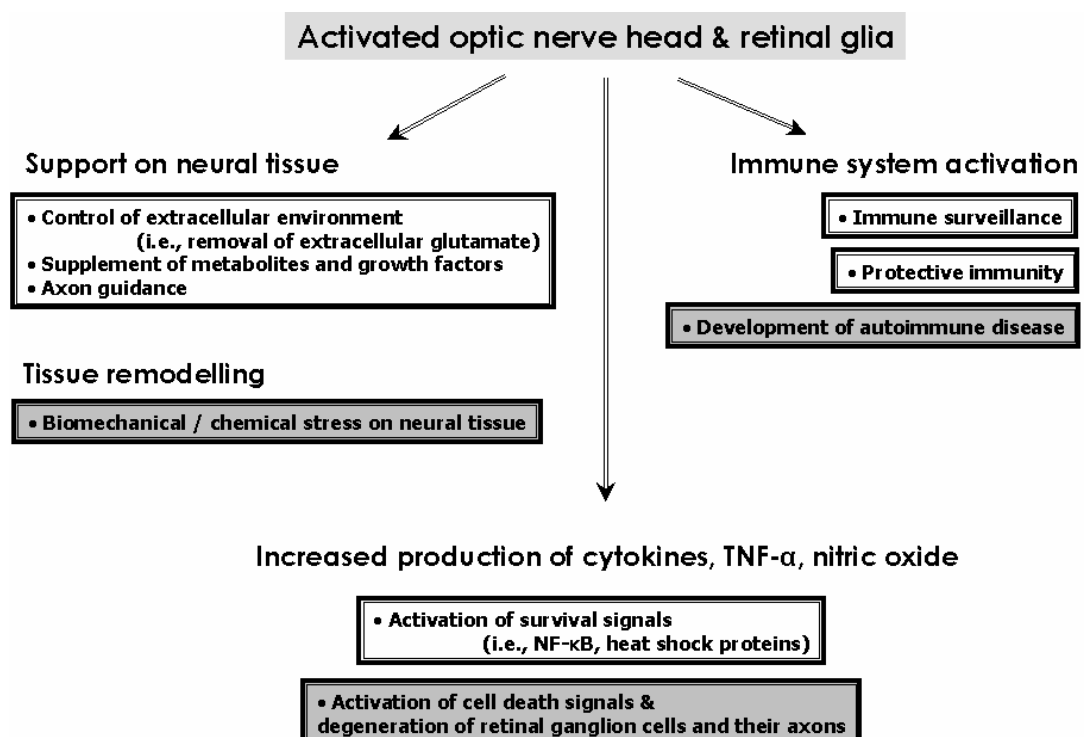


**Figure 3.** The potential supportive/protective (white boxes) and destructive (gray boxes) roles of activated glial cells in glaucoma (adapted from Tezel and Wax, 2003).<sup>56</sup>

### 1.2.6. Apoptosis of retinal ganglion cells

Regardless of the initiating cause, all optic neuropathies converge on a final common event represented by retinal ganglion cell death. Evidence from experimental models as well as from human subjects demonstrates that the activation of an intrinsic “suicide” program at least partly accounts for the loss of retinal ganglion cells exposed to various stress factors implicated in glaucoma.<sup>99-101</sup> This suicide program, referred to as apoptosis, involves a genetically coded cascade of biochemical events executed for the removal of unneeded or seriously damaged cells without eliciting an inflammatory response.<sup>15</sup>

The cells undergoing apoptosis exhibit particular morphological alterations characterized by the loss of adhesion, cellular contraction, condensation of the cytoplasm and chromatin, and blebbing of the cell membrane. These alterations facilitate the packaging of cellular organelles into membrane-bound apoptotic bodies to prevent the leakage of potentially toxic intracellular molecules and thereby protect the neighbouring cells from an inflammatory injury. The apoptotic bodies are subsequently removed by phagocytosis at the final step of the apoptotic pathway.<sup>102-104</sup>

Apoptosis can be initiated by either an extrinsic pathway upon the binding of extracellular death promoting ligands (such as TNF-alpha and FasL) to their respective receptors on the cell surface or an intrinsic pathway triggered by the release of diverse pro-apoptotic factors, like cytochrome c, from mitochondria due to loss of mitochondrial integrity.<sup>105, 106</sup> Both pathways lead to the activation of caspases, a family of intracellular proteases that cleave various cellular proteins at aspartate residues. Activation of caspases in turn gives rise to a cascade of proteolytic cleavage events that result in the morphologic changes characteristic of apoptotic cells.<sup>107</sup>

## **1.3. Current approaches of glaucoma treatment and their limitations**

Despite the extensive research to identify manageable therapeutic targets for maintaining the retinal ganglion cells alive and functional, the current treatment of glaucoma relies on pharmacological or surgical interventions all aimed at lowering the IOP for preventing further injury.<sup>5, 108</sup>

### **1.3.1. Pharmacological treatment of glaucoma**

Glaucoma treatment is usually initiated by the topical administration of medications that act on the IOP by reducing the formation or promoting the drainage of aqueous humor.<sup>108, 109</sup> Among these medications brimonidine, a selective alpha-2 adrenergic agonist, represents to our knowledge the only molecule that could also directly exert neuroprotective effects on retinal ganglion cells by increasing the levels of BDNF in experimental models of glaucoma.<sup>110, 111</sup> However, the pharmacological treatment can in some instances give rise to ocular or systemic side effects and may not be able to sufficiently lower the IOP particularly at an advanced stage of the disease, rendering the surgical treatment indispensable.<sup>112, 113</sup>

### **1.3.2. Surgical treatment of glaucoma**

The laser trabeculoplasty represents one surgical alternative to lower the IOP by reducing the resistance of trabecular meshwork against aqueous humor outflow using laser energy. However, this operation may not be adequate to perform in certain types of glaucoma or be effectual in lowering the IOP in some patients.<sup>112, 114</sup> Glaucoma filtration surgery is the most frequently applied procedure for reducing the IOP in such patients that failed to respond well to pharmacological therapy or laser treatment.<sup>5, 115, 116</sup> Depending on the type and stage of glaucoma, filtration surgery may even be recommended prior to trying medical or laser treatment.<sup>112</sup> The purpose of the filtration surgery is to create a scleral fistula that enables the drainage of aqueous humor from the anterior chamber to the subconjunctival space (Figure 4). Though this method attains an immediate effect on lowering the IOP, the

postoperative wound healing within the filtration area often occludes the artificial fistula and prevents the long-term success.<sup>117-119</sup>

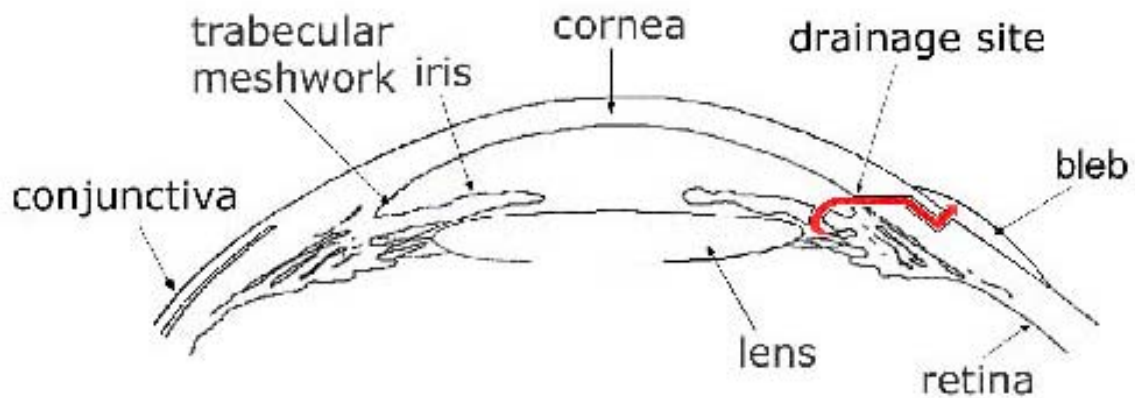


**Figure 4.** Schematic representation of the glaucoma filtration surgery performed for creating a new passage for aqueous humor drainage from the anterior chamber (image obtained from the Digital Journal of Ophthalmology of Harvard University, <http://www.djo.harvard.edu/site.php?url=/patients/pi/420#>).

### 1.3.3. Postoperative wound healing – an initially protective attempt resulting in the failure of glaucoma filtration surgery

The wound healing process in response to injury represents a protective attempt of the organism for re-establishing tissue integrity.<sup>120</sup> However, this event may give rise to undesirable consequences in certain cases, such as the obstruction of the drainage site created by glaucoma filtration surgery. The wound healing response to the tissue trauma induced by filtration surgery is initiated by the formation of a fibrin clot that transiently covers the injury site. This is followed by an inflammatory reaction during which the foreign particles are removed by neutrophils and macrophages.<sup>119</sup> The platelets and macrophages also release molecules like platelet derived growth factor (PDGF) and transforming growth factor-beta (TGF- $\beta$ ), which stimulate the fibroblasts from Tenon's capsule, the condensed connective tissue surrounding the posterior part of the eye.<sup>121-123</sup> The activated fibroblasts from Tenon's capsule migrate into the cleaned wound area and start proliferating to replace the lost cells.

These fibroblasts also deposit new extracellular matrix, and acquire contractile properties, facilitating the closure of the wound and ultimately resulting in the occlusion of the created fistula.<sup>124, 125</sup>

A variety of pharmacological agents such as corticosteroids and antimetabolites have been in clinical use in order to increase the success rate of filtration surgery.<sup>126</sup> These substances modulate the postoperative wound healing by suppressing the inflammation and preventing fibroblast proliferation, respectively. However, some antimetabolites such as fluorouracil and mitomycin C exert their effect by causing cell death,<sup>127, 128</sup> and diffusion into adjacent ocular tissues may result in impairment of cells other than the targeted ones,<sup>129, 130</sup> inducing vision threatening complications. This risk eventually necessitated the attempts to develop safer strategies, such as the administration of monoclonal anti-TGF- $\beta$  antibodies,<sup>131</sup> photoablation at the site of surgery,<sup>132</sup> and application of decorin, a naturally occurring proteoglycan inhibiting TGF- $\beta$  and PDGF.<sup>133</sup>

#### **1.4. The possible role of the Rho-kinase/ROCK signalling pathway in postoperative wound healing and retinal cell damage**

The wound healing response of fibroblasts comprises dynamic events like proliferation, motility, and contractility, which require the continuous remodelling of the actin cytoskeleton. Identifying the intracellular signaling pathways that govern the cytoskeletal arrangement in Tenon's capsule fibroblasts might therefore constitute the basis of alternative therapies specifically targeting the key mediators of these cascades. A central role in the organization of the actin cytoskeleton during various motile events is attributed to the RhoA protein from the Rho family of small GTPases, rendering this signaling pathway a likely candidate as the mediator of the wound healing activities of Tenon's capsule fibroblasts.<sup>134</sup>

The Rho family of GTPases comprises small molecular weight proteins that act as molecular switches in response to extracellular signals, being either inactive, in their GDP-bound state, or active in the GTP-bound state. The cycling of Rho-GTPases between the active and inactive states is strictly regulated by the degree of their association with GDP dissociation inhibitors (GDI) and GTPase accelerating proteins (GAP) which favour the inactive state, and the exchange of GDP for GTP by guanine nucleotide exchange factors (GEF) which promotes the active state. Activated Rho-GTPases then bind to various effector proteins that transmit the signals downstream (Figure 5).<sup>135-137</sup>

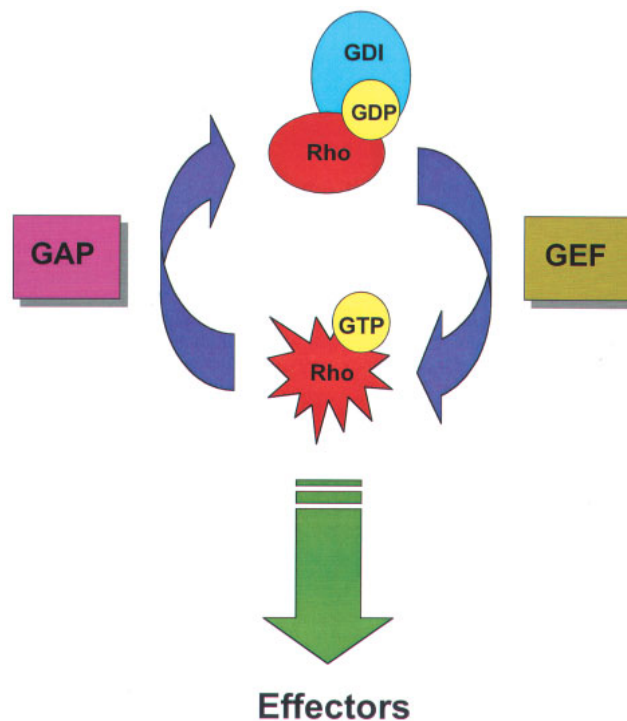


**Figure 5.** Regulation of Rho-GTPase activity.

The Rho-associated coiled-coil kinase (Rho kinase/ROCK) was the first effector of RhoA to be characterized and found to be executing the majority of the events downstream of RhoA.<sup>138</sup> ROCK is a ubiquitously expressed serine-threonine protein kinase that mainly promotes myosin II activity by inhibiting the myosin light chain phosphatase and possibly by directly phosphorylating the myosin light chain. This in turn favors the assembly of actin-myosin filaments that generate the tensile strength underlying the RhoA-ROCK associated dynamic events such as the contraction of smooth muscle cells as well as the adhesion, motility, and cell-cycle



progression in numerous cell types.<sup>139</sup> The RhoA-ROCK pathway can also regulate gene expression secondary to the cytoskeletal alterations.<sup>140, 141</sup>

As the research on the functions of ROCK progressed, the ROCK-dependent contractility was found to be a mechanism operating in a wide variety of cells including those of the ciliary muscle and trabecular meshwork. Administration of the ROCK inhibitors HA-1077 (fasudil), Y-27632, and H-1152P was reported to be inducing the relaxation of these cells by suppressing the phosphorylation of myosin light chain and thereby promoting the outflow of aqueous humor.<sup>142-144</sup> Moreover, a very recent study reports the activation of RhoA in human Tenon's capsule fibroblasts stimulated with TGF-beta and the reduction in the TGF-beta induced fibroblast contractility in response to the ROCK inhibitors mentioned above,<sup>145</sup> providing the first evidence for the involvement of the RhoA-ROCK pathway in an essential aspect of wound healing in these cells.

Interestingly, activation of ROCK by either the GTP-bound RhoA or via the caspase mediated cleavage of its autoinhibitory domain is implicated in the contraction of cells observed in the early phase of apoptosis as well (Figure 6).<sup>104</sup> Activation of this signaling pathway, an event stimulated by the repulsive axon guidance cues during development, is also likely to be underlying the collapse of the neurite network, another early feature of neuronal apoptosis.<sup>146, 147</sup> The inhibition of RhoA-ROCK signaling therefore emerges as a possible strategy for preventing or slowing-down apoptosis and axon degeneration in the CNS. The therapeutic potential of RhoA-inhibition on the latter event has indeed been the subject of numerous studies which yielded promising results in various models of CNS injury including optic nerve damage. In one study, retinal ganglion cell axons labeled anterogradely following optic nerve crush could be detected distal to the injury site in rats treated with the RhoA inhibitor C3.<sup>148</sup> In a very recent study, the regeneration of axotomized ganglion cells into a peripheral nerve graft was significantly enhanced after multiple injections of C3 alone or in combination with cyclicAMP and ciliary derived neurotrophic factor. Treatment with C3 is also reported to have increased ganglion cell survival in this study, providing important evidence for the role of RhoA pathway in axon degeneration and the subsequent neuronal death.<sup>149</sup> However, concerning the downstream RhoA effector mediating these effects, not much is

known so far except for the possible involvement of ROCK in NMDA-induced neurotoxicity in rat retinae demonstrated by the reduction in cell loss in the ganglion cell layer and the increase in retinal thickness in response to fasudil treatment.<sup>150</sup>

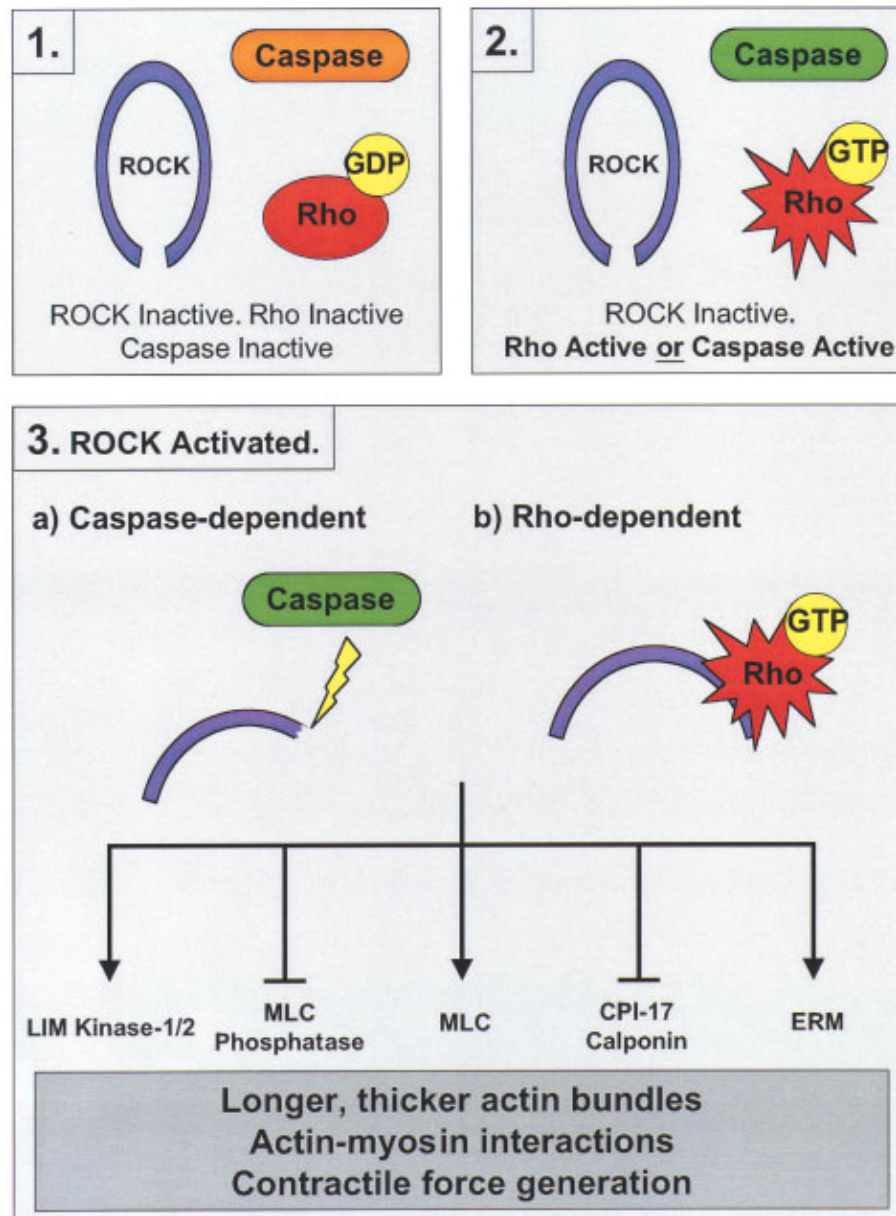


**Figure 6.** ROCK activation by Rho-GTP or caspases leads to the phosphorylation of various downstream targets favoring the generation of contractile force in apoptosis. Activated LIM kinases stabilize the filamentous actin by phosphorylating and inactivating the actin severing protein cofilin. The ROCK-dependent inhibition of CPI-17 and calponin relieves the inhibition of myosin ATPase activity of these proteins and further promotes the generation of actin-myosin contractile force. The activated ezrin-radixin-moesin (ERM) proteins contribute to the RhoA-ROCK mediated signaling by facilitating the association of activated RhoA with the plasma membrane where it can exert its effects locally.<sup>104</sup>

## 1.5. The aim of the study

The findings outlined above signify the potential of ROCK-inhibition as an ideal glaucoma treatment that may accomplish not only the reduction of IOP but also the suppression of the undesirable wound healing following filtration surgery as well as the promotion of axon regeneration and retinal ganglion cell survival. However, a more detailed characterization of the events mediated by the RhoA-ROCK pathway in cells implicated in the onset and progress of glaucoma are still required to assess the feasibility of this approach. The present study therefore addresses the influence of the ROCK-signaling pathway on the major wound healing activities of Tenon's capsule fibroblasts and the survival of retinal cells particularly at the ganglion cell layer. In this work, the impact of ROCK-signaling was studied using H-1152P, the most specific of the commercially available ROCK inhibitors at present.<sup>151</sup> This approach therefore allowed for analyzing the efficiency and safety of ROCK-inhibition as a strategy to modulate the activities of Tenon's capsule fibroblasts and retinal cells as well.

The possible role of the ROCK-signaling pathway in the wound healing activities of Tenon's capsule fibroblasts was analyzed in vitro on human cells stimulated with serum. The outcomes of H-1152P treatment on the proliferation, survival, and cytoskeletal organization of Tenon's capsule fibroblasts were characterized by biochemical and morphological analyses. Furthermore, the role of H-1152P in fibroblast motility and collagen gel contraction were investigated with particular emphasis on the extent of fibronectin network assembly. Lastly, the specificity of H-1152P was analyzed by Western blot to ensure that the observed effects reflected the outcomes of ROCK-inhibition in these cells.

Analyzing the response of retinal cells to H-1152P treatment constituted another essential part of this work not only for demonstrating the possible neuroprotective effect of this ROCK-inhibitor but also to ensure the absence of adverse effects on the retina, since several medications applied topically to the eye were found to be able to reach the posterior segment at concentrations sufficient for pharmacological activity.<sup>152</sup> In this study, the effect of H-1152P treatment on the survival of retinal cells was initially investigated in vitro on retinal explants cultured in

the absence of serum. This stringent model combining the axotomy of retinal ganglion cells with serum deprivation enabled the characterization of the response of various retinal cells under stress since the multilayered structure of the retina could be conserved for a longer period of time despite the unfavorable conditions. The effect of H-1152P treatment on the survival of retinal cells was studied by histological evaluations with particular emphasis on the ganglion cell layer. The extent of glial cell reactivity was also determined by immunohistochemistry and Western blot as an indicator of tissue stress. Furthermore, the specificity of H-1152P was analyzed as described for the Tenon's capsule fibroblasts. The outcomes of H-1152P administration on the release of various cytokines as well as the total level of glutathione were further extra- and intracellular events characterized to provide more insight into the mechanisms of H-1152P action in retinal cells.

To elucidate the direct effect of H-1152P on retinal ganglion cells, RGC-5 cells, a transformed retinal ganglion cell line offering a convenient alternative to characterize the response of retinal ganglion cells *in vitro*,<sup>153</sup> were also used in this study. The RGC-5 cells were incubated without serum to simulate the depletion of trophic support to the retinal ganglion cells as observed upon injury to the optic nerve *in vivo*. The outcomes of H-1152P treatment on the survival of serum deprived RGC-5 cells as well as the specificity of this inhibitor were analyzed by fluorescence microscopy and immunocytochemistry.

To analyze the neuroprotective potential of H-1152P *in vivo*, we also initiated a collaboration with Dr. Frank Schüttauf from the University Eye Hospital in Tübingen, in which we studied the influence of H-1152P administration on the survival of ganglion cells after optic nerve crush. The extent of glial cell reactivity was also determined with the aim of providing the first clues to the events associated with ROCK-signaling after damage to the retinal ganglion cells *in vivo*.

## 2. MATERIALS AND METHODS

### 2.1. Chemicals, culture reagents, assay kits, and other materials

#### 2.1.1. Chemicals and solutions

- **Acetic acid, anhydrous (100%)**, Merck, Darmstadt, Germany, # 100063
- **Acrylamide**, Serva, Heidelberg, Germany, # 10675
- **Alexa488-phalloidin**, Molecular Probes, Eugene, OR, # A12379
- **Ammonium persulfate**, Bio-Rad, Munich, Germany, # 123453A
- **BCIP**, Roche Applied Science, Penzberg, Germany, # 11 383 221 001
- **Bisacrylamide**, Serva, # 29195
- **Bovine serum albumin**, Serva, # 11930
- **Bromophenol blue, sodium salt**, Serva, # 15375
- **4-chloro-1-naphthol**, Sigma-Aldrich, Steinheim, Germany, # C-8890
- **Coomassie brilliant blue G-250**, Serva, # 17525
- **DAPI**, Molecular Probes, # D1306
- **Dimethylsulfoxide (DMSO)**, Merck, # 102950
- **Ethanol**, Merck, # 100983
- **Ethidium homodimer-1**, Molecular Probes, # E-1169
- **D(+)-Glucose**, Sigma-Aldrich, # G-7021
- **L-Glutamine**, ROTH, Karlsruhe, Germany, # 3772
- **Glutathione (reduced, GSH)**, Sigma-Aldrich, # G-6013
- **Glycerol**, Merck, # 104093
- **Glycine**, Merck, # 104169
- **H-1152P**, Calbiochem / Merck, # 555550
- **30% H<sub>2</sub>O<sub>2</sub>**, Merck, # 107209

- **Hepes (1M)**, Serva, # 47260
- **para-Hydroxycoumaric acid**, Sigma-Aldrich, # C-9008
- **Kaleidoscope Prestained Protein Standard**, Bio-Rad, # 161-0375
- **KCl**, Fluka / Sigma-Aldrich, # 60132
- **KH<sub>2</sub>PO<sub>4</sub>**, Merck, # A591973
- **Kodak developer & replenisher solution**, Sigma-Aldrich, # P7042
- **Kodak fixer & replenisher solution**, Sigma-Aldrich, # P7167
- **Low molecular Weight Biotinylated Protein Standard**, Bio-Rad, # 161-0308
- **Luminol**, Sigma-Aldrich, # A-4685
- **2-Mercaptoethanol**, ROTH, # 4227.1
- **Methanol**, Merck, # 106009
- **MgCl<sub>2</sub>**, Fluka, # 63068
- **Mowiol**, Hoechst, Frankfurt, Germany, # 4-80
- **Na<sub>2</sub>EDTA.2H<sub>2</sub>O**, ROTH, # 8043
- **Na<sub>2</sub>HPO<sub>4</sub>**, Merck, # A414386
- **NaCl**, Merck, # 106404
- **NaOH pellets**, Merck, # 106498
- **NBT**, Roche Applied Science, # 11 383 213 001
- **NP-40**, Fluka, # 74385
- **Paraformaldehyde**, Merck, # 104005
- **ortho-Phosphoric acid, 85%**, Merck, # 100573
- **PonceauS**, Sigma-Aldrich, # P-3504
- **2-Propanol**, Merck, # 100994
- **Protease inhibitor cocktail**, Sigma-Aldrich, # P8340
- **Sodium dodecyl sulphate (SDS)**, Serva, # 20783
- **D(+)-Sucrose**, ROTH, # 4621.1
- **TEMED**, Serva, # 35925
- **Tris base (MW:121.14)**, Sigma-Aldrich, # T1503
- **Tris-HCl (MW:157.60)**, Boehringer Mannheim, # 812846
- **Triton X-100**, Serva, # 37240
- **Tween-20**, Merck, # 822184

### 2.1.2. Cell and tissue culture reagents

- **Bovine dermal collagen solution (~3 mg/ml)**, CELLON, Strassen, Luxembourg
- **Collagen type I, from rat tail, lyophilized**, Roche Applied Science, # 1 179 179
- **D-MEM/F-12 (1:1), with phenolrot, without L-Glutamine (for cell culture)**, Gibco / Invitrogen, Carlsbad, CA, # 21 331-020
- **D-MEM/F-12 (1:1) without phenolrot, with L-Glutamine (for retina culture)**, Gibco, # 21 041-025
- **Fetal bovine serum**, Gibco, # 10270 - 106
- **10X Modified Eagle's Medium (MEM)**, Gibco, # 11700 - 069
- **Penicillin/Streptomycin**, Gibco, # 15140 - 122
- **Phosphate buffered saline (PBS), without Ca<sup>++</sup> and Mg<sup>++</sup>, for cell culture**, Gibco, # 14190 - 094
- **1X Trypsin-EDTA (0.25% Trypsin with EDTA 4Na)**, Gibco, # 25200 - 072

### 2.1.3. Assay kits

- **ApoGSH Total Glutathione Kit**, BioVision, Mountain View, CA, # K261-100
- **BCA assay**, Pierce, Rockford, IL, # 23235
- **BrdU Cell Proliferation assay**, Calbiochem, # QIA58
- **Mouse Cytokine Antibody Array I**, RayBiotech Inc., Norcross, GA, # M0308001
- **LDH**, Roche Applied Science, # 1 644 793
- **Silver staining kit**, Bio-Rad, # 161-0443

### 2.1.4. Other materials

- **Cellulose nitrate filter, 0.45 µm pore size (for retina culture)**, Sartorius, Göttingen, Germany, # 13006-50-N
- **Kodak X-Omat AR Film**, Sigma-Aldrich, # F5888
- **Millex GS 0.22 µm filter unit**, Millipore, Billerica, MA, # SLGSO33SS
- **Nitrocellulose membrane (for Western blot)**, Schleicher & Schuell, Münster, Germany, # 401396

- **OCT compound**, Sakura Finetec, Torrance, CA, # 4583
- **Superfrost slides**, R. Langenbrick, Teningen, Germany, # 03-0060
- **Whatman No.1 paper**, Schleicher & Schuell, # 426690

## **2.2. Buffers and solutions**

### **30% acrylamide / 0.8% bisacrylamide (37.5:1)**

After dissolving 300 g acrylamide in approximately 500 ml Milli-Q water, 8 g bisacrylamide was added into the solution and stirred well. The volume was adjusted to 1 liter using Milli-Q water. The solution was filtered through Whatman No.5 filter paper and stored at 4°C protected from light.

### **Alkaline phosphatase buffer**

100 mM Tris-HCl

100 mM NaCl

5 mM MgCl<sub>2</sub>

---

Dissolved in 900 ml dH<sub>2</sub>O.

The pH of the solution was adjusted to 9.5 and the final volume was brought to 1 liter with dH<sub>2</sub>O. The solution was stored at 4°C.

### **1X blotting buffer**

10X blotting buffer 100 ml

Methanol 200 ml

Milli-Q water 700 ml

---

Stirred well under a fume hood.



### **10 X blotting buffer**

0.2 M Tris-base

1.5 M glycine

0.002% sodium dodecyl sulphate (SDS)

Volume was adjusted to 1 liter with Milli-Q water.

### **Cell lysis buffer**

50 mM Tris-HCl, pH 7.4

150 mM NaCl

1% NP-40

1 mM EDTA

Tris-HCl was dissolved in approximately 75 ml of dH<sub>2</sub>O and the pH was adjusted to 7.4. NaCl, NP-40, and EDTA were then added and the volume was adjusted to 100 ml using dH<sub>2</sub>O. The solution was stored at 4°C. The protease inhibitor cocktail was added into the aliquots of cell lysis buffer at a final concentration of 1% (v/v) shortly before use.

### **4-chloro-1-naphthol stock solution (30 mg/ml)**

0.3 g of 4-chloro-1-naphthol was dissolved in 10 ml methanol, aliquotted into 1.5 ml microfuge tubes wrapped in aluminum foil, and stored at -20°C.

### **Coomassie brilliant blue solution (for Bradford Assay)**

100 mg Coomassie brilliant blue G-250

50 ml 95% ethanol (v/v)

100 ml 85% *ortho*-phosphoric acid (v/v)

The volume was adjusted to 1 liter using dH<sub>2</sub>O. The solution was filtered through Whatman No.1 filter paper and stored at 4°C.

### **Enhanced chemiluminescence (ECL) solution A**

50 mg Luminol was dissolved in 200 ml of 0.1 M Tris-HCl (pH 8.6) and stored at 4°C.

**ECL solution B**

11 mg *para*-Hydroxycoumaric acid was dissolved in 10 ml of DMSO and stored at room temperature protected from light.

**0.5 M EDTA, pH 8**

93.05 g of Na<sub>2</sub>EDTA.2H<sub>2</sub>O was dissolved in 400 ml of dH<sub>2</sub>O by stirring vigorously. The pH was adjusted to 8.0 by adding approximately 10 g NaOH pellets and the volume was brought to 500 ml with dH<sub>2</sub>O. The solution was sterile filtered using 0.22 µm filters and stored at room temperature.

**1 X electrophoresis buffer (denaturing)**

100 ml 10X electrophoresis buffer

10 ml 10% SDS (v/v)

The volume was adjusted to 1 liter using Milli-Q water.

**1 X electrophoresis buffer (non-denaturing)**

Prepared as the 1 X denaturing electrophoresis buffer omitting SDS and replacing the volume with MilliQ water.

**10 X electrophoresis buffer**

250 mM Tris

1.9 M glycine

Dissolved in a total volume of 1 liter Milli-Q water.

**Ethidium homodimer-1 (EthD-1) stock solution (2 mM)**

Under a laminar flow hood, 583.6 µl of 1:4 DMSO/dH<sub>2</sub>O mixture (v/v) was added into the vial containing 1 mg EthD-1 (MW=856.77) and mixed well. The stock solution was aliquotted at 20-50 µl into 500 µl tubes wrapped in aluminum foil and stored at -20°C.

### **0.1% glucose-PBS (w/v)**

D-glucose was dissolved in sterile PBS (culture grade) at a final concentration of 0.1% (w/v) and sterile filtered using 0.22  $\mu\text{m}$  filters under a laminar flow hood. Stored at 4°C.

### **H-1152P (10 mM stock solution)**

Under a laminar flow hood, 1 mg of H-1152P was dissolved in 255  $\mu\text{l}$  sterile  $\text{dH}_2\text{O}$ , aliquotted into sterile 500  $\mu\text{l}$  tubes wrapped in aluminum foil, and stored at -20°C.

### **2X Laemmli sample buffer**

62.5 mM Tris, pH 6.8

2% SDS (w/v)

10% glycerol (v/v)

0.1% bromophenol blue,  $\text{Na}^+$  salt (w/v)

5% beta-mercaptoethanol (v/v)

The volume was adjusted to 10 ml using  $\text{dH}_2\text{O}$  and the aliquots were stored at -20°C. The non-denaturing sample buffer was prepared as above omitting SDS and beta-mercaptoethanol.

### **Mowiol**

15 mg Mowiol was dissolved in 60 ml of phosphate buffered saline (PBS) by stirring overnight. 30 ml glycerol was added and the stirring was continued overnight. The solution was then centrifuged at 1500 rpm for 30 minutes to precipitate the undissolved Mowiol. The supernatant was aliquotted at 10 ml and stored at -20°C.

### **MTT lysis solution**

50 g SDS

3 ml 100% anhydrous acetic acid

497 ml DMSO

Stored at room temperature

**MTT stock solution (5 mg/ml)**

0.25 g MTT

50 ml PBS (cell culture grade, without Ca<sup>++</sup> and Mg<sup>++</sup>)

MTT pulver was dissolved in PBS by rotating overnight protected from light. The solution was sterile filtered using 0.22 µm filters and stored at 4°C.

**4% paraformaldehyde (w/v)**

4 g paraformaldehyde

100 ml PBS

Stirred under fume hood and heated to approximately 60°C until the solution appeared clear. Stored at 4°C.

**1X PBS**

136.9 mM NaCl

2.7 mM KCl

8.1 mM Na<sub>2</sub>HPO<sub>4</sub>

1.47 mM KH<sub>2</sub>PO<sub>4</sub>

Volume adjusted to 1 liter using dH<sub>2</sub>O. Stored at room temperature.

**PonceauS solution**

0.1 g PonceauS

200 µl acetic acid anhydrous

Volume adjusted to 20 ml using dH<sub>2</sub>O. Prepared shortly before use.

**10% SDS (w/v)**

50 g SDS was dissolved in approximately 400 ml Milli-Q water and the volume was adjusted to 500 ml with Milli-Q water.

### **Tissue homogenization buffer**

50 mM Tris-HCl, pH 7.4

2 mM MgCl<sub>2</sub>

100 mM NaCl

1% NP-40 (v/v)

10% glycerol

Tris-HCl was dissolved in approximately 75 ml of dH<sub>2</sub>O and the pH was adjusted to 7.4. NaCl, MgCl<sub>2</sub>, NP-40, and glycerol were then added and the volume was adjusted to 100 ml using dH<sub>2</sub>O. The solution was stored at 4°C. The protease inhibitor cocktail was added into the aliquots of cell lysis buffer at a final concentration of 1% (v/v) shortly before use.

### **1 M Tris**

121.14 g of Tris-base was dissolved in 800 ml dH<sub>2</sub>O. After adjusting the pH to the desired value, the final volume was brought to 1 liter using dH<sub>2</sub>O.

### **10X Tris-buffered saline (TBS)**

100 mM Tris

1.5 M NaCl

The volume was adjusted to 1 liter using dH<sub>2</sub>O. The solution was diluted 1/10 with dH<sub>2</sub>O to prepare 1X TBS.

## **2.3. Cell culture**

### **2.3.1. Culture of human Tenon's capsule fibroblasts**

Samples of human Tenon's capsule were obtained from five patients undergoing glaucoma filtration surgery. The tenets of the Declaration of Helsinki were followed for the collection of human material and informed consent was obtained from the subjects after explanation of the nature and possible consequences of the study. Strips of tissue were placed into Petri dishes in a laminar flow hood, dissected into 1-2 mm cubes and transferred into 10 mm-Petri dishes filled with a few ml of complete medium (DMEM/F-12 (1:1) with phenol red supplemented with 10% fetal bovine serum (FBS), 2 mM L-glutamine, 100 U/ml penicillin and 100 µg/ml streptomycin) sufficient to cover the tissue pieces. Sterile coverslips of 5 mm-diameter were placed on each tissue to facilitate the adhesion of the pieces to the dish and to ensure their immersion into the medium. The Petri dishes were maintained at 37°C in a humidified atmosphere of 5% CO<sub>2</sub>. The fibroblasts migrating from these tissues were harvested by trypsinization after approximately 3 weeks, renewing the medium every week. The cells between the third and seventh passages were used for the experiments. Incubations with H-1152P were performed without replenishing the inhibitor to detect whether this inhibitor can exert long-lasting effects.

### **2.3.2. Growing fibroblasts on collagen-coated coverslips**

Glass coverslips of 10-mm diameter were kept in 70% ethanol for 10 minutes, washed twice with sterile dH<sub>2</sub>O, and autoclaved or kept for 15 minutes under UV-light in a laminar flow hood. The lyophilized type I collagen from rat tail was dissolved in sterile 0.2% acetic acid (v/v) to give a final concentration of 2 mg/ml. A thin film of this solution was spread onto sterile coverslips with a diameter of 10 mm (approximately 5 µg/cm<sup>2</sup>) and air-dried in the laminar flow hood for 1 hour. The coverslips were then rinsed with sterile phosphate buffered saline (PBS) and placed into the inner wells of 24 well-plates. The outer wells were filled with PBS to prevent the evaporation of the culture medium. Fibroblasts were added at a density of 3000 cells/coverslip, allowed to attach for 3 hours, and incubated with or without H-1152P in duplicates for 4 days (see figure 7 for the structure of H-1152P).

### 2.3.3. Culture of RGC-5 cells

Cryovials containing RGC-5 cells (kindly provided by Professor Neeraj Agarwal, UNT Health Science Center, Fort Worth, TX) were removed from liquid nitrogen storage and kept in a 37°C waterbath for 1-2 minutes. The cells were transferred into 75 cm<sup>2</sup> flasks containing prewarmed complete medium, and incubated at 37°C in a humidified atmosphere of 5% CO<sub>2</sub>. The medium was replaced with fresh complete medium on the following day. For experimentation, the trypsinized cells were suspended in serum-free medium, seeded into the inner wells of 24 well-plates at a concentration of 3000 cells/well in duplicates for each treatment group, and incubated in serum-free medium for 1-5 days.

### 2.3.4. Trypsinization of the cells

Cells for subculture or experimentation were washed twice with sterile PBS and incubated with 0.25% trypsin and 0.02% EDTA (0.5 ml for 75 cm<sup>2</sup> flask) for 10-12 minutes at 37°C until all the cells detached from the culture flasks. Trypsinization was then terminated by adding 1-2 ml of complete medium into each flask. The cells were transferred into a 15-ml tube and centrifuged at 800 rpm for 8 minutes. The supernatant was removed and the cells were suspended in fresh medium containing FBS unless otherwise stated.

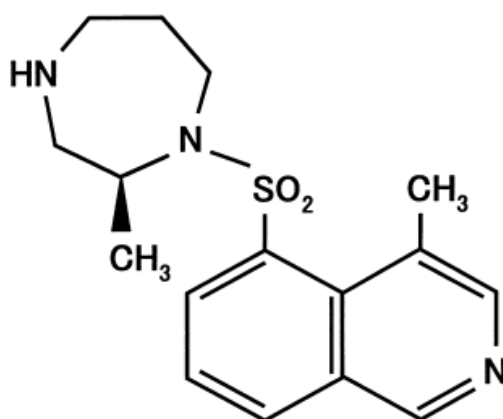


**Figure 7.** The structure of H-1152P.

## **2.4. Tissue culture**

### **2.4.1. Retinal flat mounts**

Male NMRI mice (8-9 weeks old, Harlan-Winkelmann, Borchon, Germany) were sacrificed in a CO<sub>2</sub> chamber. Under a laminar flow hood, the eyes were enucleated and collected into sterile 0.1% glucose-PBS (w/v). The cornea was cut using a scalpel and the lens and the vitreous body were removed. To facilitate the detachment of the retinae, the eye cup was sheared off with fine forceps. Retinae dissociated from the pigment epithelium were mounted onto cellulose nitrate filters pre-soaked in PBS (0.45 µm pore size, cut into approximately 1x1 cm pieces, Sartorius) with the ganglion cell layer facing upwards. The retinal flat mounts were incubated in 1 ml of DMEM/F-12 (lacking phenol red and serum) with or without H-1152P for 24 to 48 hours at 37°C and with 5% CO<sub>2</sub>.

### **2.4.2. Incubation of retinal flat mounts in the conditioned medium of retina or optic nerve**

The eyes of 8-9 week old male NMRI mice were enucleated and the retinae were prepared as flat mounts as described, taking care not to damage the optic nerve. Pieces of optic nerve obtained from different eyes were truncated to the same size (approximately 5.8 mm starting from the closest point to the optic nerve head). Each retinal flat mount and piece of optic nerve was incubated in 1 ml of DMEM/F-12 with or without 1 µM H-1152P for 24 hours at 37°C. The incubation medium was collected at the end of this period and used immediately for the incubation of freshly mounted retinae for 24 hours.

### **2.4.3. Incubation of retinal flat mounts with reduced glutathione (GSH)**

GSH was dissolved in DMEM/F-12 medium without serum at a concentration of 1 mg/ml and filter-sterilized. Flat-mounted retinae were incubated in 1 ml of this



---

medium with or without H-1152P for 24 hours at 37°C in a humidified atmosphere of 5% CO<sub>2</sub>.

#### **2.4.4. Determining the level of total glutathione in retina**

The total level of reduced and oxidized glutathione in retinae was measured using the ApoGSH™ Glutathione Colorimetric Detection Kit following the manufacturer's instructions. The assay determines the amount of the yellow colored 2-nitro-5-thiobenzoic acid generated by the reaction of GSH and 5,5'-Dithiobis(2-nitrobenzoic acid) (DTNB). The oxidized glutathione (GSSG) is also converted to GSH by glutathione reductase and NADPH, allowing the detection of total glutathione levels (Figure 8). Briefly, retinae incubated with or without H-1152P for 24 hours in serum-free medium and freshly prepared retinae (n=4 per each group) were homogenized in 200 µl of glutathione buffer. To remove the proteins from the samples, 50 µl of 5% sulfosalicylic acid was added into each tube and mixed well. The tubes were centrifuged at 8000g for 10 minutes and the supernatant was collected into new tubes. The reaction mix was prepared by adding NADPH generating mix and glutathione reductase into the glutathione reaction buffer in a 1:1:6 ratio (v/v/v) and 160 µl of this mixture was transferred into the wells of a 96-well plate. After incubating the mixture for 10 minutes to generate NADPH, 20 µl of the samples or GSH standard solutions were added and incubated further for 10 minutes. Using a multichannel pipette, 20 µl of the glutathione substrate DTNB was transferred into each well as quickly as possible to avoid the reaction time lag among wells and the samples were incubated for 10 minutes. The absorbance at 405 nm was then read using a spectrophotometric plate reader (SLT Spectra 400 ATX, Salzburg, Austria). A standard curve was prepared by plotting the concentration of each GSH-standard versus its average absorbance reading in Excel. The GSH concentration in the samples was determined from this curve and expressed as the percentage of the value detected in fresh retinae.

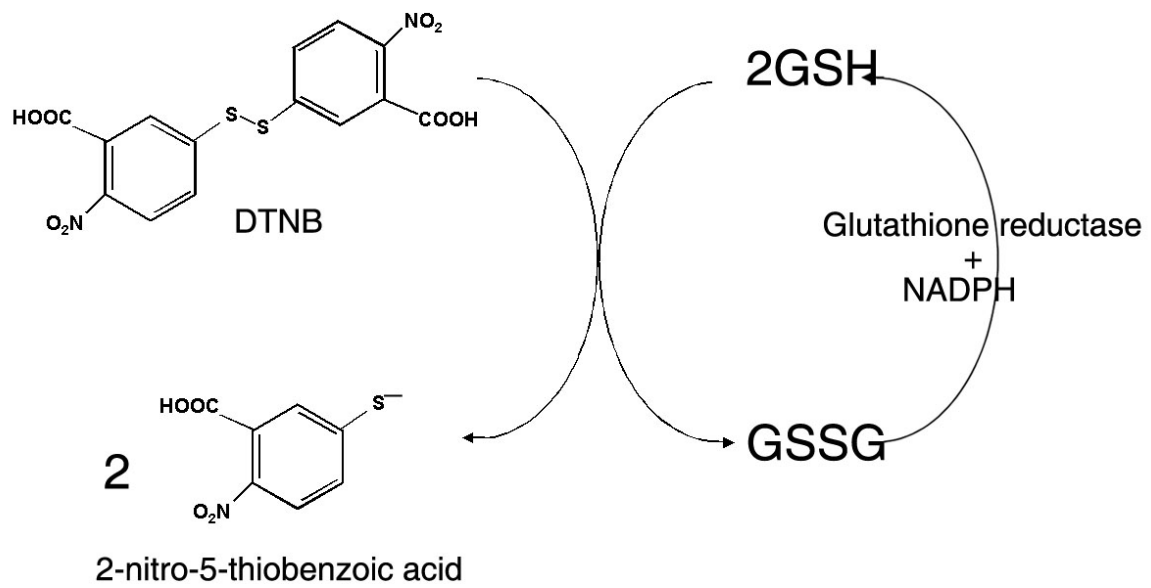


**Figure 8.** Principle of the glutathione assay.

## **2.5. Analyzing the wound healing activities of human Tenon's capsule fibroblasts**

### **2.5.1. MTT test**

MTT test allows the estimation of the amount of living cells by measuring the conversion of the light yellow 3-(4, 5-dimethylthiazolyl)-2, 5 diphenyl tetrazolium bromide to the dark blue formazan by mitochondrial dehydrogenases in viable cells.<sup>154</sup> Fibroblasts were seeded into the inner wells of 96-well culture plates at densities specified in results, with 8 to 10 wells for each treatment group. The cells were allowed to settle for 3 hours, and cultivated for 1 to 4 days in the presence or absence of H-1152P in a total volume of 200  $\mu$ L per well. The stock solution of MTT was added into each well at a volume of 20  $\mu$ l and the cells were incubated further at 37°C for 3 hours. The solution was removed by gently inverting the plates and the wells were filled with 200  $\mu$ L of MTT lysis solution. After shaking the plates vigorously for 20 minutes to facilitate the release of formazan from the lysed cells, the absorbance values in each well were read using a spectrophotometric plate reader at 570 nm with background subtraction at 690 nm.

### **2.5.2. Bromodeoxyuridine (BrdU)-incorporation**

Incorporation of BrdU into DNA was measured using a colorimetric detection kit (BrdU Cell Proliferation Assay, Calbiochem) following the manufacturer's instructions. Briefly, the fibroblasts were seeded into 96-well plates and grown for 4 days as described above. The BrdU label was introduced into the culture medium at the end of day 3 and made available for the cells during the final 24 hours of incubation. Cells incubated without the BrdU label served as background controls. Following incubation, the cells were fixed in the Fixative/Denaturing Solution containing ethanol and sodium hydroxide for 30 minutes and incubated with the monoclonal anti-BrdU antibody for 1 hour at room temperature. After washing the plates with the Wash Buffer (0.1% 2-Chloroacetamide (w/v) in PBS), the cells were incubated with horseradish peroxidase-conjugated goat anti-mouse IgGs for 30 minutes. The wells were thoroughly washed with three changes of wash buffer and flooded with dH<sub>2</sub>O.

After removing the water completely by inverting the plate over a sink and gently tapping on paper towels, the cells were incubated with 100  $\mu$ l of 3,3',5,5'-Tetramethylbenzidine substrate solution for 15 minutes. The reaction was then terminated by adding an equal volume of Stop Solution (2.5 N sulphuric acid) into each well and the absorbance values at 450 nm with background subtraction at 570 nm using a spectrophotometric plate reader. The mean absorbance value for each group was determined after subtracting the mean value of the negative control.

### **2.5.3. Migration of fibroblasts on collagen gels**

Collagen gels with an approximate depth of 1 mm were prepared by mixing cold type I collagen solution (~3 mg/ml, from bovine dermis) with 10x modified Eagle's medium and 0.2 M HEPES-0.2 N NaOH on ice at a ratio of 8:1:1 (v/v/v) and casting 25  $\mu$ l of this solution into each well (6.5 mm diameter) of a sterile 10-well slide placed into a 100-mm diameter Petri dish. To prevent the drying of gels, 1-2 ml of culture medium without serum was pipetted into the dish avoiding contact with the slides and the gels were allowed to polymerize at 37°C for 3-4 hours. Fibroblasts were harvested by trypsinization and suspended in culture medium without serum at a concentration of  $1 \times 10^6$  cells/ml. The polymerized gels were inoculated with 1  $\mu$ l of this cell suspension at the center and the cells were allowed to adhere for 2-3 hours at 37°C. The gels were then covered with culture medium containing 10% FCS and incubated with or without H-1152P. Images of the cells were acquired using a digital camera connected to an inverted microscope (Axiovert, Zeiss, Göttingen, Germany) immediately after the attachment of the cells (T0) and at certain time points throughout a 14-day incubation. The area occupied by cells on each gel was calculated using an image analysis program (Axiovision, Zeiss). At the end of the incubation period, the cells were fixed for 10 minutes in 4% paraformaldehyde (PFA) and processed for immunofluorescence staining.

### **2.5.4. Scratch (wound) assay**

Fibroblasts harvested by trypsinization were seeded in 24-well plates at a concentration of 5000 cells/well and grown until reaching confluence. A wound was

---

gently introduced in the center of the cell monolayers using a sterile 1000  $\mu\text{L}$  pipette tip. To remove the cell debris, the wells were washed twice with PBS and the cells were incubated with or without H-1152P in duplicates for 48 hours. Phase contrast images of marked regions along the wound area were obtained using an inverted microscope (Axiovert, Zeiss) immediately after creating the wound and at the end of 48 hours. The initial wound area and the areas that remained unoccupied by cells after 48 hours were measured using the Axiovision software. After the incubation, the cells were fixed for 10 minutes in PFA and processed for immunostaining.

### **2.5.5. Contraction assay**

Prior to preparing the collagen gels, fibroblasts were harvested by trypsinization, washed once with complete medium, and suspended at a concentration of  $4 \times 10^5$  cells/ml. A cold solution of type I collagen from rat tail (3 mg/ml in 0.2% acetic acid) was mixed with 10x MEM and 0.2 M HEPES-0.2 N NaOH on ice at a ratio of 8:1:1 (v/v/v). An equal volume of cell suspension was added into the neutralized collagen solution to give a final concentration of 1.2 mg/ml collagen and  $2 \times 10^5$  cells/ml. Five hundred  $\mu\text{l}$  of this solution was cast into the inner wells of a 24-well tissue culture plate and allowed to polymerize at  $37^\circ\text{C}$  for approximately 3 hours. The gels were then gently detached from the plastic surface using a sterile pipette tip and incubated with or without H-1152P for 7 days in duplicates. Images of the gels were acquired by scanning the culture plate with a flatbed scanner (Epson GT-9600, Epson, Meerbusch, Germany) immediately after the detachment of gels and at several time points throughout the incubation. The area of the gels was determined using an image analysis software (Analysis, Soft Imaging System, Münster, Germany).

## **2.6. Cytotoxicity assays**

### **2.6.1. Ethidium homodimer-1 (EthD-1) staining**

EthD-1 is a fluorescent nucleic acid dye (Excitation: 495 nm, Emission: 635 nm) which cannot penetrate intact cell membranes. The dye is thus excluded from healthy cells and is commonly used as an indicator of cell damage. Fibroblasts grown on collagen-coated coverslips, RGC-5 cells grown in 24 well-plates, and flat-mounted retinæ were incubated with 4  $\mu$ M EthD-1 in 0.1% glucose-PBS for 30 minutes. After washing with 0.1% glucose-PBS, the cells were fixed with 4% PFA-PBS for 10 minutes, permeabilized with 0.1% Triton X-100-PBS (v/v) for 5 minutes, and counterstained with 0.5  $\mu$ g/ml DAPI in PBS for 5 minutes, with PBS washes of 5 minutes repeated three times following each step. The cells were then mounted with Mowiol and analyzed by fluorescence microscopy (Zeiss) using the Openlab software (Improvision, Tübingen, Germany). Fibroblasts incubated with 70% ethanol for 20 minutes served as positive controls. Staining of the cells in flat mounted retinæ was performed following the same procedure, with fixation for 30 minutes, and permeabilization for 10 minutes. Quantification of the stained cells was performed in 8-10 areas of 0.159 mm<sup>2</sup> in flat mounted retinæ and in 5-8 areas of 0.64 mm<sup>2</sup> per well for RGC-5 cells.

### **2.6.2. Lactate dehydrogenase (LDH) assay**

LDH is a ubiquitously expressed cytoplasmic enzyme that is released into the culture medium upon damage to the plasma membrane.<sup>155</sup> The amount of LDH released by isolated retinæ incubated in serum-free medium for up to 24 hours was measured using a colorimetric assay (LDH Cytotoxicity Detection Kit, Roche Applied Science) adapted for retinal culture according to the manufacturer's instructions. Briefly, the wells of a flat bottom 96-well tissue culture plate were filled with 220  $\mu$ l of DMEM/F-12. Isolated retinæ were transferred into the wells (1 retina/well, n=3 retinæ for each group) and washed briefly to remove the LDH that might have been released during the transfer. The medium was then carefully replaced with fresh one and the retinæ were incubated for 1 (n=8 experiments), 3 (n=10 experiments), 5, 12, and 24 hours (n=4 experiments each) at 37°C. To detect the maximum amount of LDH release,

retinae (n=3) were incubated in medium containing 1% TritonX-100 (v/v) whereas medium incubated without retinae served as background controls. The supernatants were then collected into fresh tubes, diluted as described in Table 1, and transferred in triplicates into the wells of a new flat-bottom 96 well plate (100 µl/well). The plate was placed on ice and equal volume of the reaction mixture was transferred into each well. The absorbance of the samples at 492-690 nm was measured using a spectrophotometric plate reader at 2-5 minute intervals over a 30 minute period, protecting the plate from light between the measurements. After subtracting the background, the absorbance values of the samples were corrected for the dilution factor and expressed as the percentage of maximum release to estimate the extent of cell damage.

**Table 1.** Dilution factors of the retinal supernatants for LDH assay

Treatment	Time (hours)	Dilution factor
DMEM/F-12	1	Undiluted, 1:2
	3	Undiluted, 1:2, 1:5
	5	Undiluted, 1:2, 1:5
	12	1:2, 1:5
	24	1:2, 1:5, 1:10
1% Triton X-100 in DMEM/F-12	1-24	1:50, 1:100

## **2.7. Staining of cultured cells and retinæ**

### **2.7.1. Alexa488-phalloidin staining**

Fibroblasts grown in uncoated 96-well plates were fixed for 10 minutes with 4% PFA, washed with PBS, permeabilized with 0.1% Triton X-100 - PBS (PBST) for 5 minutes, and preincubated with 1% bovine serum albumin (BSA)-PBS (w/v) for 20 minutes to prevent unspecific binding. The methanolic stock solution of Alexa488-phalloidin (200 units/ml) was diluted 1:40 in 1% BSA-PBS and transferred into the wells. After a 30 minute incubation, the cells were washed three times with PBS, counterstained with DAPI as described above, mounted with Mowiol, and analyzed by fluorescence microscopy.

### **2.7.2. DAPI staining of fibroblasts embedded in collagen gels**

To stain the nuclei in whole gels after fixation, the gels were permeabilized in PBST for 15 minutes, incubated with 0.5 µg/ml DAPI in PBS for 5 minutes, washed in PBS, mounted in Mowiol, and analyzed by fluorescence microscopy.

### **2.7.3. Immunofluorescence staining of fibroblasts and RGC-5 cells**

After a 10-minute fixation in 4% PFA, the cells were washed extensively with PBS, blocked with 3% BSA in PBST for 20 minutes, and incubated with the primary antibodies diluted in the blocking buffer overnight at 4°C in a humidified chamber. Cells incubated with the blocking buffer alone served as negative controls. After 3 PBS-washes of 5 minutes each, the cells were incubated for 1 hour with the secondary antibodies diluted in blocking buffer and washed with PBS. Cells treated with biotin-labeled secondary antibodies were incubated with Cy3-conjugated Streptavidin (Jackson ImmunoResearch, 1:500 dilution in blocking buffer) for 40 minutes. The nuclei were counterstained with DAPI and the samples mounted with Mowiol were analyzed by fluorescence microscopy. The primary and the secondary antibodies as well as the dilution factors used are listed in Table 2. The



immunostaining against fibronectin was performed following the same protocol, omitting Triton X-100 from the blocking buffer.

#### **2.7.4. Preparing cryosections of collagen gels and flat mounted retinae**

Collagen gels populated with fibroblasts and flat mounted retinae were washed with PBS, fixed in 4% PFA for 30 minutes to 2 hours, incubated in 4% sucrose-PBS (w/v) overnight at 4°C, kept in 20% sucrose (w/v) -5% glycerol (v/v) for 2 days at 4°C, and embedded in OCT compound. Transverse sections of the collagen gels and retinae were cut at 16 µm using a cryostat (Leica, Bensheim, Germany) and collected onto Superfrost slides. The sections were fixed in ice-cold acetone for 10 minutes, air-dried, and stored at -20°C.

#### **2.7.5. Immunohistochemistry (IHC) on the sections of retinae and collagen gels**

After removing from -20°C, the slides were air-dried at room temperature for 30 minutes and washed three times with PBS. The sections were blocked in 3% BSA-PBS with 0.3% Triton X-100 (BSA-PBST) for 30 minutes at room temperature (RT) and incubated with primary antibodies diluted in BSA-PBST overnight at 4°C in a humidified chamber. The sections incubated with the blocking buffer alone served as negative controls. After three PBS-washes of 5 minutes each, the sections were incubated with the Cy3-conjugated secondary antibody diluted in BSA-PBST for 1 hour at room temperature, washed with PBS, counterstained with DAPI, mounted in Mowiol, and analyzed by fluorescence microscopy.

#### **2.7.6. IHC on flat-mounted retina**

After incubation, flat mounted retinae were fixed in 4% PFA-PBS, and IHC was performed according to the protocol of Wang et al.<sup>62</sup> with slight modifications. Briefly, the retinae were washed for 1 hour in PBS containing 0.2% Triton X-100. This was

followed by incubation in blocking serum (3% BSA in PBS) for 16 hours at 4°C, and with a polyclonal antibody against glial fibrillary acidic protein (GFAP) diluted in 3% BSA-PBS for 48 hours at 4°C. Retinae incubated with 3% BSA-PBS alone served as negative controls. The mounts were then washed in PBS three times for 1 hour each, and incubated with Cy3-conjugated secondary goat anti-rabbit immunoglobulins overnight at 4°C, washed in PBS, counterstained with DAPI, mounted in Mowiol, and analyzed by fluorescence microscopy. The quantification of astrocyte reactivity and the intensity of staining was performed in 4 to 5 areas of 0.64 mm<sup>2</sup> on the flat mounted retinae using the Analysis software.

**Table 2.** Primary and secondary (2°) antibodies used for immunofluorescence labelling of cultured cells and retinae

Primary Antibodies					
Antigen	Source	Type	Dilution	2° Antibody	Supplier (Catalog #)
Adducin	Rabbit	P	1:100	4	A (ab18314)
Alpha-smooth muscle actin (Clone 1A4)	Mouse	M	1:75	1	B (M0851)
CD11b	Rat	P	1:100	5	C (MCA74GA)
Cleaved-caspase 3	Rabbit	M	1:100	4	D (9664)
Fibronectin	Rabbit	P	1:400	4	B (A0245)
GFAP	Rabbit	P	1:400	4	B (Z334)
Ki-67 (clone Ki-S5)	Mouse	M	1:100	2 / 3	B (M7240)
Phospho(S726)-adducin	Rabbit	P	1:100	4	A (ab14375)
Phospho(T445)-adducin	Rabbit	P	1:100	4	E (sc-16738)

Secondary Antibodies					
Number	Anti-	Conjugation	Source	Dilution	Supplier (Catalog #)
1	Mouse IgG	Alexa488	Goat	1:400	F (A11001)
2	Mouse IgG	Biotin	Rabbit	1:100	B (E0354)
3	Mouse IgG (H+L)	Cy3	Goat	1:400	G (115-165-146)
4	Rabbit IgG (H+L)	Cy3	Goat	1:400	G (111-165-003)
5	Rat IgG (H+L)	Biotin	Rabbit	1:200	B (E0468)

**A:** Abcam (Cambridge, UK); **B:** DAKO (Glostrup, Denmark); **C:** Serotec (Oxford, UK); **D:** Cell Signaling Technology (MA); **E:** Santa Cruz Biotechnology (Santa Cruz, CA); **F:** Molecular Probes (Eugene, OR); **G:** Dianova (Hamburg, Germany); **M:** Monoclonal; **P:** Polyclonal.

## **2.8. Protein purification**

### **2.8.1. Protein extraction from cells**

Fibroblasts grown in 75 cm<sup>2</sup> flasks for 4 days were washed twice with ice-cold PBS. 500 µl of ice-cold cell lysis buffer was added into each flask and the flasks were kept on ice for 5 minutes. The cells were transferred into a microfuge tube and maintained under gentle agitation at 4°C for 15 minutes. Cell lysates were cleared by centrifugation at 12000 rcf for 20 minutes in a precooled microcentrifuge at 4°C (Heraeus, Kendro Laboratory Products, Hanau, Germany). The supernatants were collected and stored at -80°C.

### **2.8.2. Protein extraction from retinae**

After incubation, free floating retinae (n=8 for each treatment group) were collected into 1.5 ml Eppendorf tubes, homogenized in liquid nitrogen, and lysed in 300 µl of ice-cold tissue lysis buffer. The lysates were cleared by centrifugation at 12000 rcf for 20 minutes at 4°C (Heraeus). The supernatants were collected and stored at -80°C.

### **2.8.3. Determining the protein concentration by Bradford assay**

Bradford assay allows the detection of protein concentration by quantitating the binding of Coomassie brilliant blue to the unknown proteins and comparing this binding to that of different amounts of a standard protein, such as BSA. Duplicate aliquots of the BSA standards (25-500 µg/ml) and the samples were prepared by diluting the 0.5 mg/ml BSA stock solution and the samples with 0.15 M NaCl at a total volume of 100 µl. Blank tubes were filled with only 100 µl of 0.15 M NaCl. After adding 1 ml of Coomassie brilliant blue solution into each tube, the tubes were vortexed, left at room temperature for 2 minutes, and the absorbance values at 595 nm were measured using 1 cm-pathlength plastic microcuvettes (1 ml). A standard curve was prepared by plotting the concentration of each BSA-standard versus its

average absorbance reading in Excel. The protein concentration in the samples was determined from this curve and corrected for the dilution factor.

#### **2.8.4. Determining the protein concentration by bichinonic acid (BCA) assay**

The BCA assay allows the estimation of the protein concentration based on the reduction of  $\text{Cu}^{+2}$  to  $\text{Cu}^{+1}$  by proteins in an alkaline environment and the spectrophotometric detection of the purple-colored reaction product formed by the chelation of two BCA molecules with one  $\text{Cu}^{+1}$  ion. Determining the protein concentration via the BCA method was performed using the Micro BCA™ Protein Assay Kit (Pierce) according to the manufacturer's instructions. This assay adapted for use in microplates allows the quantitation of protein concentration in a linear working range of 2-40  $\mu\text{g/ml}$  and is compatible with a wide range of substances including Tris (upto 50 mM) as well as detergents like SDS, NP-40, and Triton X-100 at concentrations as high as 5%. Briefly, 150  $\mu\text{l}$  of BSA standards ranging from 0.5 to 200  $\mu\text{g/ml}$ , blanks, and unknown samples diluted in  $\text{dH}_2\text{O}$  were pipetted into the wells of a 96-well microplate in duplicates. The working reagent containing BCA, cupric sulfate pentahydrate, sodium carbonate, sodium bicarbonate, sodium tartrate, and sodium hydroxide was prepared as instructed and transferred into each well at 150  $\mu\text{l}$ . The plate was shaken thoroughly for 30 seconds and incubated at 37°C for 2 hours. After allowing the plate to cool to room temperature, the absorbance values at 570 nm were read using a spectrophotometric plate reader. The values were corrected for the blanks and the protein concentration of the unknown samples were determined from the standard curve as described for the Bradford assay.

## **2.9. SDS-Polyacrylamide gel electrophoresis (PAGE) and Western blot**

### **2.9.1. SDS-PAGE**

One dimensional sodium dodecyl sulphate (SDS)-PAGE is a commonly used protocol to separate proteins based primarily on their molecular weight. The binding of SDS to the denatured protein introduces an overall negative charge and the length of the SDS-protein complex becomes proportional to its molecular weight. SDS-PAGE was performed using the Mini-Protean Electrophoresis Cell from Bio-Rad. The 12% resolving gel was prepared by mixing the solutions listed in Table 3, cast between vertically aligned glass plates separated by 0.75 mm spacers, overlaid with 2-propanol, and allowed to polymerize for approximately 1 hour. After decanting the 2-propanol, the 5% stacking gel solution was cast, a 10-well comb was inserted, and the gel was allowed to polymerize for 30-45 minutes. The comb was then removed and the gel assembly was inserted into an electrode cell placed in a buffer tank filled with 1X Electrophoresis buffer.

The protein samples were thawed on ice, aliquotted at the volumes desired, and mixed with an equal volume of 2X Laemmli sample buffer. The samples were then kept at 95°C for 5 minutes, centrifuged briefly, and loaded into the wells, with 20 µg of protein per lane. The Kaleidoscope Prestained Protein Standard or the Low molecular Weight Biotinylated Protein Standard from Bio-Rad was loaded into separate wells as molecular weight markers. The gel was connected to a power supply and run at a constant voltage of 100 V until the bromophenol blue in the loading buffer reached the bottom of the gel.

### **2.9.2. Non-denaturing gel electrophoresis**

Electrophoresis under non-denaturing conditions allows the separation of proteins in their native state based on their size and charge. Non-denaturing gel electrophoresis was performed following the procedure for SDS-PAGE, omitting SDS and  $\beta$ -

mercaptoethanol from the gel solutions and loading the samples into the gels without heating.

**Table 3.** Solutions used for casting 5-12% polyacrylamide gels

<b>Solution</b>	<b>12 % resolving gel (volume)</b>	<b>5 % stacking gel (volume)</b>
<b>30% acrylamide, 0.8% bisacrylamide (w/v)</b>	4.2 ml	900 $\mu$ l
<b>1 M Tris-HCl, pH 8.8</b>	3.75 ml	-
<b>1 M Tris-HCl, pH 6.8</b>	-	650 $\mu$ l
<b>10% SDS (w/v)</b>	100 $\mu$ l	30 $\mu$ l
<b>Milli-Q water</b>	2 ml	3.5 ml
<b>10% ammonium persulfate (w/v)</b>	100 $\mu$ l	30 $\mu$ l
<b>TEMED</b>	5 $\mu$ l	5 $\mu$ l

### 2.9.3. Silver staining of gels

Silver staining is a highly sensitive method for detecting proteins as low as 0.1 ng/mm<sup>2</sup> in polyacrylamide gels. This method was performed using the Bio-Rad Silver Stain Kit according to the manufacturer's instructions. After electrophoresis, the mini-gels were fixed in 40% methanol/10% acetic acid (v/v) for 30 minutes and incubated with the oxidizer (containing potassium dichromate and nitric acid) for 5 minutes. The gels were then washed thoroughly for 15 minutes using large volumes of Milli-Q water and changing the water at least 6 times within the first 5 minutes. This was followed by a 20-minute incubation in the silver nitrate reagent and a quick rinse with Milli-Q water (30 seconds maximum). The developer solution (containing sodium carbonate and paraformaldehyde) was then poured over the gels and replaced with fresh one upon the appearance of a brown or smokey precipitate (usually within the first 30 seconds). The gels were kept in the developer until the desired intensity was obtained, changing the solution every 5 minutes if necessary. The color development was stopped by incubating the gels in 5% acetic acid (v/v) for 15 minutes, with 2-3 changes of this solution. The gels were then dried on filter papers and sealed in

plastic bags. All the incubations were done under gentle rotation in a fume hood and Milli-Q water was used for the preparation or dilution of the solutions.

#### 2.9.4. Transfer of proteins onto nitrocellulose membranes

Following electrophoresis, the transfer of the proteins from the gel to a nitrocellulose membrane was performed using the Mini Trans-Blot Electrophoretic Transfer Cell from Bio-Rad. The nitrocellulose membrane and pieces of Whatman 3MM paper cut approximately to the size of the gel, fiber pads, and the gel removed from the glass plates were soaked in 1 X Blotting buffer. The membrane sandwich was assembled in a nonconducting cassette as illustrated in Figure 9, gently removing air-bubbles by rolling a Pasteur pipette over each layer. The cassette was inserted into the electrode cell placed into the buffer tank with the gel facing the cathode (black side of the cell) and the membrane facing the anode (red side of the cell). The buffer tank was filled with the blotting buffer and connected to a power supply. Transfer of the proteins was performed at a constant voltage of 100 V for 1 hour or at 10 V overnight. The membrane was then removed from the cassette and processed for PonceauS staining.



**Figure 9.** Schematic representation of the membrane-gel sandwich assembly for the electrophoretic transfer of proteins from the gel to the nitrocellulose membrane.



### **2.9.5. PonceauS staining**

Staining with PonceauS was carried out to verify transfer onto the nitrocellulose membranes and equal protein loading. The membranes were incubated with freshly prepared PonceauS solution for 5 minutes under gentle rotation. The solution was decanted and excess dye was removed by washing with dH<sub>2</sub>O for 2 minutes. The membranes were then scanned using a flatbed scanner (Epson) and destained completely with several changes of dH<sub>2</sub>O.

### **2.9.6. Western blot**

The nitrocellulose membranes were washed briefly in Tris-buffered saline (TBS), blocked in 5% nonfat milk in TBS containing 0.1% Tween-20 (TBST) for 30 minutes, washed with two changes of TBST and TBS for 10 minutes each, and incubated with the primary antibodies diluted in blocking buffer overnight at 4°C. Membranes covered with the blocking buffer only served as negative controls. After repeating the washes with TBST and TBS, the membranes were incubated with the secondary antibodies diluted in the blocking buffer for 1 hour at room temperature. Membranes treated with biotin-conjugated secondary antibodies were incubated further with HRP-conjugated Streptavidin (DAKO, diluted 1:1000 in blocking buffer) for 1 hour at room temperature. The membranes were then washed as described above and signal detection was performed using suitable substrates for the enzymes coupled to the secondary antibodies. All the incubations were performed under gentle rotation. The primary and secondary antibodies as well as the dilution factors used are listed in Table 4.

### **2.9.7. Signal detection by NBT/BCIP**

Color development by nitroblue tetrazolium chloride (NBT) and 5-bromo-4-chloro-3-indolyl phosphate (BCIP) was performed on membranes incubated with alkaline phosphatase-conjugated secondary antibodies. The developing solution was prepared shortly before use by adding 55 µl of NBT stock solution (100 mg/ml) and 37.5 µl BCIP stock solution (50 mg/ml) into 10 ml of alkaline phosphatase buffer. The membranes were incubated in this solution without shaking until the desired band

intensity was reached. The reaction was terminated by 20 mM Tris (pH 8.0), 5 mM EDTA. The membranes were then rinsed in dH<sub>2</sub>O, air-dried, and stored in plastic folders.

### **2.9.8. Signal detection by 4-chloro-1-naphthol**

Color development by 4-chloro-1-naphthol was performed on membranes incubated with horseradish peroxidase-conjugated secondary antibodies. The developing solution was prepared shortly before use by pipetting 100 µl of 4-chloro-1-naphthol stock solution into 10 ml of 50 mM Tris-HCl, pH 7.6, filtering the solution, and adding 10 µl of 30% H<sub>2</sub>O<sub>2</sub>. The membranes were incubated in this solution without shaking for approximately 30 minutes or until the desired band intensity was reached, rinsed in dH<sub>2</sub>O, air-dried, and stored in plastic folders.

### **2.9.9. Signal detection by enhanced chemiluminescence (ECL)**

Signal detection was performed by ECL on membranes incubated with horseradish peroxidase-conjugated streptavidin. The ECL solution was prepared by mixing 10 ml of Solution A with 3 µl of 30% H<sub>2</sub>O<sub>2</sub> and 1 ml of Solution B shortly before use. The membranes were placed on a piece of plastic sheet, incubated with the ECL solution for 2 minutes, and covered with another piece of plastic sheet or Saran wrap. After removing excess solution and air bubbles, the membrane-plastic sheet sandwich was put into a film cassette. A piece of Kodak X-Omat AR film was placed on the membranes in a dark room and the cassette was sealed. The exposure time varied between 30 seconds to 1 minute for the membranes incubated with anti-GFAP and adducin antibodies and overnight for the membranes incubated with phospho-adducin antibodies. The film was then removed from the cassette, incubated with the developer solution for 5 minutes, washed briefly under running tap water, fixed for 5 minutes in the fixer solution, kept in a water bath for 5 minutes, and air-dried. The intensity of the bands was detected using the Quantity One software (version 4.6.2, Bio-Rad).

**Table 4.** Primary and secondary (2°) antibodies used for Western blot

Primary Antibodies				
Antigen	Source	Dilution Factor	2° Antibody used (dilution factor)	Supplier (catalog #)
Adducin	Rabbit	1:1000	3 (1:2000)	A (ab18314)
EGF (mouse)	Goat	1:500	1 (1:500)	B (AF2028)
GFAP	Rabbit	1:2000	2 (1:2000) / 3 (1:2500)	C (Z334)
IFN-gamma	Rabbit	1:1000	2 (1:1000)	D (500-P32)
IL-6	Rabbit	1:1000	2 (1:1000)	D (500-P26)
IL-8	Rabbit	1:1000	2 (1:1000)	D (500-P28)
IL-10	Rabbit	1:1000	2 (1:1000)	D (500-P20)
Phospho(S726)-adducin	Rabbit	1:500	3 (1:500)	A (ab14375)
Phospho(T445)-adducin	Rabbit	1:200	3 (1:250)	*

Secondary Antibodies				
Number	Anti-	Conjugation	Source	Supplier (Catalog #)
1	Goat IgG (H+L)	HRP	Rabbit	E (305-035-003)
2	Rabbit IgG (H+L)	AP	Goat	E (111-055-003)
3	Rabbit IgG (H+L)	Biotin	Donkey	E (711-065-152)

**A:** Abcam (Cambridge, UK); **B:** R&D Systems, **C:** DAKO (Glostrup, Denmark); **D:** PeproTech, (Rocky Hill, NJ); **E:** Jackson ImmunoResearch Inc., (West Grove, PA); **AP:** Alkaline phosphatase; **HRP:** Horseradish peroxidase; \*: kindly provided by Prof. Kozo Kaibuchi, Nagoya University, Japan.

## **2.10. Cytokine arrays**

### **2.10.1. Membrane-based mouse cytokine array**

The cytokine profile of the retinal conditioned medium was analyzed using the RayBio Mouse Cytokine Antibody Array I (RayBiotech) according to the manufacturer's instructions with slight modifications. This array consists of membranes coupled with antibodies against 22 cytokines in duplicates as well as biotin-conjugated IgGs producing positive signals allowing the comparison of the relative expression levels among different membranes. The membranes were initially kept in the blocking buffer overnight at 4°C and incubated with the freshly collected conditioned media of retinae for 2 hours at room temperature. After washing with two changes of the wash buffers supplied, the membranes were incubated with biotin-labeled anti-cytokine antibodies first at 4°C overnight, then at room temperature for an additional 2 hour-period. This was followed by several washes and a 2 hour-incubation with horseradish peroxidase conjugated streptavidin. Signal detection was performed by ECL as instructed and the spot intensity was measured using the ImageQuant software (Molecular Dynamics, CA).

### **2.10.2. Bio-Plex flow cytometric cytokine assay**

The concentration of various cytokines in our samples of retina and optic nerve incubation media were kindly analyzed by Bio-Rad Laboratories, Munich, Germany using the Bio-Plex suspension array. The Bio-Plex mouse cytokine assay kit consists of an array of 18 sets of beads, each being internally dyed with different ratios of two spectrally distinct fluorophores and conjugated with an antibody against a cytokine. The bead suspension was incubated with the samples in microplates, then with a biotinylated detection antibody, and finally with the reporter molecule streptavidin-phycoerythrin. The microplates were analyzed in the Bio-Plex array reader. Each bead was excited by two laser beams, one for the excitation of the dye in the bead to identify its spectral address, and one for the excitation of the reporter molecule for the quantification of the captured cytokine. The fluorescent signals of the beads were recorded and translated by the Bio-Plex Manager software.

## **2.11. Protein database search and sequence analysis**

The amino acid sequences of mouse EGF, IFN-gamma, IL-6, IL-10, and their receptors were retrieved from the GenBank protein database (<http://www.ncbi.nlm.nih.gov/entrez/query.fcgi?db=Protein>). The accession numbers of these sequences are listed in Table 5. Searching the *Mus musculus* protein database using the amino acid sequences of the cytokines as query was performed using the BLASTP algorithm.<sup>156</sup> The optimal global alignment of the amino acid sequences of IFN-gamma and IL-6 with their respective receptors was performed using the ALIGN algorithm (version 2.0).<sup>157</sup> Both algorithms were accessed from Biology Workbench 3.2 (<http://workbench.sdsc.edu/>).

**Table 5.** GenBank accession numbers of the amino acid sequences of EGF and the cytokines analyzed

<b>Protein (<i>Mus musculus</i>)</b>	<b>Accession number</b>
EGF	NP_034243
EGF receptor isoform 1	NP_997538
IFN-gamma	NP_032363
IFN-gamma receptor 1	NP_034641
IL-6	NP_112445
IL-6 receptor, alpha	NP_034689
IL-10	NP_034678
IL-10 receptor, alpha	NP_032374

## **2.12. In vivo effects of H-1152P after optic nerve crush (ONC)**

The experiments on animals were carried out in accordance with the ARVO Statement for the Use of Animals in Ophthalmic and Vision Research. Female Brown Norway Rats (Charles River, Sulzfeld, Germany) were anesthetized by intraperitoneal administration of chloral hydrate. Two microliters of H-1152P (1, 10, and 100  $\mu$ M) or PBS was injected intraocularly using a heat-pulled glass capillary connected to a microsyringe, avoiding injury to the lens. The optic nerve of the left eye was then exposed and partially crushed approximately 2 mm back from the eye globe for 15 seconds whereas the right eye served as sham-control. Five days after the crush, the fluorescent tracer Fluorogold was injected into the Superior colliculus. The rats were sacrificed two days after the tracing surgery and the retinae were either prepared as flat mounts (n=2 rats per treatment) or processed for the immunohistochemical analysis of GFAP and CD11b expression (n=1 rat per treatment). The operations on animals and the quantification of the live (Fluorogold-positive) RGCs were performed by Dr. Frank Schüttauf (University Eye Hospital, Tübingen) and his group.

## **2.13. Statistical analysis**

The data were analyzed by two tailed Student's t-test and the  $p$  values smaller than 0.05 were accepted as significant.

## 3. RESULTS

### 3.1. Effect of ROCK Inhibition on the wound healing activities of human Tenon's capsule fibroblasts

#### 3.1.1. Optimal concentration of the ROCK inhibitor H-1152P

To analyze the cycling rate of Tenon's capsule fibroblasts as well as the effect of various concentrations of H-1152P on this process, MTT test was performed on cells seeded at densities decreasing serially from 5000 to 625 cells per well and incubated with or without H-1152P for 1, 2, and 4 days. After 24 hours, the addition of H-1152P induced a slight but non-significant decrease in the extinction values (Figure 10a). This pattern appeared essentially unchanged until the end of day 2 (Figure 10b). On day 4, the extinction values in untreated cells increased approximately two-fold and the administration of H-1152P at 1, 10, and 50  $\mu$ M resulted in significant decreases by 16%, 34%, and 51%, respectively ( $p < 0.0005$ ). This H-1152P dependent decrease became more pronounced at lower seeding densities, amounting to 27% ( $p < 0.03$ ), 60% ( $p < 0.0005$ ), and 67% ( $p < 0.005$ ) reduction with 1, 10, and 50  $\mu$ M H-1152P, respectively, in fibroblasts plated at a density of 625 cells/well. Since the decrease observed after incubation with 50  $\mu$ M H-1152P did not significantly surpass the effect obtained with 10  $\mu$ M, we deduced the latter concentration of this inhibitor as being optimal for causing a considerable reduction in the amount of viable fibroblasts (Figure 10c).

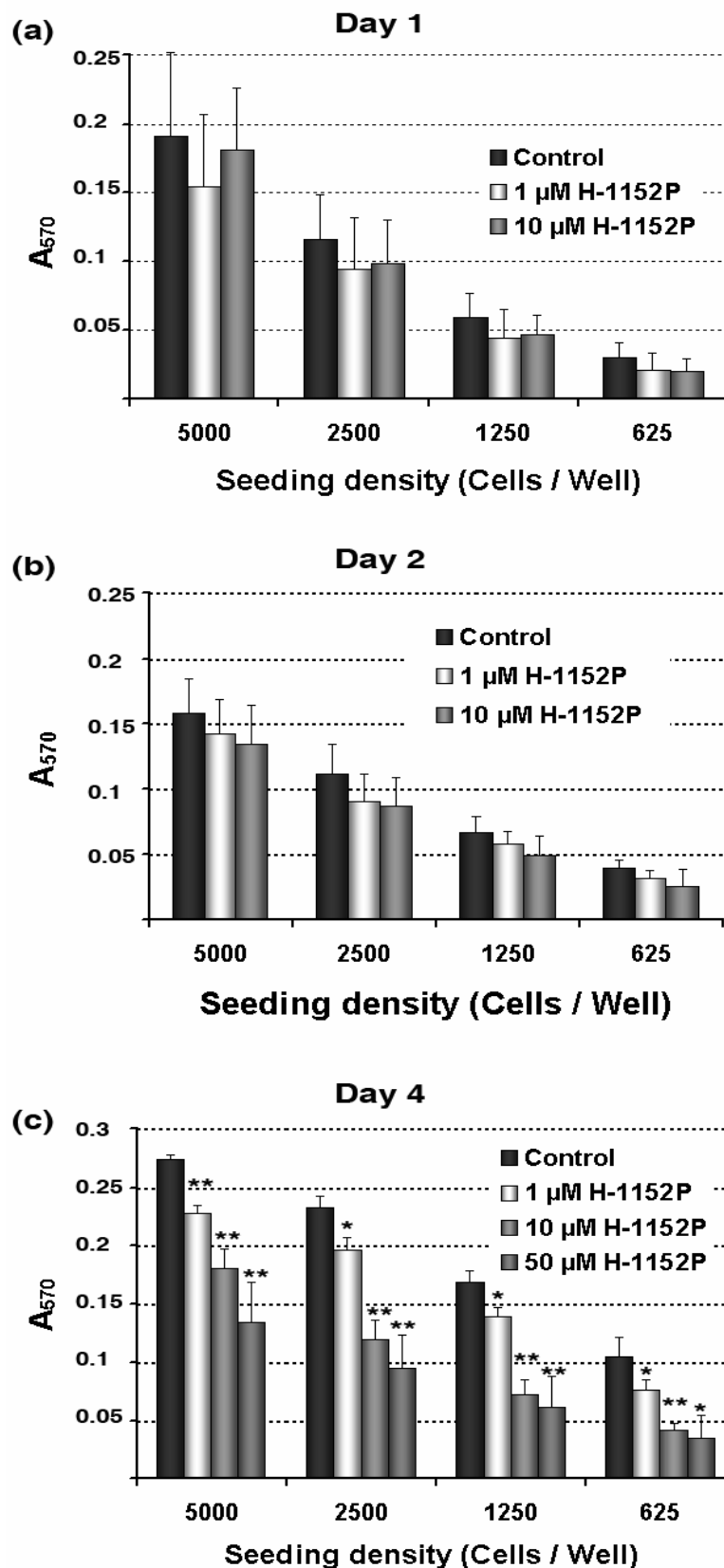


**Figure 10.** Dose dependent effect of H-1152P on the amount of viable fibroblasts. Cells seeded at densities varying between 5000 to 625 cells/well were incubated with or without H-1152P for **(a)** 1 day (n=5 experiments), **(b)** 2 days (n=3 experiments), and **(c)** 4 days (n=4 experiments) after which they were subjected to MTT test. \* $p < 0.03$ , \*\* $p < 0.001$ .



### 3.1.2. Anti-proliferative effect of H-1152P

To clarify whether the H-1152P dependent reduction in the amount of viable fibroblasts resulted from an impairment of cell proliferation or the toxicity of this inhibitor, fibroblasts plated at the densities mentioned above were incubated with or without H-1152P for 4 days and the levels of BrdU incorporated into the DNA of proliferating cells was measured using a colorimetric assay. The absorbance values of untreated cells revealed a gradual increase at lower seeding densities, which were reduced by H-1152P administration in a dose-dependent manner. Addition of 10  $\mu$ M H-1152P was sufficient to keep the extinction values between 0.1 and 0.135 regardless of the initial cell number, accounting for significant decreases in cell proliferation by 80 to 90% compared to controls ( $p < 0.01$ , Figure 11).

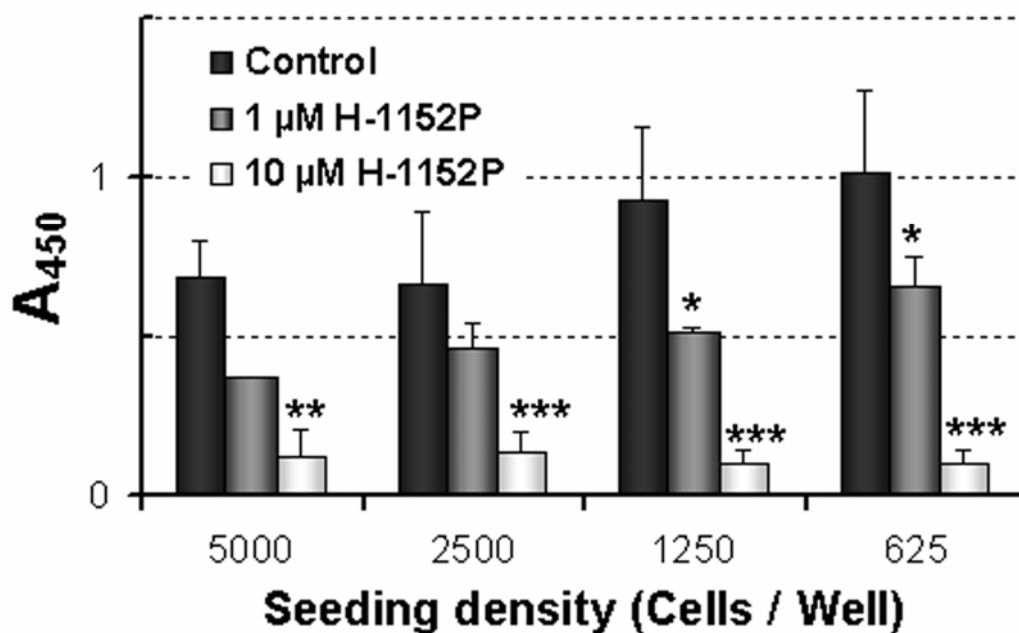


**Figure 11.** BrdU incorporation into fibroblasts during the final 24 hours of a 4 day incubation period. The mean absorbance values were calculated from three independent experiments with the exception of the 5000 cells/well group ( $n=2$ ). \* $p < 0.04$ , \*\* $p < 0.01$ , \*\*\* $p < 0.00005$ .

To further confirm the anti-proliferative effect of H-1152P, an immunostaining was performed with antibodies against Ki-67, a nuclear protein associated with cell proliferation,<sup>158</sup> on fibroblasts that were grown for 4 days on collagen coated coverslips. The results revealed an upregulation of Ki-67 expression in approximately 50% of the nuclei in untreated controls, whereas only about 5% of the cells stained positively for this marker after treatment with 10  $\mu$ M H-1152P ( $p < 0.01$ , Figure 12a and b).

The extent of cell damage at this time point was determined by performing ethidium homodimer-1 staining. Incubating the fibroblasts with 70% ethanol induced significant cellular toxicity, as demonstrated by the strong ethidium homodimer-1 staining in the positive controls. In contrast, very weak staining was observed in both the H-1152P-treated and untreated fibroblasts grown on collagen coated coverslips indicating the viability of these cells. The number of DAPI stained cells were reduced in a dose-dependent manner without an accompanying increase in the intensity of EthD-1 staining in H-1152P treated cells, suggesting that H-1152P inhibits the proliferation of Tenon's capsule fibroblasts without exerting toxic effects (Figure 12c).

### **3.1.3. Short-term application of H-1152P**

The application of a growth inhibitor as a single dose might be desirable for in vivo use. Therefore, the effect of a short-term exposure was investigated by performing MTT test on fibroblasts that were incubated for 1 day with or without H-1152P and for 3 days in fresh medium lacking this inhibitor. The short-term exposure to H-1152P appeared to be sufficient to induce a mild decrease of approximately 20% in the amount of viable fibroblasts. This decrease was statistically significant ( $p < 0.04$ ) in all the groups except for the cells seeded at the lowest density (Figure 13).

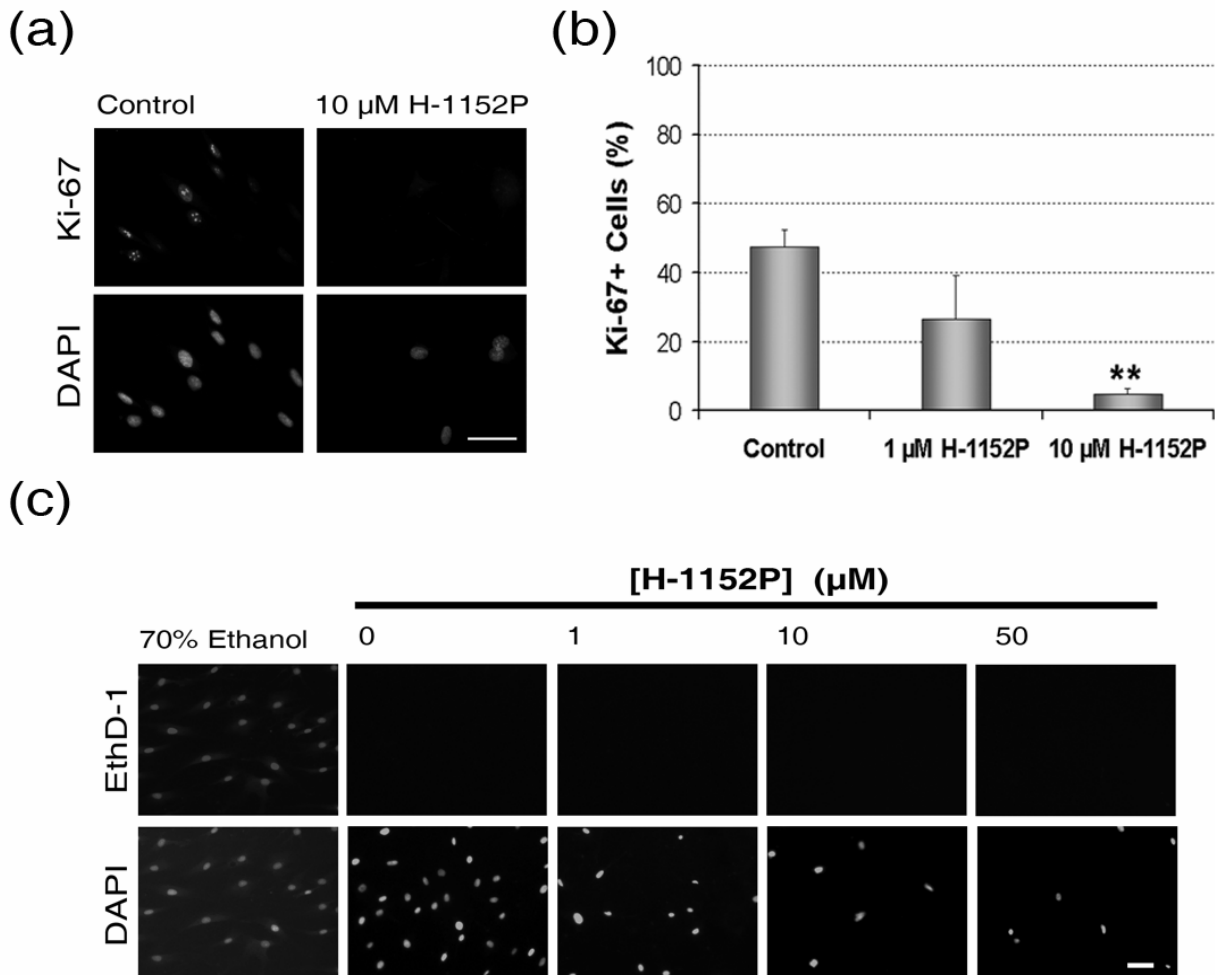


**Figure 12.** The anti-proliferative effect of H-1152P on Tenon's capsule fibroblasts. (a) Fibroblasts grown on collagen-coated coverslips were incubated for 4 days and used for Ki-67 immunostaining to analyze cell proliferation. DAPI counterstaining was performed to visualize the nuclei, (b) Quantification of (Ki-67)+ nuclei (n=2 experiments). \*\* $p$ <0.01, (c) Ethidium homodimer-1 (EthD-1) staining demonstrating the viability of fibroblasts after 4 days in contrast to the cells of the positive control which were treated with 70% Ethanol. The images for Ki-67 and Ethd-1 stainings are representative of two independent experiments. Bar=50  $\mu$ m.

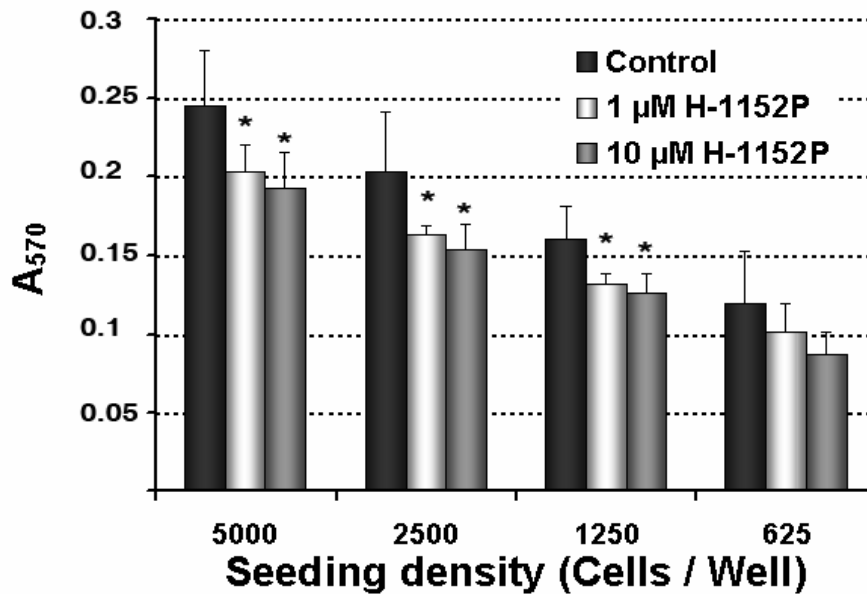


**Figure 13.** Short-term application of H-1152P. Fibroblasts seeded into 96 well-plates were incubated for 24 hours with or without H-1152P. The medium was then replenished and the cells were incubated further for three days in the absence of H-1152P. Cell proliferation/viability was then quantified by performing MTT test at the end of this period. \* $p < 0.04$ .

### 3.1.4. Rearrangement of the actin cytoskeleton in response to H-1152P

The H-1152P induced changes in the organization of the actin cytoskeleton were visualized by performing Alexa-phalloidin staining on fibroblasts grown for 4 days. Untreated fibroblasts exhibited numerous stress fibers aligned as parallel bundles. Administration of H-1152P led to a dose-dependent decrease in the abundance and length of these bundles, resulting in a gradually weakening staining for filamentous actin and a gain in cell diameter. This was accompanied by the sprouting of randomly oriented protrusions, the lengths of which exhibited a dose-dependent increase in H-1152P treated cells (Figure 14a).

A particular event observed in normal tissues under circumstances requiring mechanical force development and in pathological tissues with hypertrophic scarring is the transition of fibroblasts into myofibroblasts, an intermediate cell type between fibroblasts and smooth muscle cells, with stress fibers rich in alpha-SMA.<sup>159</sup> To

analyze the extent of this differentiation in Tenon's capsule fibroblasts after 4 days, immunostaining for alpha-SMA was performed on cells that were grown as described above. Only few alpha-SMA positive cells could be detected both among the untreated fibroblasts and the cells that received H-1152P for 4 days. Yet, the staining in controls was more intense, revealing prominent alpha-SMA bundles (Figure 14b).

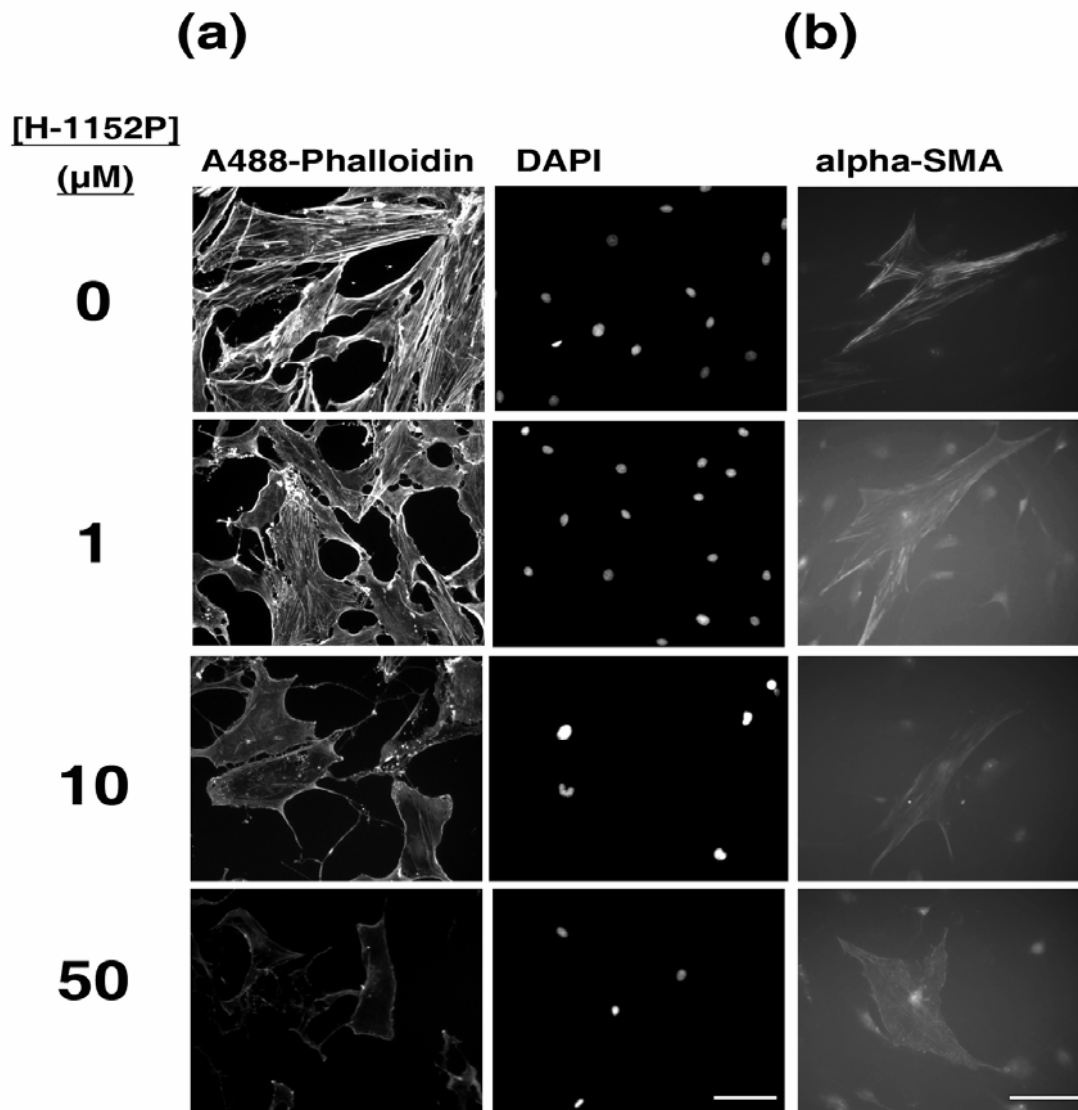


**Figure 14.** Changes in the organization of actin cytoskeleton in response to H-1152P. **(a)** Fibroblasts seeded in 96 well-plates at a density of 1250 cells/well were fixed after 4 days of incubation and stained with Alexa 488-phalloidin and DAPI to visualize the actin filaments and cell nuclei, respectively. The images shown are representative of three independent experiments. Bar=50  $\mu$ m. **(b)** Alpha-SMA immunostaining in fibroblasts after 4 days of incubation to detect the extent of myofibroblast differentiation. The staining appeared very weak in both the treated and untreated groups and localized mainly to the perinuclear region. The images demonstrate the few cells in which alpha-SMA organized as bundles could be detected and are not representative for the entire well. The experiment was performed twice with duplicates for each treatment group. Bar=25  $\mu$ m.

### 3.1.5. Fibroblast migration in response to H-1152P

The effect of H-1152P on the migration of Tenon's capsule fibroblasts was studied by inoculating restrained collagen gels with a small colony of fibroblasts and measuring the area occupied by cells over a 14 day-incubation period with or without H-1152P as well as performing an in vitro wound healing assay. Untreated fibroblasts in the former assay acquired an elongated shape with a protruding edge and spread out radially on the gel, invading an area approximately 8-fold larger than the initial size and reaching confluence at the end of 14 days. In the presence of 1  $\mu\text{M}$  H-1152P fibroblasts did not seem to be impaired in this respect. However, the cells acquired a less polarized morphology and the increase in area covered by the cells was reduced by a factor of 3 at a concentration of 10  $\mu\text{M}$  ( $p < 0.03$ , Figure 15a and b). Migration appeared to be restricted to the surface of the gels at least for the first 14-days after the attachment of fibroblasts to the gel, since no cells could be detected inside the gels in any of the treatment groups within this period. However, a dose-dependent decrease was observed in the amount of fibronectin deposited into the extracellular matrix in response to H-1152P. In untreated controls, strongly stained long fibrils aligned parallel to the longitudinal axis of cells were detected both at the inoculation zone and along the tracks towards the farthestmost points reached by the cells, with the staining intensity being stronger at the center, possibly due to the higher cell density at this location. The micrographs demonstrating the fibronectin immunostaining are therefore presented separately for the center and the periphery to avoid misinterpretation while comparing the staining intensity in treated and untreated groups. The fibroblasts treated with 10  $\mu\text{M}$  H-1152P were loosely arranged and their ECM exhibited almost no fibrils (Figure 15c).

Migration of Tenon's capsule fibroblasts into the wound area created at the center of confluent monolayers of these cells was also suppressed by the ROCK-inhibitor in a dose-dependent manner. Untreated fibroblasts rich in stress fibers were able to migrate into the wound area and organize a dense cellular network, leaving only 10% of the initial wound area unoccupied after 48 hours. Administration of 10  $\mu\text{M}$  H-1152P significantly suppressed the recovery, with 35% of the initial wound region not being populated at the end of 48 hours (Figure 16a and b,  $p < 0.005$ ,  $n = 2$  experiments). The expression of Ki-67 in fibroblasts at the wound center and the

deposition of fibronectin in this area also exhibited a dose-dependent reduction in response to H-1152P (Figure 16c).

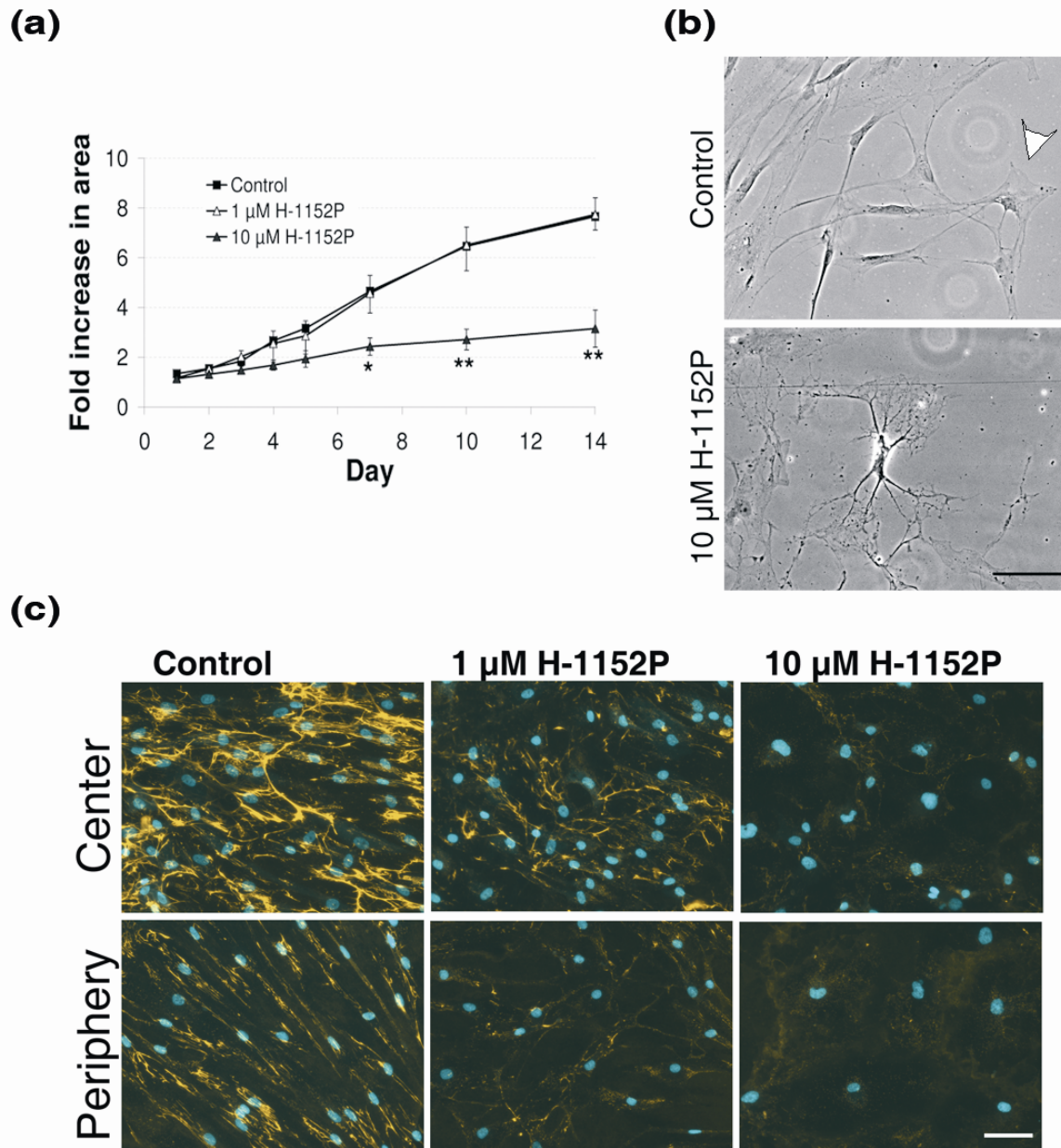


**Figure 15.** Effect of H-1152P on fibroblast migration on restrained collagen gels. **(a)** Collagen gels on multiwell glass slides (n=5 to 8 gels per slide) were inoculated with an equal amount of fibroblasts. After the attachment of cells, the slides were incubated with or without H-1152P and the changes in the area occupied by cells were monitored over 14 days. The mean increase in area was calculated from two independent experiments. \* $p < 0.05$ , \*\* $p < 0.03$ . **(b)** Phase contrast images of the cells on collagen gels. Arrowheads point to the leading edge in untreated cells. **(c)** Representative images of fibronectin immunostaining at the inoculation zone (center) and the periphery of the collagen gels covered with fibroblasts after 14 days. Bar=50 μm.

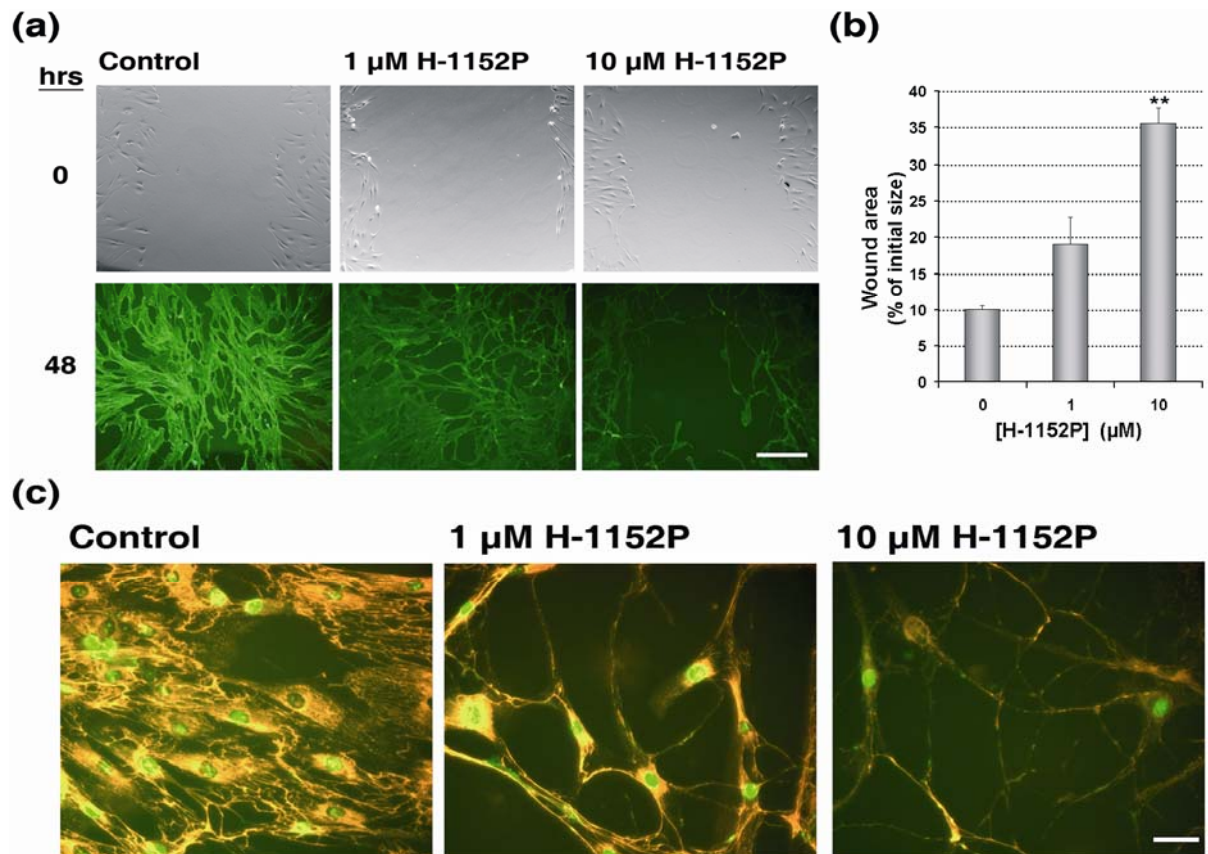


**Figure 16.** In vitro wound healing assay. **(a)** Phase contrast images of the fibroblasts immediately after the induction of the wound into the confluent cell layer (0 hrs) and Alexa 488-phalloidin stainings exhibiting the cellular organization at the wound center after 48 hours. Bar= 100  $\mu\text{m}$ . **(b)** Percentage of wound area after 48 hours. The mean values are calculated from two independent experiments with duplicates for each treatment group. \*\* $p < 0.005$ . **(c)** Double immunostaining for Ki-67 (green) and fibronectin (orange) at the wound area after 48 hours. Bar= 25  $\mu\text{m}$ .



### 3.1.6. Effect of H-1152P on collagen gel contraction

Wound contraction facilitates the healing process by drawing the wound margins closer as well as reducing the amount of new tissue required to re-establish integrity.<sup>160, 161</sup> Floating or restrained collagen gels populated with fibroblasts are commonly utilized in vitro models simulating this process. In this study, the impact of H-1152P on wound contraction was investigated by measuring the area of fibroblast populated floating collagen gels incubated with or without this inhibitor over a 7-day period. The area of the collagen gels was decreased by 25% at the end of 7 days in untreated controls, whereas only a 5% contraction was observed in the presence of 10  $\mu$ M H-1152P ( $p < 0.005$ , Figure 17a). Untreated cells were densely packed under these 3D-culturing conditions and exhibited a dendritic morphology, whereas the cells that received H-1152P treatment were more loosely arranged, with distorted protrusions. In all the treatment groups, cell density gradually declined from the center towards the periphery of the gels (Figure 17b and c). The immunostaining performed on cross-sections of the gels using anti-fibronectin antibodies revealed a similar trend in the assembly pattern of this protein, with stronger staining intensity at the center possibly due to the local differences in the cell density. The fibronectin network appeared nevertheless more prominent in untreated gels compared to the H-1152P-treated groups (Figure 17d).

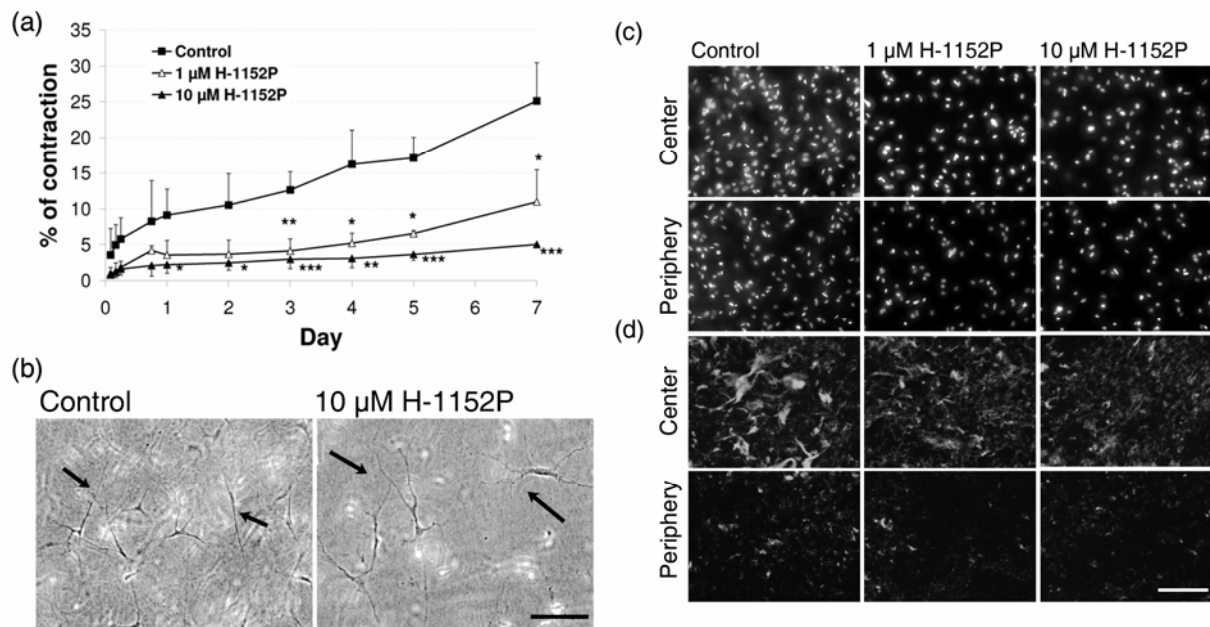


**Figure 17.** Effect of H-1152P on Tenon's capsule fibroblasts in three-dimensional collagen gel culture. **(a)** Fibroblast populated collagen gels were gently detached from the wells in which they were cast and incubated with or without H-1152P (n=2 gels per treatment group). The area of the collagen gels was measured over 7 days with an image analyzer program and the percentage of contraction at each time point was calculated with respect to the initial gel size. Data shown are the mean values of three independent experiments. \* $p < 0.04$ , \*\* $p < 0.01$ , \*\*\* $p < 0.005$ . **(b)** Phase contrast images of the fibroblasts in collagen gels. Arrows indicate the protrusions, which acquire a more distorted morphology in response to H-1152P. **(c)** DAPI staining of the gels viewed from above and **(d)** fibronectin immunostaining on the cross sections of gels showing the organization of cells and the deposition of fibronectin into the ECM, respectively, after 7 days incubation with or without H-1152P. Bar=50 μm.

### 3.1.7. Specificity of H-1152P action

Like most kinase inhibitors, H-1152P suppresses the activity of ROCK mainly by occupying the ATP-binding domain of this enzyme and thus depriving the kinase of its source for the gamma-phosphoryl group required for the phosphorylation of its substrates.<sup>162</sup> However, owing to the sequence homology between the ATP-binding domains of ROCK and PKA, H-1152P can also inactivate PKA at higher concentrations.<sup>163, 164</sup> To clarify whether H-1152P interferes with the PKA pathway in Tenon's capsule fibroblasts at the concentrations tested, Western blots were carried out to analyze the levels of PKA-dependent adducin phosphorylation in these cells. Adducin is a cytoskeletal protein which recruits the actin filaments to the spectrin-based membrane skeleton. The PKA-mediated phosphorylation of alpha- and gamma-adducin occurs predominantly at serine(S)726 and S662 in the MARCKS domain, respectively. PKA can phosphorylate alpha-adducin at S408, S436, and S481 as well.<sup>165</sup> In this study, the PKA-dependent phosphorylation of adducin was detected by performing immunoblots using antibodies recognizing the phosphoS726/S662 residues. The signal intensity of the bands normalized to the protein levels in the corresponding lane did not appear to be considerably altered for phospho(p)-alpha-adducin. Control blots performed using a polyclonal antibody recognizing alpha-adducin displayed a similar trend in the total amount of this protein, suggesting that the PKA-dependent phosphorylation of alpha-adducin is not impaired by H-1152P. In contrast, the levels of phospho-gamma-adducin appeared slightly reduced in response to H-1152P, and it was not possible to detect the changes in the total level of this isoform. However, increasing the concentration of H-1152P did not result in a further decrease in the intensity of p-gamma-adducin bands. H-1152P treatment therefore appeared less likely to have significantly interfered with the PKA-dependent phosphorylation of the gamma-isoform (Figure 18).

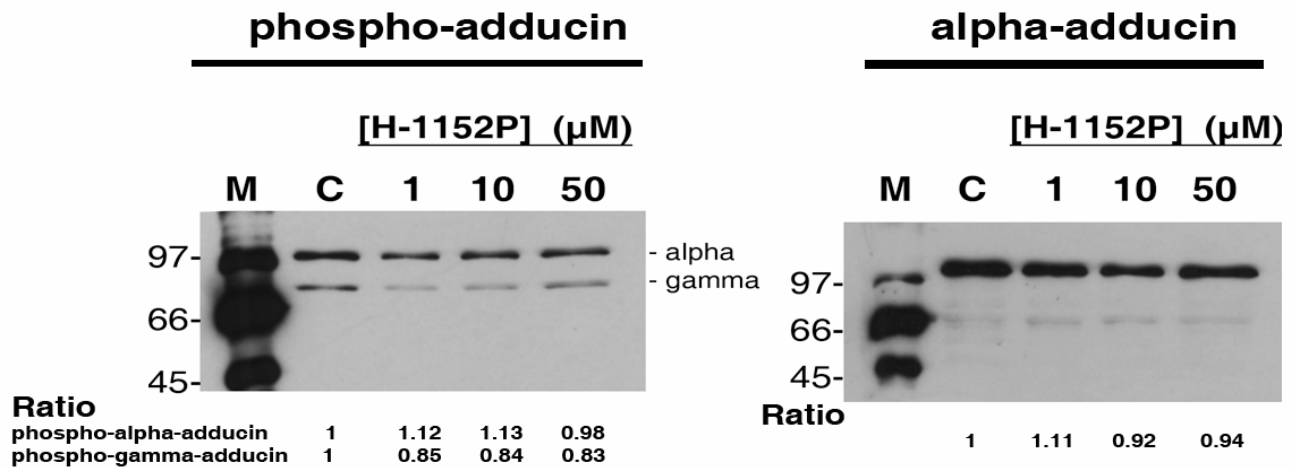


**Figure 18.** H-1152P appears less likely to interfere with the PKA-dependent phosphorylation of adducin. Representative Western blot showing the levels of alpha- and gamma-adducin ( $M_r$  approximately 103 and 85 kDa) phosphorylated at Serine 726 and 662, respectively, in fibroblasts incubated for 4 days with or without H-1152P (phospho-adducin). The total level of alpha-adducin in response to H-1152P treatment is shown on the right. The lower molecular weight bands on this blot might represent degradation products of alpha-adducin or correspond to other proteins weakly recognized by the antibody that became detectable after extended film exposure. The signal intensity of each band was normalized to the levels of the total protein in the corresponding lane (visualized by PonceauS staining). The ratio of the normalized signal intensity in treated fibroblasts to the signal intensity in control fibroblasts (C) is given below the respective lane. M: Molecular weight marker (in kDa).

## **3.2. Effect of ROCK inhibition on retinal cell survival in vitro**

### **3.2.1. Time course of cell damage in retinae under serum deprivation**

Prior to analyzing the effect of the ROCK inhibitor H-1152P on the survival of serum deprived retinal cells, it was necessary to determine the time course of cell damage under these conditions. For this purpose, isolated retinae were incubated in DMEM/F-12 medium without serum and the amount of LDH released from damaged cells was measured at certain time points over a 24-hour period.

The percentage of damaged cells, calculated from the ratio of LDH released from untreated retinae to the maximal amount of LDH released from retinae permeabilized with 1% Triton X-100, amounted to less than 1% after 1 hour. However, this value displayed a gradual and significant increase over time ( $p < 0.005$  at all the time points tested in comparison to 1 hour), reaching 12% by the end of 24 hours (Figure 19). Considering the prominent increase in cell damage within this period, we decided to concentrate on the outcomes of H-1152P treatment on the survival of retinal cells after 24 hours of serum deprivation, with particular emphasis on the fate of the cells in the ganglion cell layer.

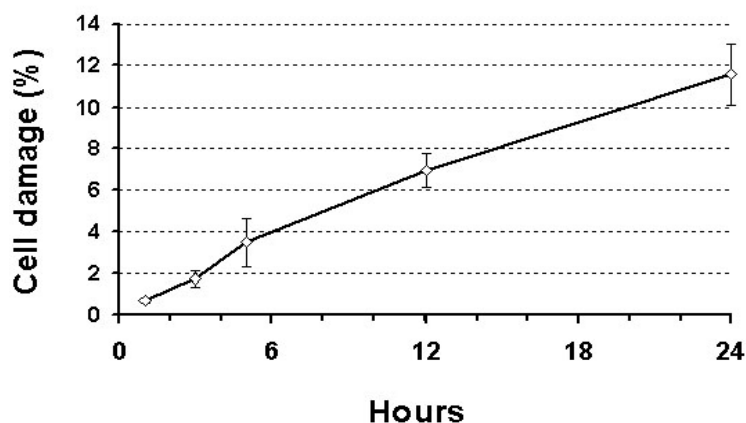


**Figure 19.** Time course of cell damage in retinae under serum deprivation determined by LDH release. The amount of LDH released was expressed as the percentage of maximum release to estimate the extent of cell damage. The mean values were calculated from 4 to 10 independent experiments (see Materials and Methods section 2.4.2).

### 3.2.2. Neuroprotective effect of H-1152P on the ganglion cell layer

Measurement of LDH release allowed for efficiently screening the time course of cell damage in retinae under serum deprivation. However, it was not possible to distinguish the response of a certain group of cells in this model. Moreover, the likely influence of RhoA on the expression of LDH in neural cells, as suggested by the alterations in the isoforms of this enzyme in rat cerebral neurons treated with the RhoA inhibitor botulinum C3 transferase,<sup>166</sup> rendered this model inappropriate for analyzing the effects of ROCK inhibition. The impact of H-1152P treatment on the extent of cell damage in the ganglion cell layer was therefore analyzed in isolated retinae prepared as flat mounts on cellulose nitrate filters with the ganglion cell layer exposed. The damaged cells in these retinae incubated with or without H-1152P for 24 hours were detected by EthD-1 staining and the ratio of the EthD-1 stained cells to the amount of total (DAPI-stained) cells was in turn calculated to determine the extent of cell damage.

After 24 hours of incubation without serum, cells strongly stained with EthD-1 constituted 57% of the total cell population in the GCL of untreated retinae (n=11). Treatment with H-1152P at concentrations ranging from 1 to 100 nM failed to induce a considerable difference in this high level of damage (n=2 retinae for 1 and 10 nM, n=4 retinae for 100 nM). However, the ratio of EthD-1 positive cells was significantly reduced to 34% in retinae incubated with 1  $\mu$ M of H-1152P (n=8,  $p<0.00005$ ). A mild decrease to 44% in cell damage was also observed in retinae that received 20  $\mu$ M of this inhibitor (n=6,  $p<0.05$ ). Yet, increasing the concentration to 100  $\mu$ M (n=3) did not generate a neuroprotective effect (Figure 20a and b).

To determine the outcomes of H-1152P treatment over a longer incubation period, flat mounted retinae were incubated with or without 1  $\mu$ M H-1152P for 48 hours and cell damage in the ganglion cell layer was analyzed as above. Serum deprivation for 48 hours severely impaired the cell survival in the GCL of untreated retinae as demonstrated by the increase in the number of EthD-1 positive cells. This, together with the decrease in cell density as seen in the DAPI-staining, accounted for

the rise in cell damage to over 70% (n=2). However, treatment with 1  $\mu$ M H-1152P (n=2) significantly reduced this ratio to 40% (Figure 21).

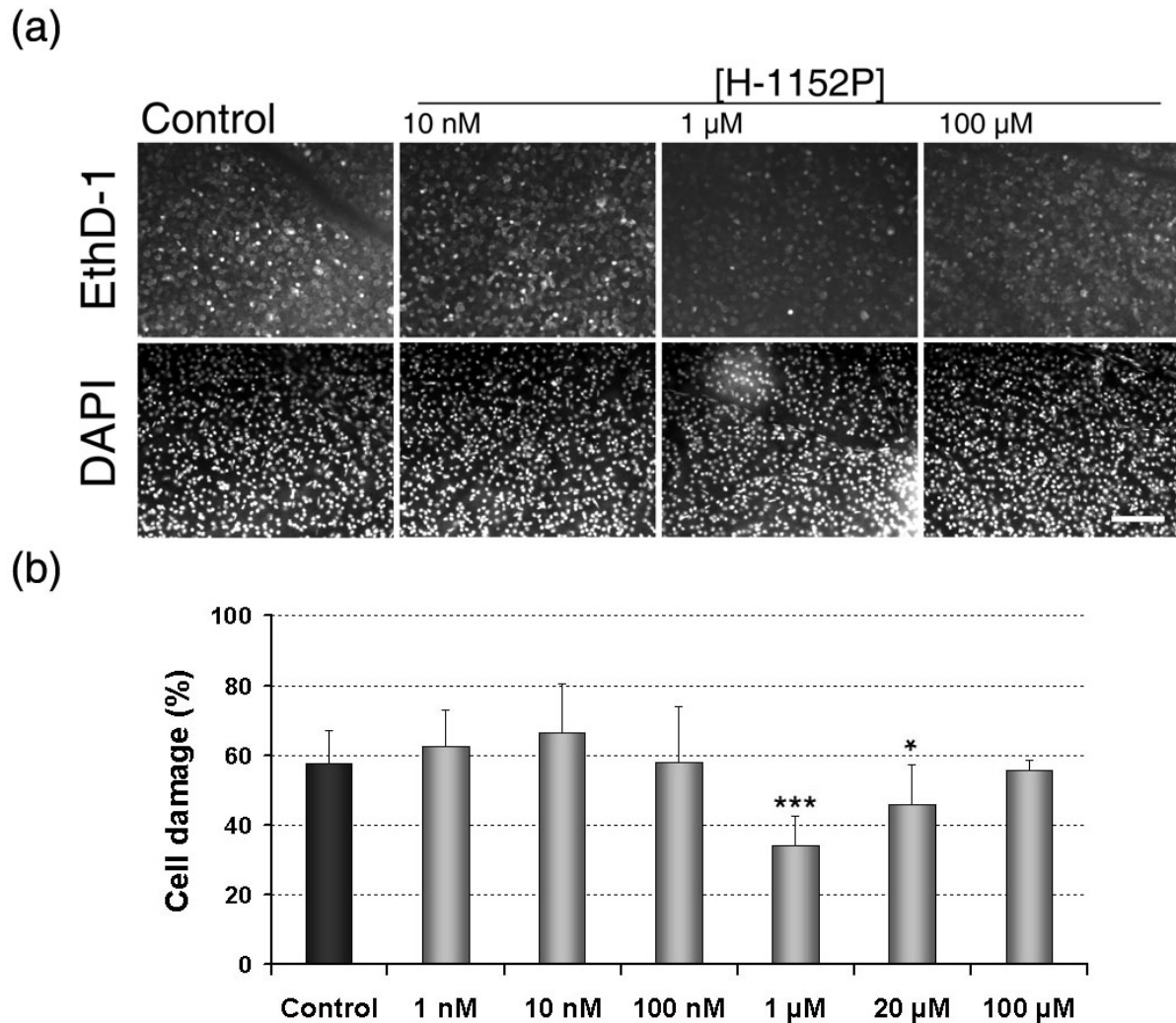


**Figure 20.** The dose-dependent neuroprotective effect of H-1152P on the ganglion cell layer of retinae under serum deprivation. **(a)** EthD-1 staining of the retinal flat mounts to detect the damaged cells after 24 hours incubation with or without the ROCK inhibitor H-1152P. DAPI counterstaining was performed to determine the total number of cells in the fields analyzed. Bar= 100  $\mu$ m, **(b)** Percentage of damaged cells in the ganglion cell layer after 24 hours incubation. \* $p$ <0.05; \*\*\* $p$ <0.001 compared to control.

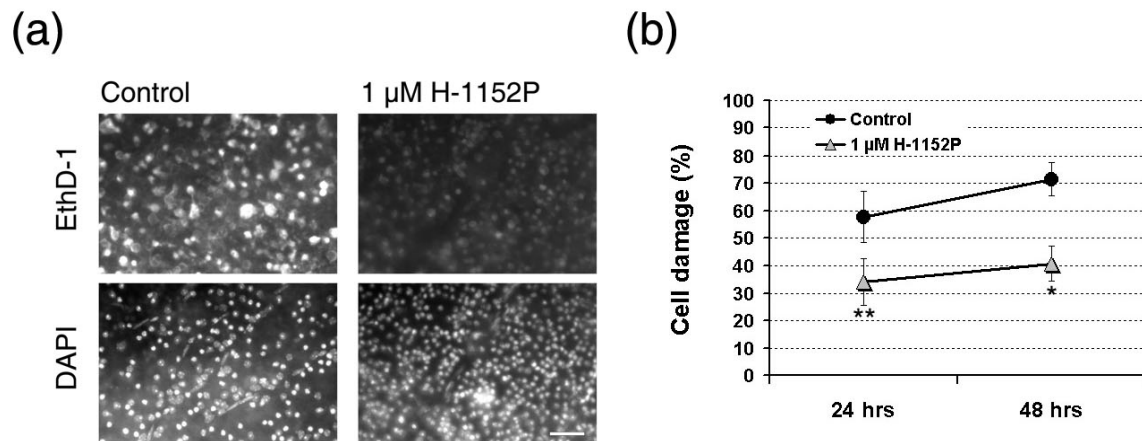


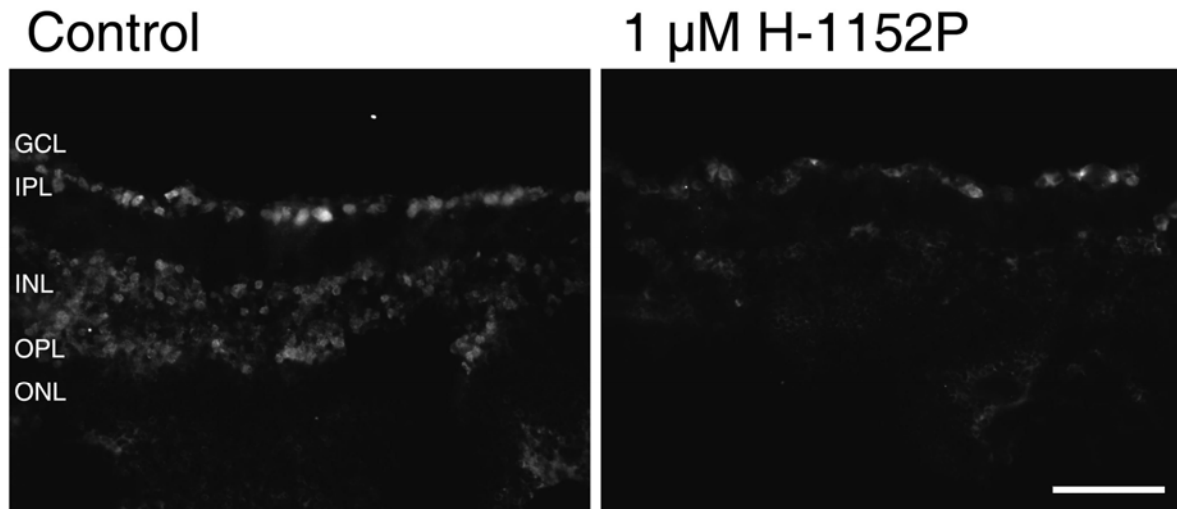
**Figure 21.** H-1152P dependent suppression of cell death in the GCL after 48 hours of serum deprivation (a) determined by EthD-1 and DAPI stainings. Note the decrease in cell density in untreated controls. (b) Percentage of cell damage after 48 hours incubation calculated from two independent experiments (see Figure 20 b for the 24 hour-incubation period).

### 3.2.3. Reduced caspase-3 activation in response to H-1152P

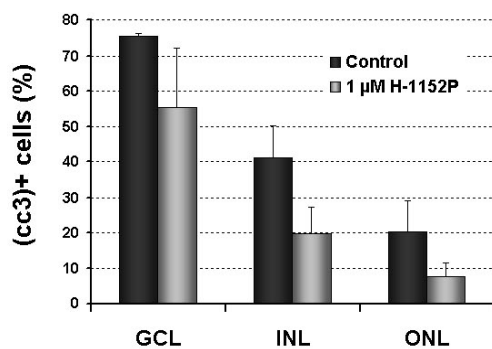
Staining with the EthD-1 dye allowed for detecting the high degree of damage induced by serum deprivation in the ganglion cell layer of isolated retinæ, which could be suppressed to a certain extent with H-1152P. However, it was not possible to differentiate the cells that were committed to apoptosis using this approach. An early intracellular event triggered by various apoptotic signals like FasL, TNF-alpha, cytochrome-C released from mitochondria, and elevated intracellular calcium is the activation of caspase-3 by proteolytic cleavage.<sup>167, 168</sup> Based on this, immunostainings for cleaved caspase-3 were performed on retinal transverse cryosections to detect the extent of apoptosis in all the layers of serum deprived retinæ treated with or without H-1152P for 24 hours. In untreated retinæ, the cleaved caspase-3 positive cells constituted 75% of the cells in the ganglion cell layer, 41% of the cells in the inner nuclear layer, and 20% of the cells in the outer nuclear layer, whereas the addition of 1 μM H-1152P reduced these values to 55% in GCL, 20% in INL, and 7.6% in ONL. The intensity of the staining was also reduced by approximately 50% in all the layers after H-1152P treatment (Figure 22).



(a)



(b)



(c)

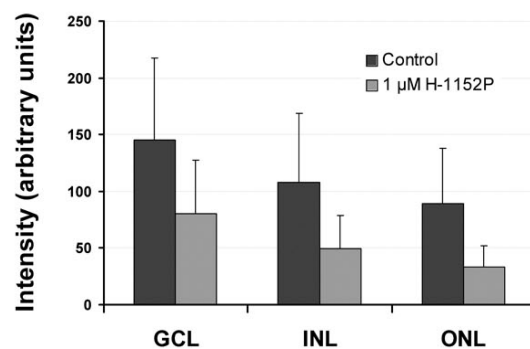


**Figure 22.** H-1152P reduces the activation of caspase-3 in all the cell layers of serum deprived retinae. **(a)** Cleaved caspase-3 immunostaining on transverse sections of retinae incubated without (control, n=2) or with 1  $\mu$ M H-1152P (n=2) for 24 hours. Bar= 50  $\mu$ m (GCL: Ganglion cell layer, IPL: inner plexiform layer, INL: inner nuclear layer, OPL: outer plexiform layer, ONL: outer nuclear layer), **(b)** Percentage of cleaved caspase-3 positive cells and **(c)** the intensity of staining in all the retinal cell layers quantified in 4 to 12 sections per retina .

### 3.2.4. Specificity of H-1152P action in mouse retinal cells

To clarify whether H-1152P interferes with the PKA pathway in mouse retinae at a concentration of 1  $\mu$ M, Western blots were carried out to analyze the levels of adducin isoforms as well as the ROCK- and PKA-dependent phosphorylation of this protein.

The total level of adducin was detected using the polyclonal antibody recognizing the alpha- (110 kDa) and gamma- (80 kDa) isoforms. Both of these isoforms appeared to be expressed at similar levels in untreated as well as H-1152P treated retinae after 24 hours. Additional bands of smaller molecular weights, which could represent the degradation products of adducin, were also detected in both samples at a similar intensity, suggesting that the H-1152P treatment induced no significant difference in the total level of this protein after 24 hours of serum deprivation (Figure 23a).

The PKA-dependent phosphorylation of adducin was analyzed using the polyclonal antibody recognizing the alpha-, beta-, and gamma-adducin isoforms phosphorylated at S726, S713, and S662 in the MARCKS domain, respectively. This antibody allowed the detection of three bands with molecular weights corresponding to the adducin isoforms in untreated retinae. These bands were also present at slightly higher levels in the lysates of retinae treated with 1  $\mu$ M H-1152P indicating that H-1152P at this concentration did not cause a reduction in the PKA-dependent phosphorylation of adducin (Figure 23b and d).

The ROCK-dependent phosphorylation of adducin was analyzed using a polyclonal antibody which was reported to recognize only the alpha-adducin isoform phosphorylated at T445 in the neck domain and the degradation products thereof.<sup>169</sup> In untreated retinae a weak band of 110 kDa presumably corresponding to this isoform was indeed detectable. However, a band of approximately 74 kDa which was of considerably higher intensity as well as several weaker bands of intermediate and lower size were also present. All these bands were found to be expressed at approximately 50% lower levels in retinae treated with 1  $\mu$ M H-1152P (Figure 23c and e). This decrease in the ROCK-dependent phosphorylation of adducin in H-

1152P treated retinæ without an accompanying decrease in the PKA-dependent phosphorylation and the total level of adducin suggests that H-1152P administered at 1  $\mu$ M specifically inhibits the ROCK activity without interfering with the PKA pathway in mouse retinæ.

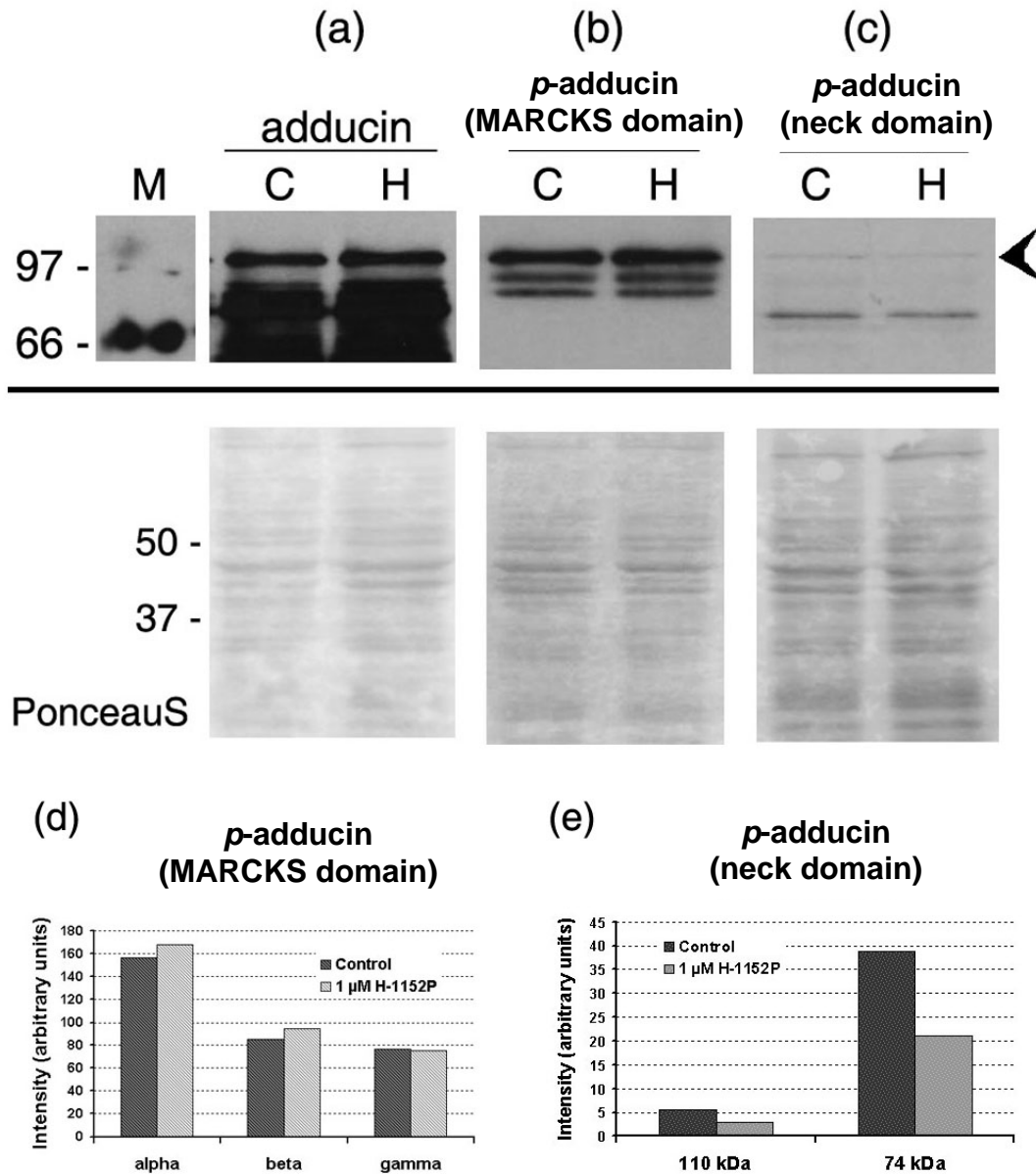


**Figure 23.** H-1152P at 1  $\mu$ M inhibits the ROCK-pathway without interfering with the PKA-pathway in mouse retina. **(a-c)** Representative Western blots demonstrating the levels of adducin phosphorylated at the MARCKS and neck domains by PKA and ROCK, respectively. The arrowhead indicates the alpha-isoform. The total level of this protein in retinæ incubated with (H) or without (C) 1  $\mu$ M H-1152P for 24 hours is shown on the left (adducin). PonceauS staining was performed to verify equal protein loading. M: Molecular weight marker (in kDa). Densitometric analysis of the adducin isoforms phosphorylated at the MARCKS **(d)** or neck domains **(e)** confirms the distinct reduction in ROCK activity without a considerable change in PKA activity.

Interestingly, adducin was reported to be one of the numerous proteins subject to caspase-3 mediated cleavage in cells undergoing apoptosis.<sup>170</sup> The potential caspase-3 cleavage sites in alpha-adducin and the fragments that can be recognized by the phosphorylation domain specific antibodies used in this study are illustrated in Figure 24. The 74 kDa fragment, which contains the domain phosphorylated by ROCK but not the domain phosphorylated by PKA is of particular interest, since such a fragment was indeed reported to be generated by caspase-3 in renal proximal tubular epithelial cells undergoing apoptosis.<sup>170</sup> The 74 kDa band detected in the lysates of serum deprived mouse retinae might therefore be an additional indicator of the caspase-3 activity and the decrease in the intensity of this band in response to ROCK inhibition might provide further support to the previous findings regarding the H-1152P dependent reduction in caspase-3 activation.

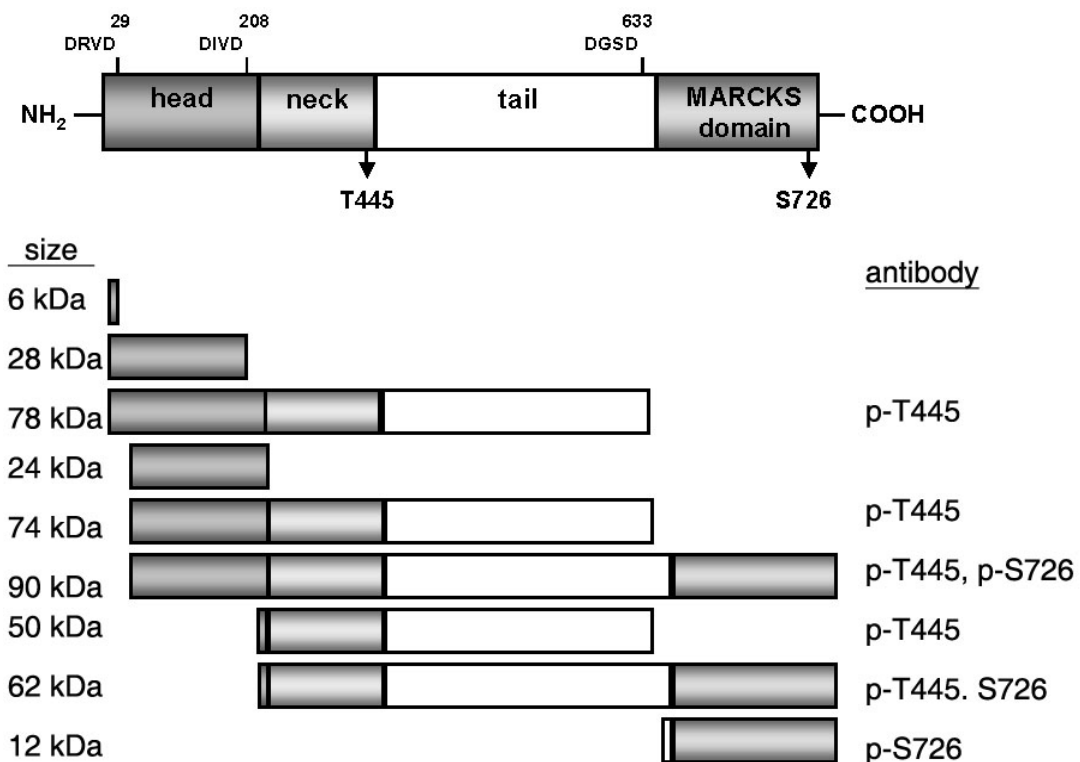


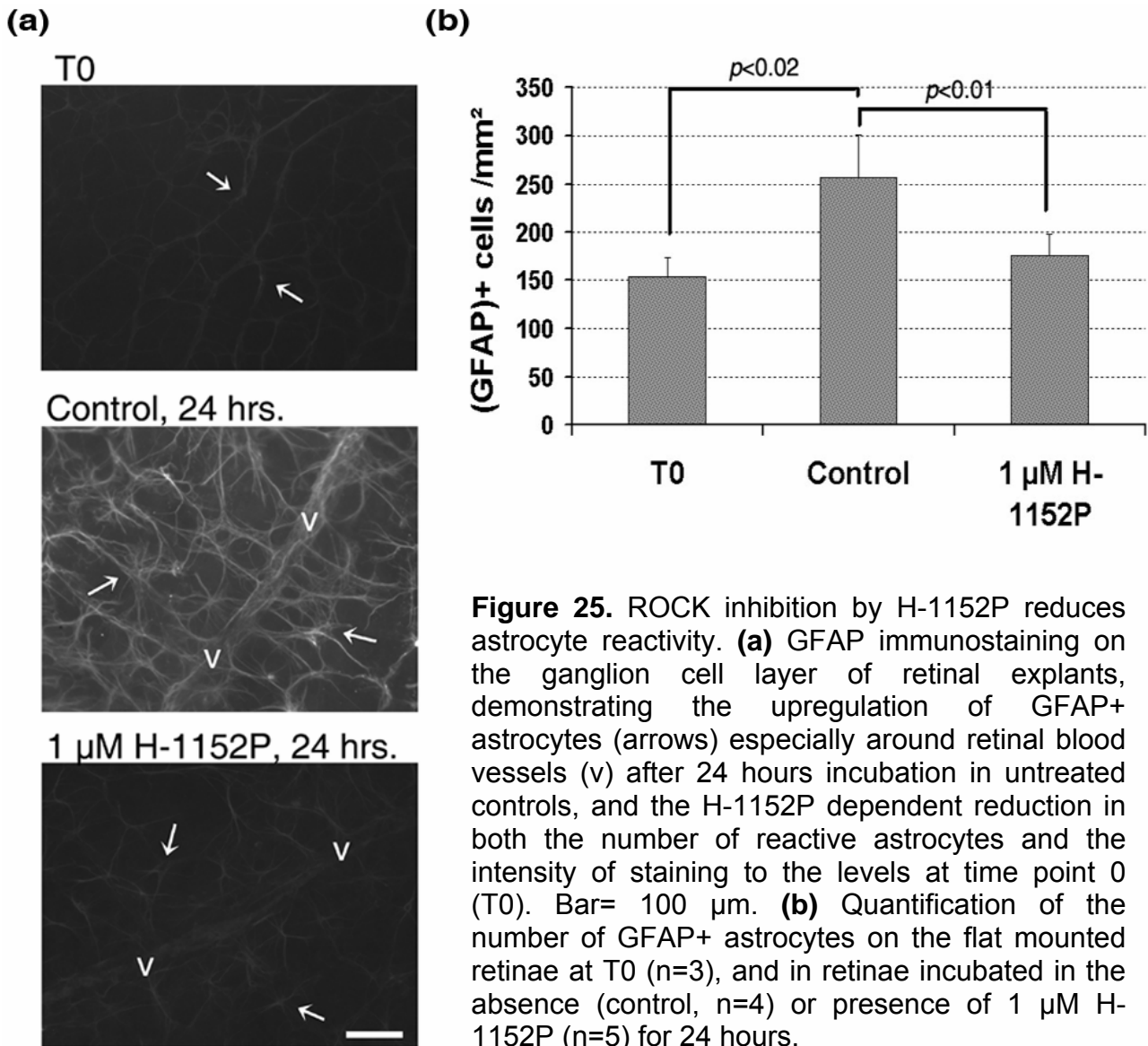
**Figure 24.** DXXD motifs on alpha-adducin that can be recognized by caspase-3 and hypothetical fragments that could be generated by caspase-3 mediated cleavage at these sites (adapted from van de Water et al., 2000).<sup>170</sup> The fragments that can be recognized by the anti-phospho-adducin antibodies used in this study are marked on the right. MARCKS: Myristoylated alanine rich kinase.

### 3.2.5. Decrease in glial cell reactivity in response to ROCK inhibition

In order to understand the mechanism by which the retinal cells benefit from H-1152P-mediated ROCK inhibition, it was necessary to characterise the cellular changes induced by this treatment in more detail. Considering the involvement of glial cell reactivity in the pathologic course of neuronal damage,<sup>62, 171</sup> we focused on the response of astrocytes, Müller cells, and microglia in the retina. Therefore, immunostainings were initially performed using an antibody against GFAP on retinal flat mounts incubated for 24 hours in serum-free medium with or without 1  $\mu$ M H-1152P to detect the extent of glial cell activation on the nerve fiber/ganglion cell layer. An additional group of retinae, fixed immediately after mounting, served as controls reflecting the basal level of astrocytes at the starting conditions (T0).

GFAP immunostaining at T0 was mainly localized to the spots damaged during mounting and appeared very weak in undamaged areas. A significant increase was observed in both the number of reactive astrocytes and the intensity of GFAP staining, especially around the retinal blood vessels in untreated retinae after 24 hours of serum deprivation, while the retinae incubated with 1  $\mu$ M H-1152P displayed a weaker staining pattern similar to T0 (Figure 25).

Immunostainings of retinal transverse sections performed to detect the response of not only the astrocytes but also the Müller cells also revealed only a few GFAP+ cells on the nerve fiber layer (NFL) at T0. Incubation in serum-free medium led to the upregulation of GFAP in untreated retinae as demonstrated by the strong staining on the NFL and the profound increase in GFAP+ Müller cells. However, treatment with H-1152P appeared to suppress this process in a dose-dependent manner. Retinae that received 1  $\mu$ M H-1152P contained considerably less reactive astrocytes on the NFL and few activated Müller cells while the retinae treated with 20  $\mu$ M of this inhibitor exhibited only a few weakly stained astrocytes on the NFL and almost no GFAP+ Müller cells (Figure 26).



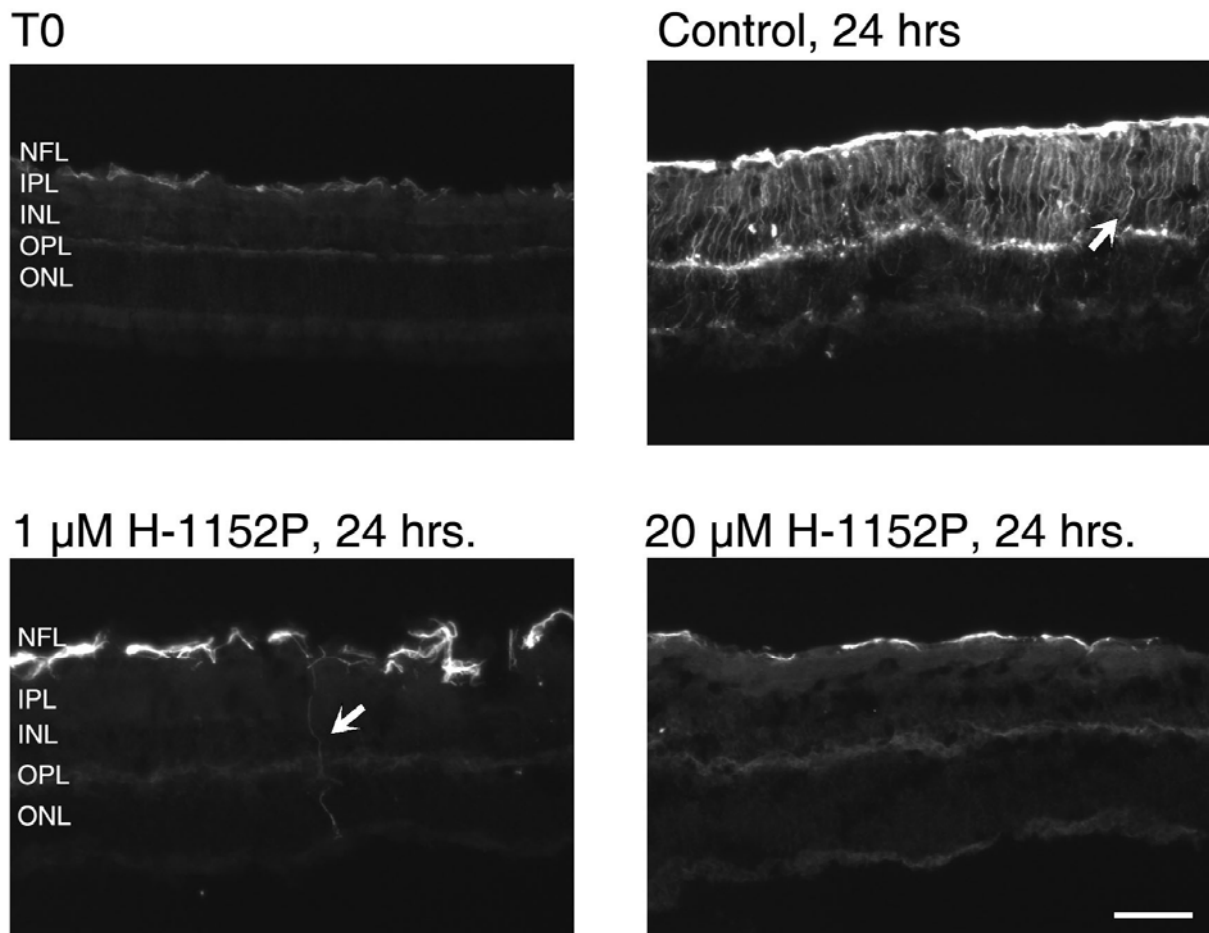


**Figure 26.** GFAP immunostaining of retinal transverse sections, showing GFAP upregulation not only on the nerve fiber layer (NFL), but also in Müller cells (arrows) in untreated controls, and the dose-dependent impairment of this process in retinæ incubated with H-1152P. Bar= 50  $\mu$ m (IPL: inner plexiform layer, INL: inner nuclear layer, OPL: outer plexiform layer, ONL: outer nuclear layer).

Upregulation of GFAP in untreated retinæ after 24 hours incubation and the H-1152P associated decrease were also confirmed by Western blot analysis of the corresponding cytoplasmic protein extracts. GFAP is a 49 kDa protein with several splice variants, which might be phosphorylated and glycosylated to varying degrees,<sup>172, 173</sup> resulting in several bands on Western blots. Figure 27 demonstrates the significant upregulation of all the detectable isoforms in untreated retinæ after 24 hours compared to T0. Among these isoforms, a band of approximately 37 kDa, which could hardly be detected at T0, was of particular interest, since it constituted the main portion of the GFAP positive bands in untreated retinæ after 24 hours of serum

deprivation. In contrast, treatment with 1  $\mu$ M H-1152P led to a significant reduction of 32 to 47% in the intensity of the 37 and 49 kDa isoforms, respectively ( $p < 0.04$ , Figure 27).

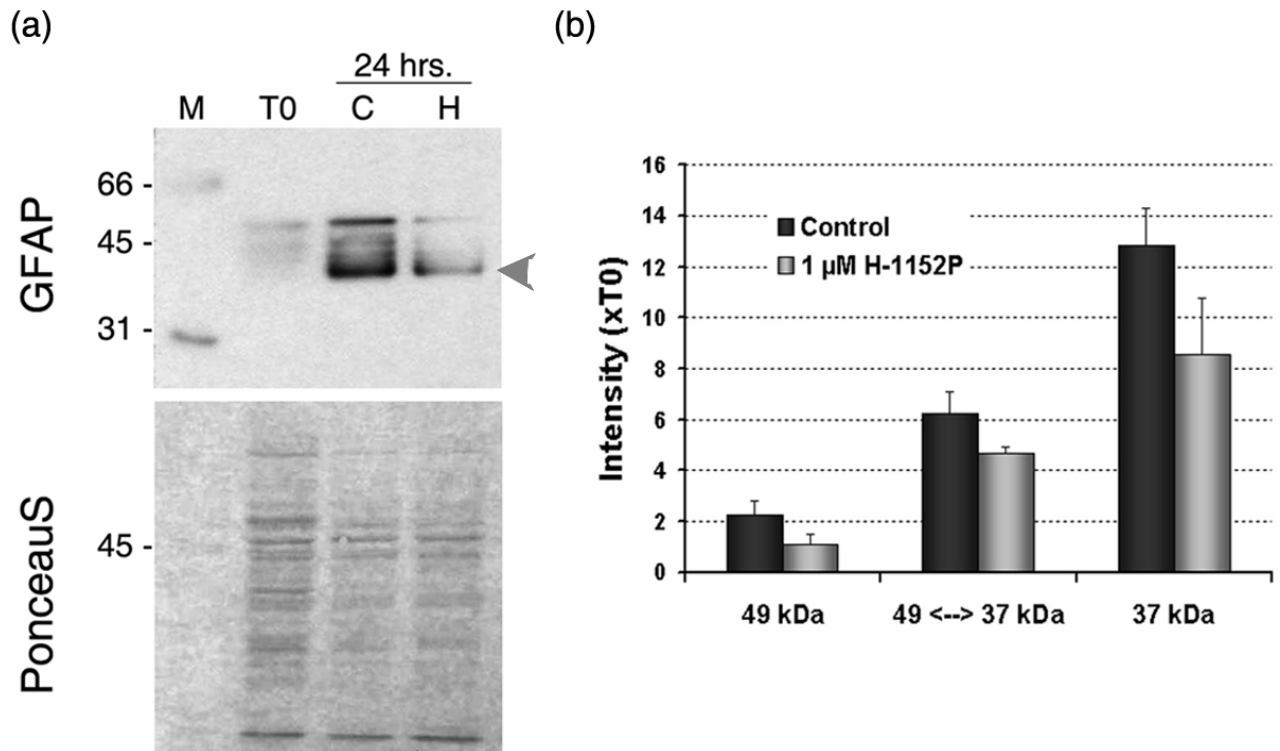


**Figure 27.** ROCK-inhibition induced decrease in the levels of GFAP isoforms. **(a)** Representative immunoblot demonstrating the upregulation of all the detectable GFAP isoforms in untreated retinae (C) after 24 hours of serum deprivation compared to the initial levels (T0), and the decrease in the intensity of these bands in retinae treated with 1  $\mu$ M H-1152P (H). M: Molecular weight marker in kDa. PonceauS staining was performed to verify equal protein loading. The arrowhead indicates the approximately 37 kDa isoform which was strongly upregulated in untreated retinae after 24 hours of serum deprivation. **(b)** Densitometric analysis of the intensity of the GFAP isoforms, expressed as fold increase with respect to the intensity at T0. The mean values were calculated from four independently performed blots. The H-1152P-associated decrease in intensity was significant for all the isoforms ( $p < 0.04$ ).



As mentioned earlier, the microglia constitute another type of glial cell in the CNS playing a critical role in host defense under pathological conditions. In normal adult rats, resting microglial cells exhibiting a ramified morphology characterized by several long, frequently bifurcated processes, are scattered throughout the ganglion cell and the inner plexiform layers. The activation of these cells is marked by the acquisition of a more amoeboid shape and an increase in proliferation as well as the upregulation of certain cell-specific marker proteins, such as the type 3 complement / integrin receptor CD11b, which can be detected using the monoclonal antibody clone OX-42 or CD11b specific antibodies. To characterize the response of microglia on the ganglion cell layer of isolated mouse retinae after serum deprivation, immunostainings were performed using an anti-CD11b antibody on freshly prepared retinal whole mounts as well as on retinae incubated for 24 hours.

In freshly prepared retinae, a network of ramified microglia with thin processes stained weakly for CD11b could be detected on the ganglion cell layer. However, a considerable increase was observed in the levels of this protein after 24 hours of serum deprivation. The CD11b-positive microglia in the control group also acquired a rounder shape with retracted protrusions. In contrast, the microglia in retinae incubated with 1  $\mu$ M H-1152P exhibited a weaker staining for CD11b and possessed longer processes resembling the ramified morphology of quiescent microglia (Figure 28), suggesting that the treatment with H-1152P also reduces the extent of microglial activation in isolated retinae under serum deprivation.

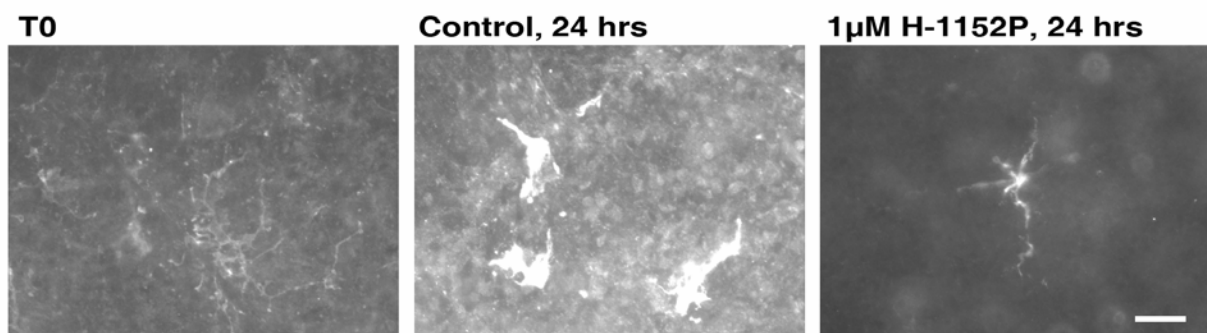


**Figure 28.** Representative images of the CD11b immunostaining demonstrating the activation of microglia on the ganglion cell layer of retinal whole mounts incubated without H-1152P for 24 hours (control). Microglia in retinae treated with 1  $\mu$ M H-1152P exhibited a more ramified morphology similar to the quiescent microglia detected in freshly prepared retinal whole mounts (T0). Bar = 100  $\mu$ m.

### **3.2.6. H-1152P induced changes in the levels of proteins released from the retina and the optic nerve**

In most cases, a white spot located at the position of the excised optic nerve was observed in the culture media of untreated retinae after 24 hours of incubation without serum. This radially diffusing spot was usually absent in H-1152P treated retinae, or was of a smaller size. The position of this spot suggested leakage from damaged axons or cells at the optic nerve head, or secretion of soluble proteins presumably from non-neuronal cells as seen in the central nervous system following nerve injury. Considering this, we wanted to analyze the protein content of the culture medium after 24 hours incubation, and the effect of H-1152P treatment.

SDS-PAGE analysis revealed numerous bands in the incubation medium of untreated retinae, the majority of which showed a decreased intensity in H-1152P treated samples. The effect of H-1152P treatment on the optic nerve led to even more dramatic consequences, leaving almost no proteins detectable in the corresponding supernatant in contrast to the incubation medium of the untreated nerve. Among the proteins common to the conditioned media of the retina and the optic nerve, an approximately 20 kDa band, which also underwent a H-1152P dependent reduction, was of particular interest. Certain bands in the incubation media of retina or optic nerve, including the 20 kDa band were detected in the lysates of these tissues as well (Figure 29). These findings suggested the secretion or leakage of various proteins from cells/cell structures present in both the retina and the optic nerve, and a decrease in the amount of most of these proteins by ROCK inhibition.

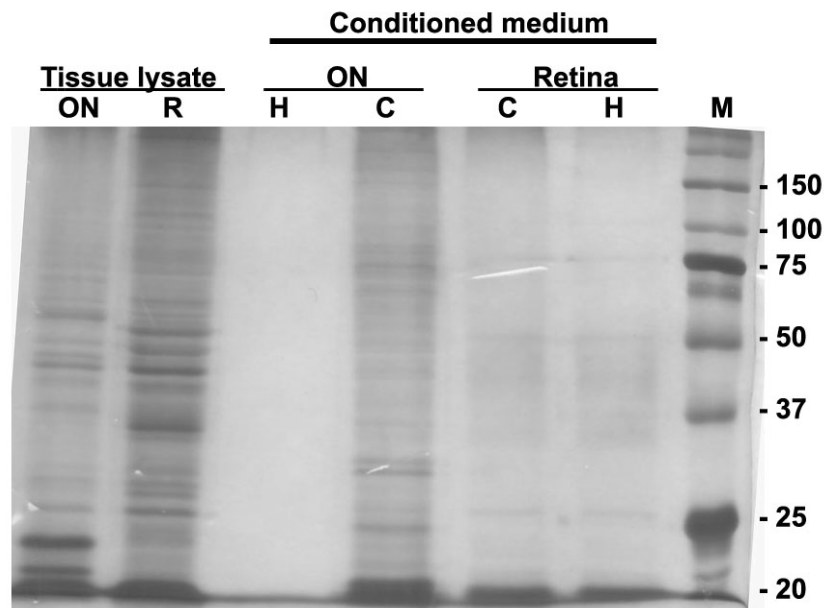


**Figure 29.** SDS-PAGE analysis of the culture media and cytoplasmic extracts of retinae (R) or optic nerve (ON) after 24 hours incubation with (H) or without 1  $\mu$ M H1152P (C). M: Molecular weight marker (in kDa).

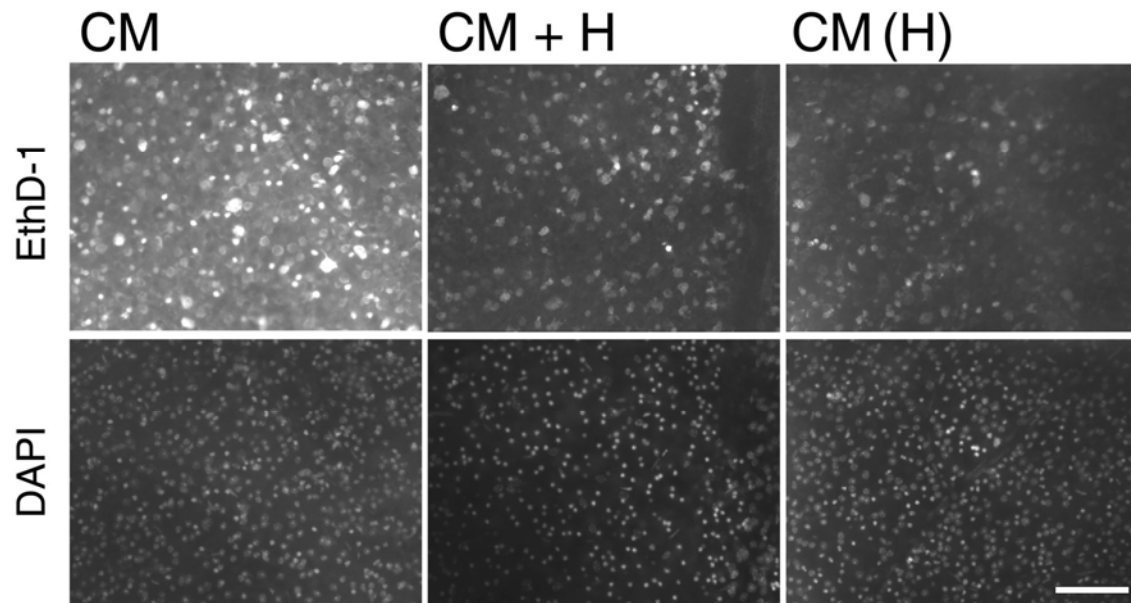
### 3.2.7. Reduction in the toxicity of the conditioned media of retina and optic nerve incubated with H-1152P

The source of the soluble proteins detected in the culture medium of both the retina and the optic nerve are likely to be the damaged ganglion cell axons, endothelial cells, astrocytes, or microglia. Reactive astrocytes and microglia are indeed known to produce growth factors and immunomodulatory cytokines, the balance of which being critical for neuron survival. Considering this, we wanted to analyze whether the medium content after 24 hours-incubation was toxic to retinal cells, and whether ROCK inhibition resulted in any difference. With this purpose, pieces of ON (5,8 mm/ml) were incubated for 24 hours with or without 1  $\mu$ M H1152P. This conditioned medium was then used for incubating freshly prepared retinal explants. As controls, retinal explants were coincubated with ON pieces of the same size in fresh medium containing or lacking 1  $\mu$ M H-1152P. The percentage of damaged cells was then assessed by EthD-1 staining as described.

As seen in Figure 30, coincubation of ON with the retina yielded similar results to those obtained from retinæ incubated alone, with a decrease in cell damage in the presence of 1  $\mu$ M H-1152P. However, incubation of the retinæ with the conditioned medium of optic nerve significantly increased the extent of cell damage to 71% (n=5,  $p<0.02$ ). Addition of H-1152P into this conditioned medium induced a mild but insignificant reduction to 62% (n=2). However, the extent of cell damage was found to be significantly lower when the conditioned medium of the optic nerve incubated with 1  $\mu$ M of H1152P was used (45%,  $p<0.006$ ).

Incubation of freshly prepared retinæ with the conditioned medium of untreated or H-1152P treated retinæ also yielded similar results. The percentage of cell damage in the GCL reached 72% in the control group incubated for 24 hours in the conditioned medium of untreated retinæ (n=3,  $p<0.05$ ). Addition of H-1152P into this conditioned medium induced a slight but insignificant recovery with 58% cell damage (n=3). However, the culture medium of the retinæ incubated with 1  $\mu$ M of H-1152P resulted in a significantly lower damage of approximately 43% (n=3,  $p<0.02$ , Figure 31). These findings suggested that H-1152P might be exerting its protective effect mainly by reducing the amount of certain secreted molecules, and probably to a less extent by inhibiting their activity.

(a)



(b)

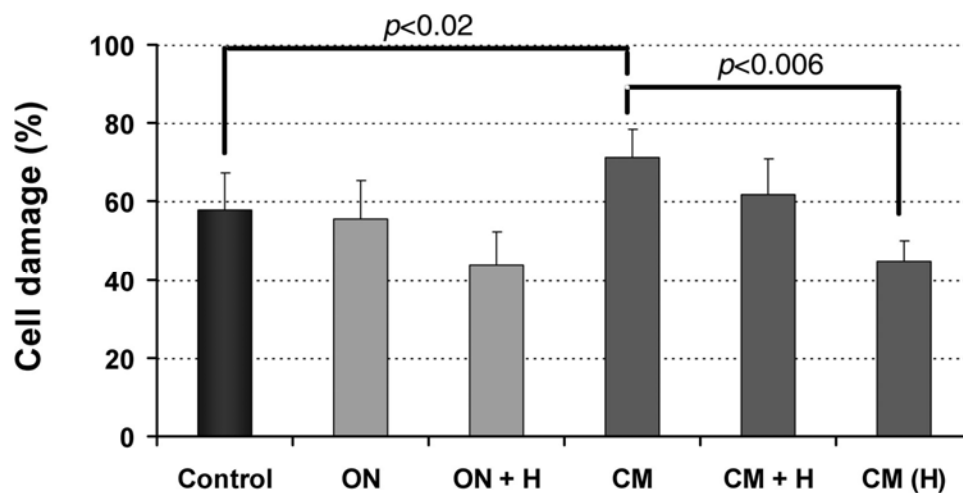


**Figure 30.** H-1152P associated decrease in the toxicity of the optic nerve conditioned medium. **(a)** Representative images of the EthD-1 and DAPI stainings in the ganglion cell layer (GCL) of retinae incubated with the conditioned medium of optic nerve alone (CM) or with the addition of 1  $\mu$ M H-1152P into this medium (CM+H) for 24 hours. Note the reduction in the number of EthD-1 positive cells and the intensity of staining in retinae treated with the conditioned medium of optic nerve incubated with 1  $\mu$ M H-1152P (CM(H)) for 24 hours. Bar=100  $\mu$ m. **(b)** Quantification of the percentage of cell damage in the GCL after 24 hours. Control refers to the extent of cell damage in retinae incubated with DMEM/F-12 for 24 hours (see Figure 13b). ON indicates the retinae that were coincubated with a 5.8 mm piece of optic nerve (n=2) whereas ON+H stands for retinae that were coincubated with the optic nerve piece in the presence of 1  $\mu$ M H-1152P (n=3).

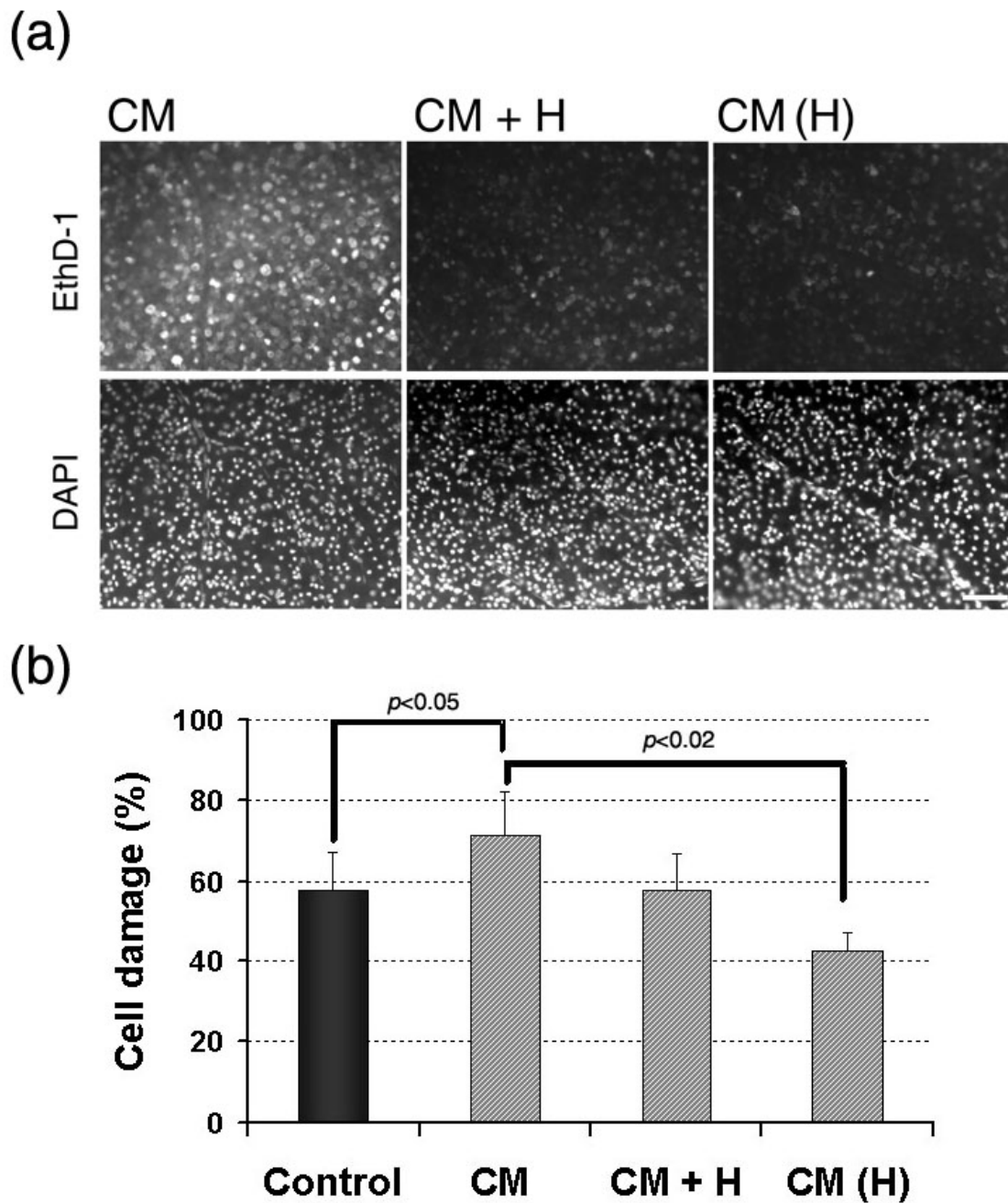


**Figure 31.** H-1152P associated decrease in the toxicity of retinal conditioned medium. **(a)** Representative images of the EthD-1 and DAPI stainings in the ganglion cell layer (GCL) of retinæ incubated with retinal conditioned medium alone (CM) or with the addition of 1  $\mu$ M H-1152P into this medium (CM+H) for 24 hours. The number of EthD-1 positive cells and the intensity of staining underwent a considerable reduction when the conditioned medium of retinæ incubated with 1  $\mu$ M H-1152P (CM(H)) for 24 hours was applied. Bar=100  $\mu$ m. **(b)** Quantification of the percentage of cell damage in the GCL after 24 hours. Control denotes the extent of cell damage in retinæ incubated with serum-free DMEM/F-12 for 24 hours (see Figure 20b).

### 3.2.8. Characterization of the secreted proteins

To identify the small molecular weight proteins which were released into the incubation medium, Western Blot analysis was initially performed for IL-6, IL-10, IFN-gamma, and EGF using antibodies that were already present in our laboratory. In all cases, a strong band of 50 kDa and a relatively weaker band of approximately 30 kDa as well as some intermediary bands were detected in the supernatant of untreated controls, the intensity of which appeared significantly lower in the supernatants of H-1152P treated retinae. However, it was difficult to derive a conclusion about the role of ROCK inhibition from the levels of these cytokines, since the size of especially the major 50 kDa band was considerably larger than the size of these cytokines (Figure 32).

We first interpreted these observations as an artifact, but the repetition of these experiments with new samples yielded similar results, and it was less likely to be the failure of the antibodies used, since the cytokines loaded onto the gel as control could be visualized in the blots as shown for EGF (Figure 32). The possibility that these bands represented the dimers or tetramers of cytokines also appeared unlikely since the denaturing conditions applied and the presence of beta-mercaptoethanol were expected to have disrupted such quaternary protein structures. Interestingly, these bands disappeared from blots performed under native conditions, suggesting that the antibodies might be recognizing some other protein(s) that share sequence similarity to the cytokines under denaturing conditions.

To identify the proteins that bear sequence similarity to these cytokines, a *Mus musculus* protein database was searched using the amino acid sequences of mouse EGF, IFN-gamma, IL-6, and IL-10 as query. The proteins that are retrieved for IFN-gamma, IL-6, and IL-10 are listed in Table 6 together with the percentage of identical amino acids as well as the percentage of positive residues and gaps in the alignment region. Of particular interest was the ionotropic glutamate receptor delta-1 which was found to contain stretches of conserved residues in both interferon-gamma and interleukin-10. The database search using EGF amino acid sequence yielded 100 proteins, among which the low density lipoprotein receptor-related protein, being also present in the list of proteins retrieved for IFN-gamma, may deserve further attention.

The low density lipoprotein receptor-related protein, which can exist in a soluble as well as a membrane bound form,<sup>174</sup> is a multifunctional receptor implicated in the regulation of growth factor/cytokine metabolism and is reported to be expressed in isolated Müller cells.<sup>175</sup> Interestingly, the receptors of many of the cytokines can also exist in a soluble form and modify the activity of cytokines by acting as agonists or antagonists.<sup>176</sup> Aligning the amino acid sequences of IFN-gamma and IL-6 receptor with the sequences of IFN-gamma and IL-6 has indeed shown that these receptors encoded by 400-500 amino acids also share short stretches of conserved residues with their respective ligands (Figure 33), suggesting that the soluble receptors of the cytokines analyzed here might also have been recognized by the antibodies used in the immunoblots.

**Figure 32.** ROCK inhibition significantly reduces the release of approximately 50 and 30 kDa proteins recognized by anti-cytokine antibodies. Equal volumes of the culture media of retinae incubated with or without 1  $\mu$ M H1152P (H and C, respectively) were analyzed by Western blot, using antibodies against IFN-gamma, IL-6, IL-10, and EGF (M: Molecular weight standard in kDa, E: 100 ng EGF, -: negative control incubated with the alkaline phosphatase-conjugated goat anti-rabbit IgG).

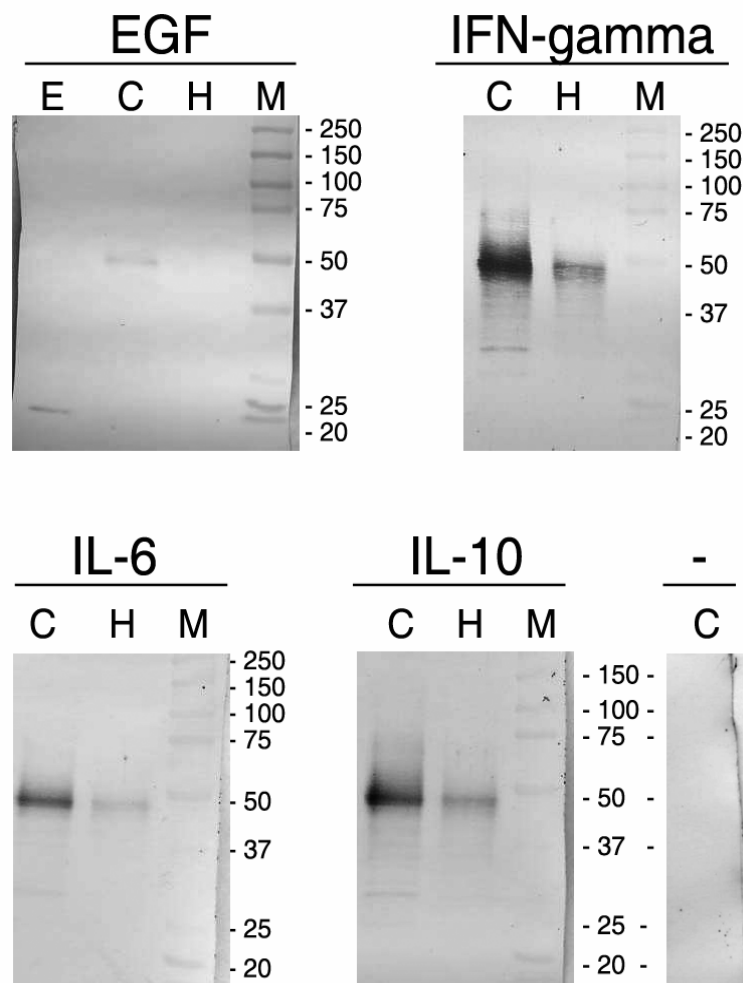




**Table 6.** Mouse proteins sharing conserved regions with IFN-gamma, IL-6, and IL-10

Cytokine	Protein (GenBank accession number)	Identities (%)	Positives (%)	Gaps (%)
<b>IFN-gamma</b>	muscle and microspikes RAS (NP_032650.1)	15/68 (22%)	34/68 (50%)	
	transcriptional regulator, SIN3B (NP_033214.1)	21/114 (18%)	46/114 (40%)	15/114 (13%)
	vomer nasal 1 receptor, A9 (NP_444454.1)	16/64 (25%)	31/64 (48%)	2/64 (3%)
	glutamate receptor, ionotropic, delta 1 (NP_032192.1)	14/40 (35%)	25/40 (62%)	3/40 (7%)
	similar to low density lipoprotein (XP_926267.1)	19/74 (25%)	34/74 (45%)	8/74 (10%)
	olfactory receptor 661 (NP_666959.1)	27/93 (29%)	41/93 (44%)	6/93 (6%)
	low density lipoprotein receptor-related protein (XP_904952.1)	19/74 (25%)	34/74 (45%)	8/74 (10%)
<b>IL-6</b>	Zonadhesin (NP_035871.1)	15/43 (34%)	22/43 (51%)	2/43 (4%)
	similar to Carboxypeptidase D precursor (XP_001001063.1)	12/36 (33%)	16/36 (44%)	
	basic FGF repressed, zinc binding protein (NP_061376.1)	13/34 (38%)	18/34 (52%)	
<b>IL-10</b>	interleukin 20 (NP_067355.1)	36/135 (26%)	62/135 (45%)	6/135 (4%)
	interleukin 19 (NP_001009940.1)	28/131 (21%)	60/131 (45%)	5/131 (3%)
	interleukin 22 (NP_058667.1)	26/100 (26%)	49/100 (49%)	5/100 (5%)
	interleukin 10-related T cell-derived inducible (NP_473420.1)	25/100 (25%)	49/100 (49%)	5/100 (5%)
	similar to Interleukin-22b precursor (IL-22b) (XP_001000613.1)	23/85 (27%)	44/85 (51%)	5/85 (5%)
	dystonin isoform e (NP_034211.1)	23/87 (26%)	42/87 (48%)	7/87 (8%)
	neurobeachin like 1 (XP_996048.1)	17/46 (36%)	26/46 (56%)	10/46 (21%)
	glutamate receptor, ionotropic, delta 1 (NP_032192.1)	15/46 (32%)	26/46 (56%)	1/46 (2%)
	polymerase (RNA) II (DNA directed) polypeptide (NP_033115.1)	15/47 (31%)	27/47 (57%)	3/47 (6%)
	isoprenylcysteine carboxyl methyltransferase (NP_598549.1)	29/97 (29%)	41/97 (42%)	14/97 (14%)

**(a)**

```

      10      20      60      70      80      100
m_IFNg_rec  MGPQAAAGRMI LLV LMLS AKVGS---CWEYQNMSQTPIFTVQVKVYSGSWTDS---IYEQIMYPDVSAW---
      : : : : : : : : : : : : : : : : : : : : : : : : : : : : : : : : : : : : : : : : : : : : :
mouse_IFNg  MN---ATHCILALQLFLMAVSG---CYCHGTVIES---LESLN NYFNSSGID---VEEKSLFLDI---W---
      10      30      40      50

      120 150 160 170 190 210
m_IFNg_rec  KVGQKESDYA---LSVL---VVNGESQGT MFGDG-VYVEHNRSGEILHTKHTVEKEE---CELNISVLDSR
      : : : : : : : : : : : : : : : : : : : : : : : : : : : : : : : : : : : : : : : : : : : : :
mouse_IFNg  RNWQKDGD---MKIL---QSQIISF---YL---RLFEVLKDNQAISN-----NISVIESHL
      60      70      80      90

      230 240 280 300 310 380
m_IFNg_rec  ISSFWQVRTEKSK---TKKNSF---LSVVKS---ESKYSLVTPH---TQRRSF SLL
      : : : : : : : : : : : : : : : : : : : : : : : : : : : : : : : : : : : : : : : : : : : : :
mouse_IFNg  ITTFFS---NSK---AKKDAF---MSI----AKFEVNNPQ
      100      110      120

      380 400 420 430 440 460
m_IFNg_rec  TQRRSF SLL---SLTAYHSRN---DLESLPNNNSETKMAEHDP PPVPVKAP---VGGKES
      : : : : : : : : : : : : : : : : : : : : : : : : : : : : : : : : : : : : : : : : : : : : :
mouse_IFNg  VQRQAFNEL---IRVVH---QLLPES S-----LRKR-----KRS
      130      140      150

```

**(b)**

```

      10      20      30
IL6-m       M---KFLSARD FHPVAF LGL----MLV---TTTAFPT---SQVRR  GDFTE----
      : : : : : : : : : : : : : : : : : : : : : : : : : : : : : : : : : : : : : : : : : : : : :
sIL6Rm      MLTVGCTLLVALLAAPAVALVLGSCRALEVANGTVTSLPGASGSQNRE---GDYLC----
      10      20      30      40      70 90

      40 50 60 70 80 90
IL6-m       DTPNRPVYTTSQVGGLITHVL-W---EIVEMRK----ELCNGNSDCMNND DALAENNLK L
      : : : : : : : : : : : : : : : : : : : : : : : : : : : : : : : : : : : : : : : : : : : : :
sIL6Rm      DVPPEEPKLSCFRKNPLVNAICEWR-EILEGDKVYHIVSLCVANSVGS KSSHNEAFHSLKM---
      110 120 130 180 190 200 210

      100 110 120 130
IL6-m       PEIQRN---DGCY---QTGY---NQE---ICLLKISSGLLEYHSYLEYMKNNLKD NKDK
      : : : : : : : : : : : : : : : : : : : : : : : : : : : : : : : : : : : : : : : : : : : : :
sIL6Rm      PDPPANLV-DPSYLLQFQLRYR PVWSK EFTVLLL PVAQYQCVIHDALRGVKHV VQVRGKEEL
      220 250 260 270 280 290

      140 150 160 170
IL6-m       ---ARVLQRDTETLIH-IFNQE----VKDLHKIVLPTPI---SNAL-----
      : : : : : : : : : : : : : : : : : : : : : : : : : : : : : : : : : : : : : : : : : : : : :
sIL6Rm      TTPAGILWNPTQVSVEDSANHE----VQESSMSLPTFLVAGGSLAFGLLLCVFIILR---
      320 330 340 360 370

      180 190 200 210
IL6-m       LTDKLESQKEWLRTKTIQ----FILKSLEE-FLKVTLRSTRQT-
      : : : : : : : : : : : : : : : : : : : : : : : : : : : : : : : : : : : : : : : : : : : : :
sIL6Rm      LKQKWKSEAEK-ESKTTSP PPPPYSLG PLKPTFLLVPL LTPHSSG
      390 400 410 420 430

```

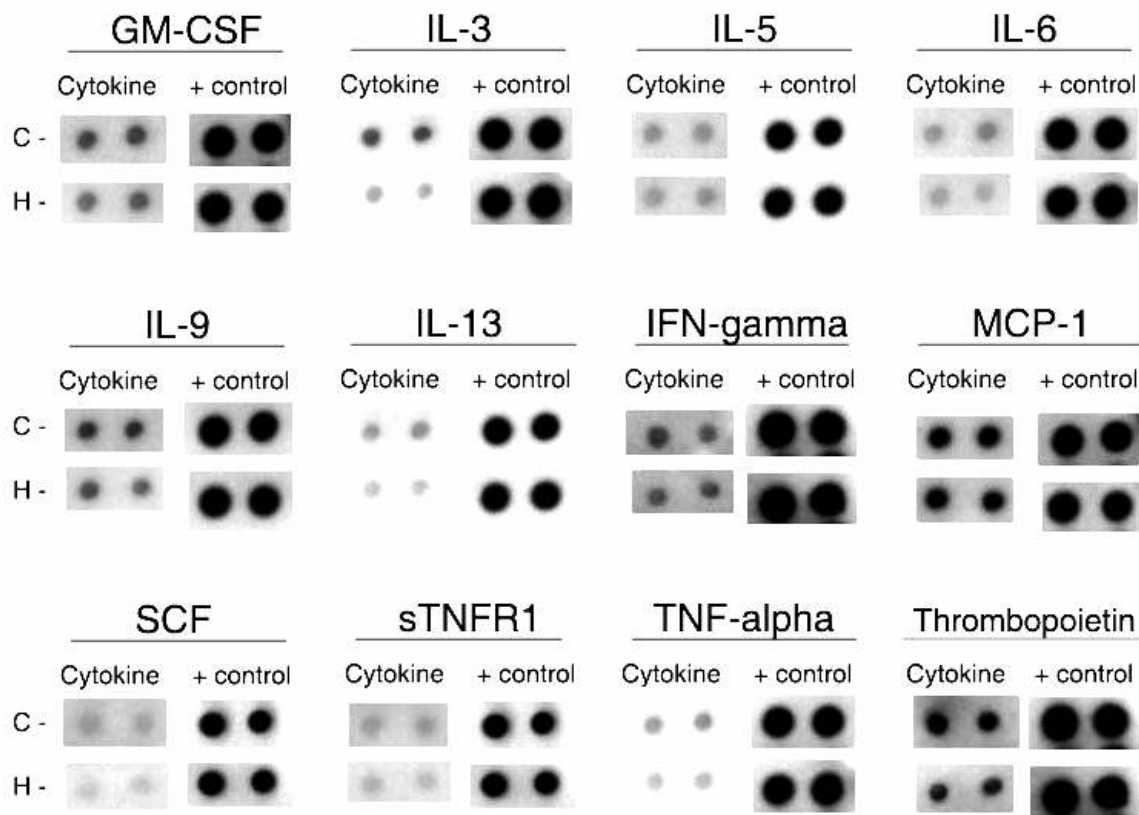
**Figure 33.** Optimal global alignment of the amino acid sequences of **(a)** mouse interferon-gamma (IFNg) with the mouse IFNg receptor (m\_IFNg\_rec) and **(b)** mouse IL-6 (IL6-m) with the soluble mouse IL6 receptor (sIL6Rm). The identical amino acids are matched with “:” whereas “.” Denotes conservative replacement.

### **3.2.9. Changes in the cytokine profile of the conditioned medium of the retina and optic nerve in response to ROCK-Inhibition**

To analyze the cytokine profile of the culture medium after the 24-hour incubation of retinae in serum-free medium, a membrane-based cytokine array which allowed for the simultaneous detection of 22 mouse cytokines was utilized. Incubation of the retinae in the presence of 1  $\mu$ M H-1152P led to a significant reduction in the amount of 11 of the cytokines that could be detected in the culture medium using this array. Among these, the cytokines IL-3, IL-6, and TNF-alpha were reduced by approximately 30% in a H-1152P dependent way whereas the levels of GM-CSF, IL-5, IL-9, IL-13, IFN-gamma, SCF, soluble TNF receptor (STNFR)1, and thrombopoietin exhibited a 15% decrease ( $p < 0.05$ , Figure 34).

To confirm these results and to determine the concentrations of the cytokines in the culture supernatants of the retinae and the optic nerve, we also had our samples analyzed with the Bio-Plex multiple cytokine array system by the Bio-Rad Laboratories. The Bio-Plex flow-cytometric mouse cytokine array allowed for the simultaneous detection of 18 mouse cytokines. In the culture media of retinae, 8 of these cytokines were below the measurable range. All the other cytokines, with the exception of IL-1a, IL-12 (p70) and MIP-1a were increased at least 1.5 fold in the supernatants of untreated retinae compared to H-1152P treated samples. Of particular interest were the cytokines IL-1beta, IL-3, IL-4, IL-10, and TNF-alpha, which were reduced by at least 40% in response to ROCK inhibition. The concentrations of all these cytokines were in pg/ml, which might explain our failure to detect a band corresponding to these cytokines on Western blots. The optic nerve supernatants contained even lower concentrations of cytokines, with IL-1a, IL-12, and MIP-1a being the only detectable ones. Here, IL-12 (p40) showed a 2.3 fold increase in H-1152P treated samples, and MIP-1a had a 1.3 fold higher concentration in controls (Table 7).

(a)



(b)

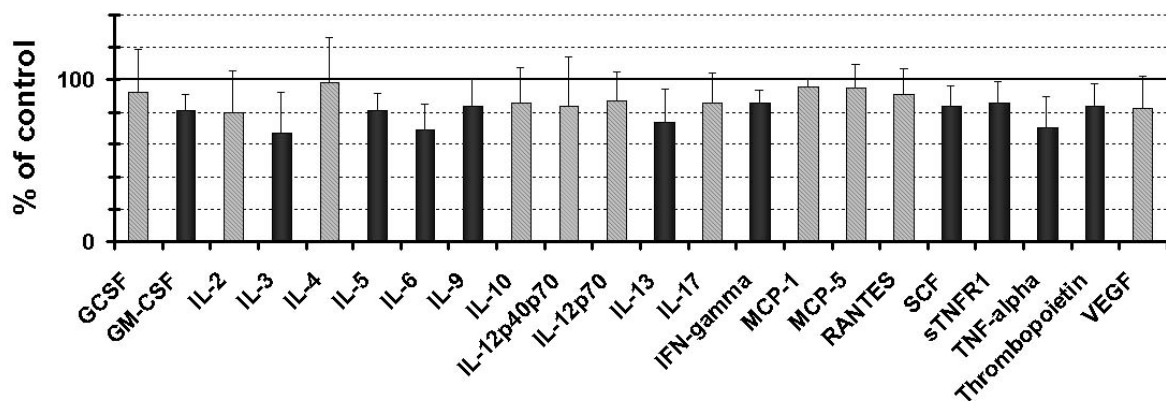


**Figure 34.** Cytokine profile of the retinal conditioned medium (a) Representative images of the spots corresponding to various cytokines on membranes incubated with the conditioned medium of untreated retinae (C) or retina incubated with 1  $\mu$ M H-1152P (H). The positive controls on each membrane are shown to allow the comparison of the spot intensity on different membranes. (b) Cytokine intensity in response to H-1152P treatment. The mean intensity value for each cytokine, calculated from 6 independent experiments, is expressed as the percentage of the intensity of that cytokine in untreated controls. Cytokines that were significantly reduced ( $p < 0.05$ ) by H-1152P are denoted in black.

**Table 7.** Cytokine concentrations (pg/ml) in the culture media after 24 hours measured by Bio-Plex assay

Cytokine	Retina		Optic Nerve	
	Control	1 $\mu$ M H1152P	Control	1 $\mu$ M H1152P
<b>G-CSF</b>	-	-	-	-
<b>GM-CSF</b>	-	-	-	-
<b>IFN-gamma</b>	0,88	-	-	-
<b>IL-1°</b>	3,86	3,72	*0,17	*0,21
<b>IL-1b</b>	10,17	4,8	-	-
<b>IL-2</b>	-	-	-	-
<b>IL-3</b>	21,33	7,29	-	-
<b>IL-4</b>	52,62	31,37	-	-
<b>IL-5</b>	-	-	-	-
<b>IL-6</b>	-	-	-	-
<b>IL-10</b>	73,67	41,85	-	-
<b>IL-12 (p40)</b>	7,17	4,31	1,18	2,78
<b>IL-12 (p70)</b>	1,97	1,87	-	*0,15
<b>IL-17</b>	-	-	-	-
<b>KC</b>	-	-	-	-
<b>MIP-1a</b>	14,61	13,7	14,61	10,9
<b>TNF-alpha</b>	19,62	10,49	-	-
<b>RANTES</b>	-	-	-	-

**G-CSF:** Granulocyte-colony stimulating factor, **GM-CSF:** Granulocyte-macrophage CSF, **IFN-gamma:** Interferon-gamma; **IL:** Interleukin; **KC:** Keratinocyte-derived chemokine, **MIP-1a:** Macrophage inflammatory protein-1 alpha, **TNF-alpha:** Tumor necrosis factor alpha; **RANTES:** Regulated upon activation normal T-cell expressed and secreted; \*value extrapolated beyond the standard range; - value below the detectable range.

### 3.2.10. Effect of H-1152P in the presence of exogenous glutathione

So far, we were able to demonstrate the neuroprotective effect of H-1152P on retinal cells in a very stringent experimental model which combined axotomy with depletion of trophic support. To improve the culture conditions and to analyze the impact of H-1152P treatment under less severe circumstances, the incubation medium was supplied with the antioxidant glutathione (GSH) and the ratio of EthD-1 positive cells in the ganglion cell layer of retinae incubated with or without H-1152P for 24 hours was determined.

Administration of glutathione into the serum-free medium induced a mild but insignificant decrease in the percentage of cell damage in untreated retinae ( $n=5$ ) as well as in retinae incubated with 0.1 ( $n=2$ ) and 1  $\mu\text{M}$  H-1152P ( $n=5$ ). However, exogenous glutathione significantly enhanced the neuroprotective effect of 20  $\mu\text{M}$  H-1152P, with the extent of cell damage decreasing from 44% (20  $\mu\text{M}$  H-1152P without glutathione) to 29.5% ( $n=5$ ,  $p<0.03$ , Figure 35).

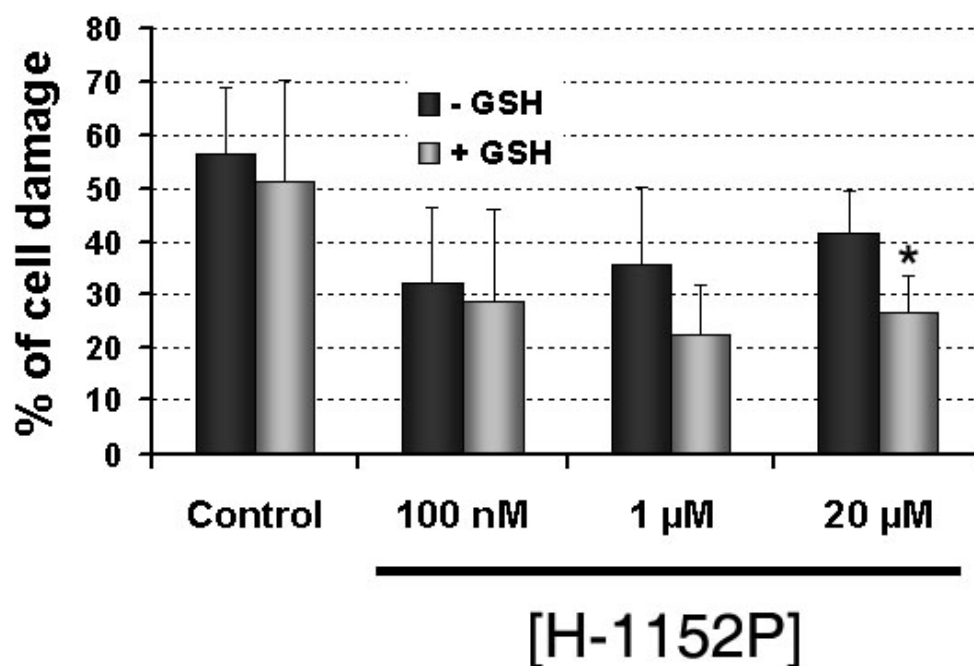


**Figure 35.** Effect of exogenous glutathione (GSH, 1 mg/ml) on cell survival in the ganglion cell layer of retinae incubated in serum-free medium for 24 hours. \* $p<0.03$ .

### 3.2.11. Effect of H-1152P on the level of total glutathione after 24 hours of serum deprivation

Having observed a glutathione dependent improvement in the neuroprotective effect of 20  $\mu\text{M}$  H-1152P, we wanted to analyze the effect of H-1152P on the levels of this antioxidant after 24 hours of serum-deprivation. With this purpose, a colorimetric assay was used for measuring the levels of total (oxidized and reduced) glutathione in freshly isolated retinae as well as in retinae incubated without serum for 24 hours.

Figure 36 demonstrates that the 24-hour incubation in serum-free medium caused a 55% decrease in the level of total glutathione in both untreated retinae and in retinae that received 1  $\mu\text{M}$  of H-1152P whereas treatment with 20  $\mu\text{M}$  H-1152P decreased the glutathione levels by 67%.

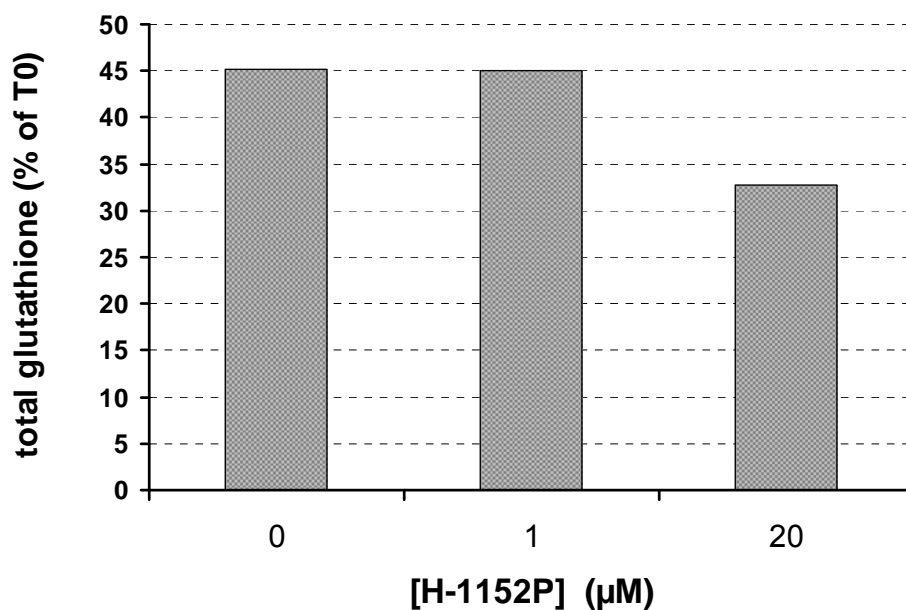


**Figure 36.** The effect of 24-hour serum deprivation and H-1152P treatment on the level of total (oxidized and reduced) glutathione in retinae. The amount of glutathione after each treatment is expressed as the percentage of the initial level (at T0).

### **3.3. Effect of ROCK-inhibition on RGC-5 cells**

#### **3.3.1. Concentration dependent effects of H-1152P on the survival of serum starved RGC-5 cells**

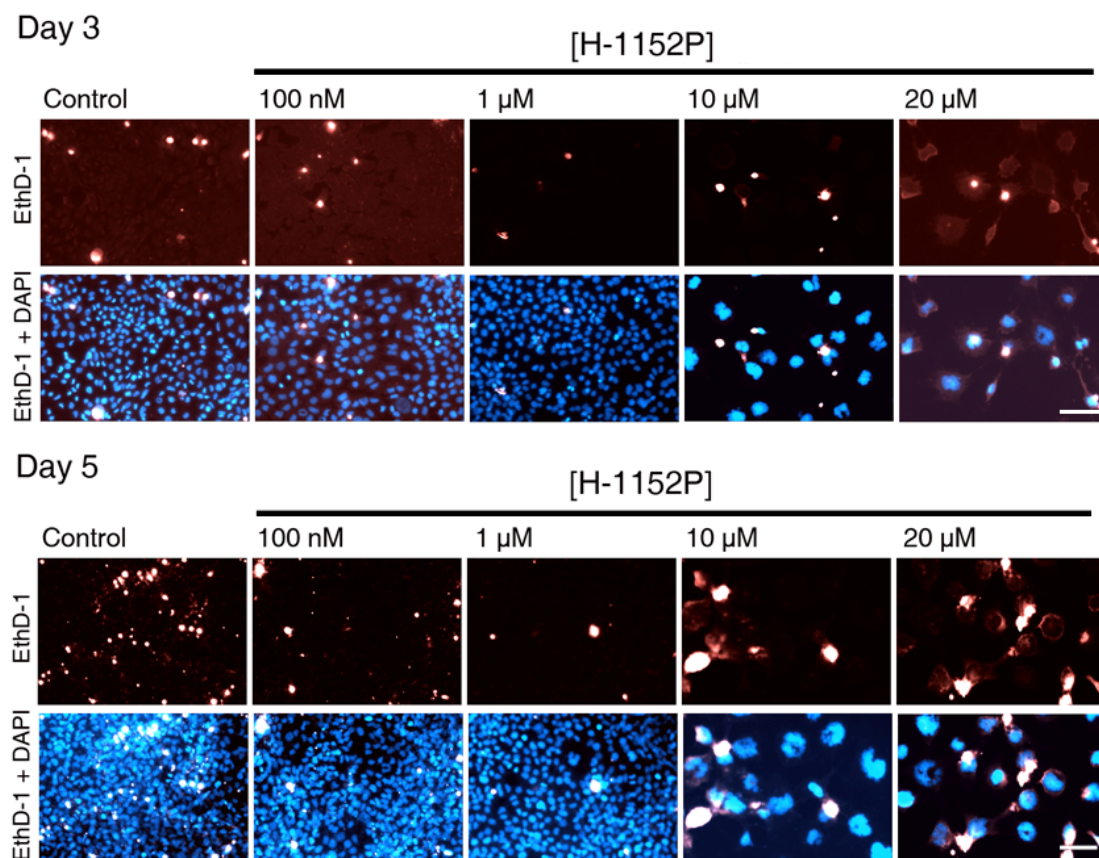
The results obtained on isolated mouse retinae favored the view that ROCK inhibition promotes the survival of retinal cells mainly by suppressing glial cell reactivity. However, the direct effect of ROCK inhibition on retinal neurons, and in particular the RGCs, remained unclear. To elucidate this question, the transformed rat ganglion cell line RGC-5, which offers an easy alternative to study the response of retinal ganglion cells in vitro was utilized.<sup>153</sup> The cells were incubated without serum to simulate the depletion of trophic support to the retinal ganglion cells as observed upon injury to the optic nerve in vivo. The extent of cell damage in RGC-5 cells incubated without serum for 3 to 5 days with various concentrations of H-1152P was then determined by EthD-1 and DAPI stainings.

In contrast to the retinal cells of the NMRI mice, the RGC-5 cells proved to be very robust and were able to proliferate even in the absence of serum (see the DAPI stainings of untreated cells after 3 and 5 days in Figure 29). After 3 days, only 15% of the cells in the control group were distinctly stained with EthD-1. H-1152P exerted a moderate protective effect resulting in 9% cell damage when introduced at 100 nM and significantly reduced the cell damage to 5% when administered at 1  $\mu$ M ( $p < 0.01$ ). However, increasing the concentration to 10 and 20  $\mu$ M led to dramatic alterations in cell morphology characterized by a 2-3 fold increase in cell diameter. In addition, a marked reduction amounting approximately to a factor of 15 was observed in the number of cells that remained in the wells after 3 days of incubation with H-1152P at these concentrations. The proportion of EthD-1 stained cells underwent a dramatical increase reaching 42% ( $p < 0.02$ ) and 50% in groups treated with 10 and 20  $\mu$ M of H-1152P, respectively. Incubation with H-1152P at concentrations above 10  $\mu$ M also led to the fragmentation of nuclei in the majority of the cells as demonstrated by the DAPI-stainings (Figure 37).



The extent of cell damage after five days of serum deprivation spread to 23% of the cells in untreated controls. The protective effect of H-1152P at 100 nM and 1  $\mu$ M concentrations became more significant at this time point, with decreases in this value to 11% ( $p<0.01$ ) and 9% ( $p<0.02$ ), respectively. However, the dramatic increases in cell volume and the amount of fragmented nuclei after treatment with 10 and 20  $\mu$ M of H-1152P were discernible at this time point as well, associated with a further rise in cell damage to 69% ( $p<0.01$ ) and 77%, respectively (Figure 37).

(a)



(b)

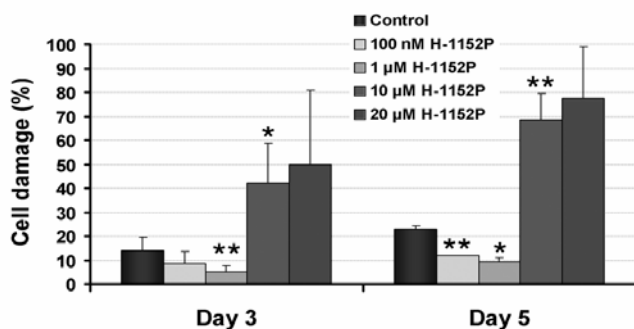


**Figure 37. (a)** Concentration dependent effect of H-1152P on the survival of serum starved RGC-5 cells after 3 and 5 days determined by EthD-1 and DAPI stainings. Bar= 100  $\mu$ m. **(b)** Percentage of damaged (EthD-1 positive) RGC-5 cells. \*:  $p<0.02$ ; \*\*:  $p<0.01$ .

### 3.3.2. Reduced caspase-3 activation in serum starved RGC-5 cells treated with H-1152P

Having observed an approximately 60% reduction in the extent of cell damage in RGC-5 cells incubated with 1  $\mu$ M H-1152P, we wanted to investigate the impact of H-1152P treatment on the progress of apoptosis in these cells. With this purpose, immunostaining for cleaved caspase-3 was performed on cells grown without serum for 1 to 5 days. After 1 day, 5% of the untreated cells were stained positively for cleaved caspase-3 and the administration of H-1152P at 1  $\mu$ M caused no considerable difference. After 2 days, this value was doubled in the controls and significantly reduced to 6.47% ( $p < 0.03$ ) in cells treated with 1  $\mu$ M H-1152P. These ratios remained unaltered until the end of day 3 whereas after day 5 the H-1152P associated decrease appeared to be no longer significant (Figure 38).

### 3.3.3. Specificity of H-1152P action in RGC-5 cells

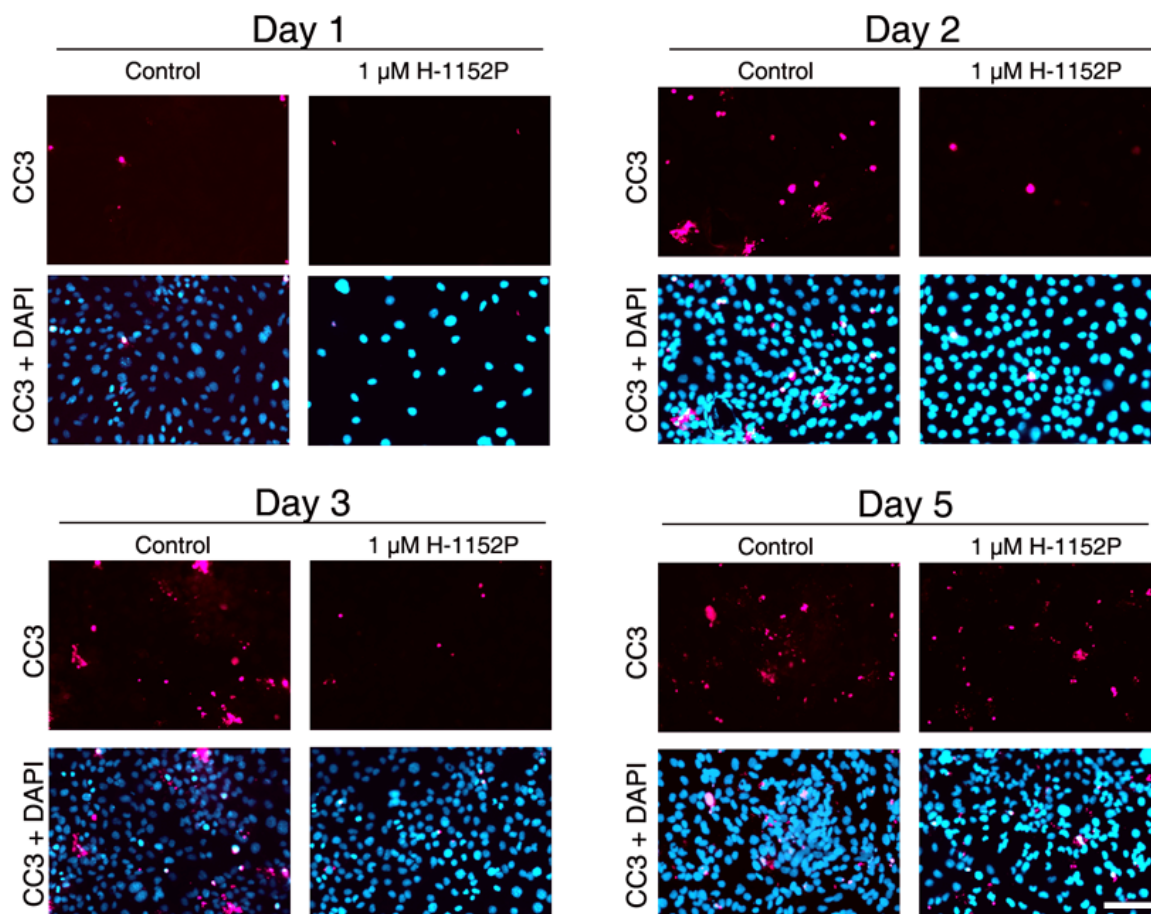
To identify the signaling pathway that is primarily targeted by H-1152P at a concentration of 1  $\mu$ M, immunostainings were performed with the adducin antibodies recognizing distinct domains phosphorylated by ROCK and PKA.

After 1 day of serum deprivation, a cytoplasmic staining of varying intensity was observed with the  $p$ -(S726)adducin antibody in RGC-5 cells regardless of the treatment. The intensity of this staining underwent a gradual decrease over 5 days in untreated cells whereas strongly stained cells were still discernible in the H-1152P treated group at this time point, suggesting that the treatment with 1  $\mu$ M of H-1152P did not interfere with the PKA-dependent phosphorylation of adducin. Interestingly, both the untreated and the H-1152P treated cells that exhibited a particularly strong staining appeared to have condensed nuclei characteristic of apoptotic cells (Figure 39).

The immunostainings with the  $p$ -(T445)adducin antibody revealed some strongly stained cells in untreated controls, the number of which considerably

increased after 3 and 5 days. In contrast, only a few positively stained cells could be detected in the group treated with 1  $\mu\text{M}$  H-1152P, suggesting the inhibition of the ROCK-dependent phosphorylation of adducin in the latter group. Untreated cells that were strongly stained with this antibody also exhibited condensed or fragmented nuclei especially during the first two days of incubation. However, the nuclei of  $p$ -(T445)adducin positive cells treated with H-1152P appeared to have undergone less shrinkage particularly at the end of day 1 and 2 (Figure 40).

(a)



(b)

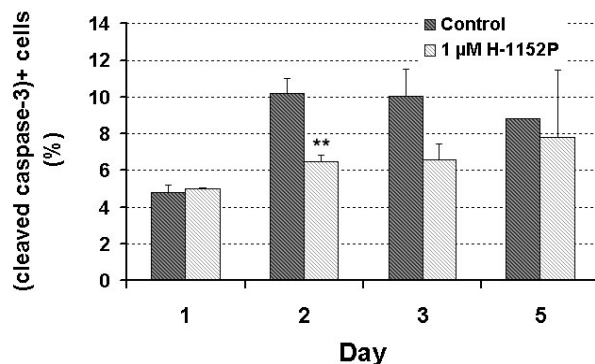


**Figure 38.** Extent of caspase-3 activation in serum deprived RGC-5 cells. (a) Immunostainings for cleaved caspase-3 (CC3) on cells treated with or without H-1152P for 1 to 5 days. Bar= 100  $\mu\text{m}$ . (b) Percentage of cleaved caspase-3 positive cells calculated from two independent experiments with duplicates for each treatment group. \*\* $p < 0.03$ .

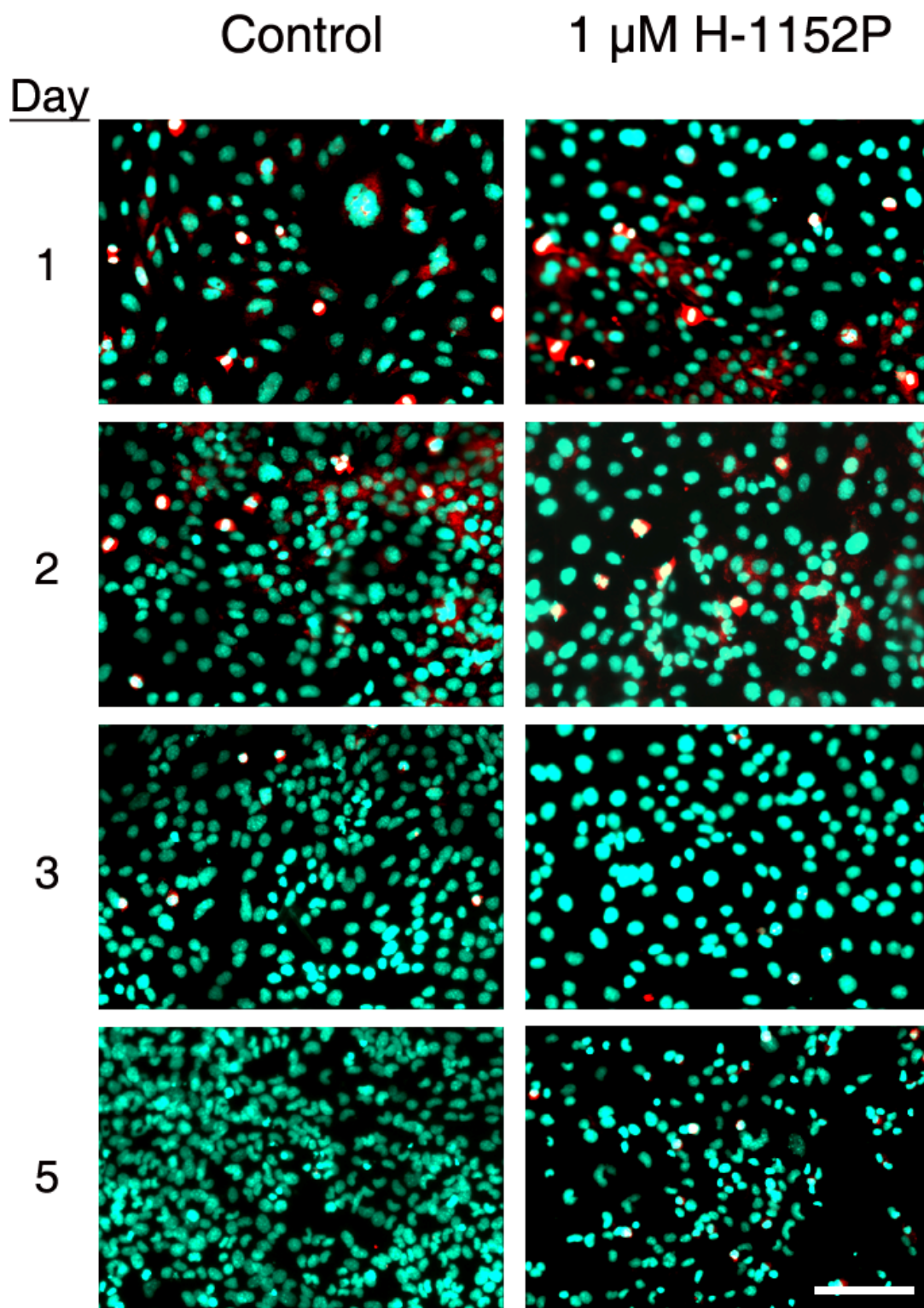


**Figure 39.** Merged images of the *p*-(S726)adducin immunostaining (red) with DAPI-staining (green) demonstrating the PKA-mediated phosphorylation of adducin as an indicator of PKA activity in RGC-5 cells treated with or without H-1152P for 1 to 5 days. Note the condensed nuclei in both untreated and H-1152P treated cells which exhibit a very strong cytoplasmic immunostaining for *p*-(S726)adducin. Bar=100 μm.



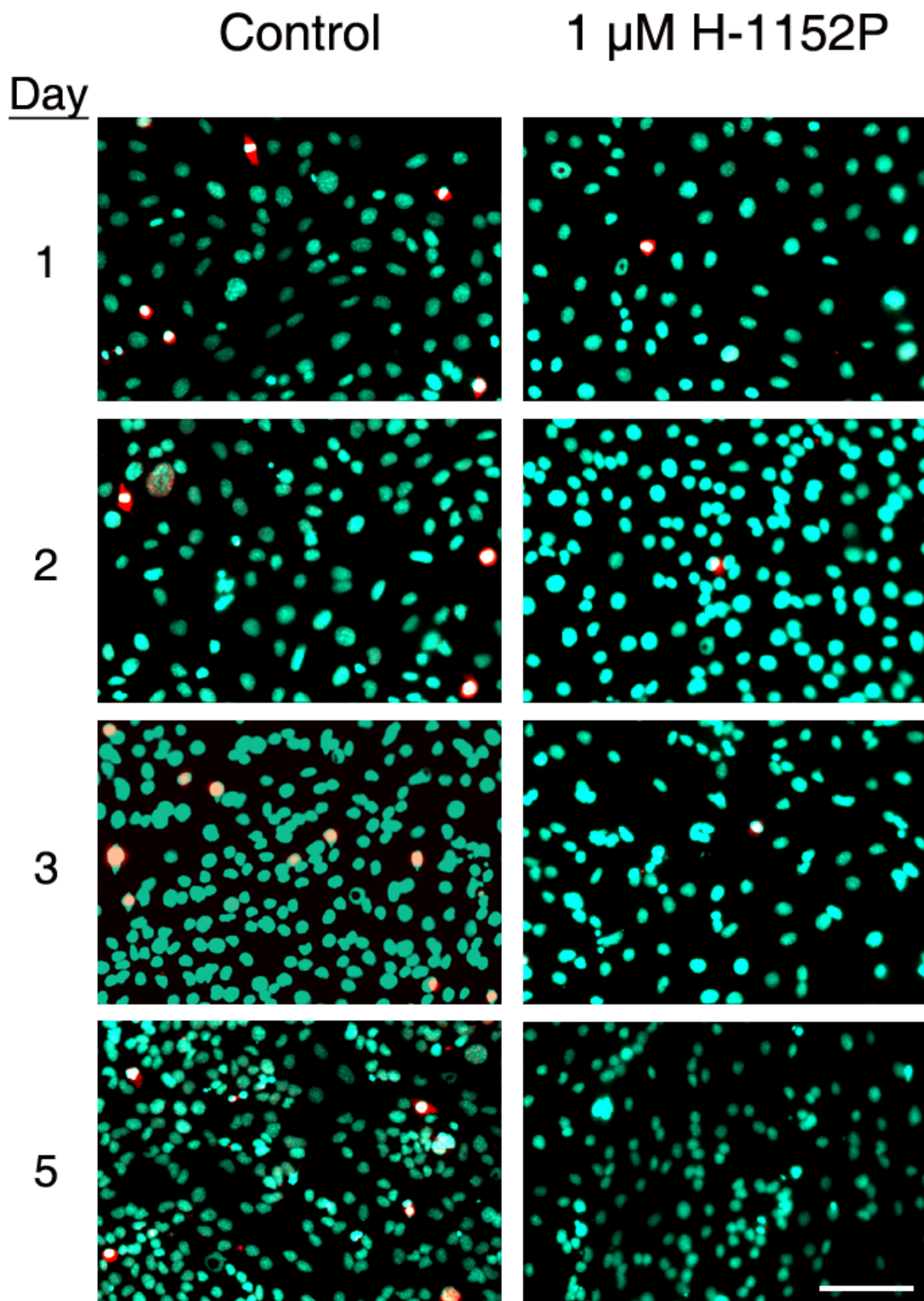


**Figure 40.** Merged images of the  $p$ -(T445)adducin immunostaining (red) with DAPI-staining (green) demonstrating the H-1152P dependent decrease in the ROCK-mediated phosphorylation of adducin in RGC-5 cells incubated for 1 to 5 days. Note that the nuclei of the H-1152P treated cells positively stained with this antibody do not exhibit a dramatic condensation as opposed to the untreated cells during the first 2 days of incubation. Bar=100  $\mu$ m.

### **3.4. Effect of ROCK-inhibition on retinal ganglion cell survival after optic nerve crush**

Based on the in vitro findings demonstrating the neuroprotective potential of H-1152P on retinal cells, we wanted to analyze the outcomes of H-1152P treatment on retinal ganglion cells in a degenerating model in vivo. With this purpose, unilateral optic nerve crush was performed in collaboration with Dr. Frank Schüttauf (University Eye Hospital, Tübingen) on rats that received intraocular injections of H-1152P (1-100  $\mu$ M) or PBS. Five days after the operation, the retrograde tracer Fluorogold was injected into the Superior colliculus to label the RGCs. The quantification of the surviving RGCs as well as the immunohistochemical analysis of glial cell reactivity were performed 1 week after the crush.

In rats that received an intraocular injection of PBS prior to the optic nerve crush, a 53% reduction was detected in the density of the retrogradely labelled RGCs in comparison to the sham-operated eyes. This considerable cell loss was accompanied by a notable glial cell reactivity, demonstrated by the strong GFAP expression in the nerve fiber layer and in Müller cells as well as the presence of CD11b positive microglia particularly in the inner and outer plexiform layers. However, injection of 1  $\mu$ M H-1152P led to a 1.6 fold increase in the density of the fluorogold positive RGCs together with a decrease in the reactivity of particularly the Müller cells and microglia compared to controls. Yet, similar to the in vitro observations, the neuroprotective effect of H-1152P was gradually weakened when the inhibitor was administered at higher concentrations prior to the optic nerve crush, with 100  $\mu$ M of this inhibitor resulting in almost the same degree of cell loss as observed in PBS-treated rats (Figure 41).

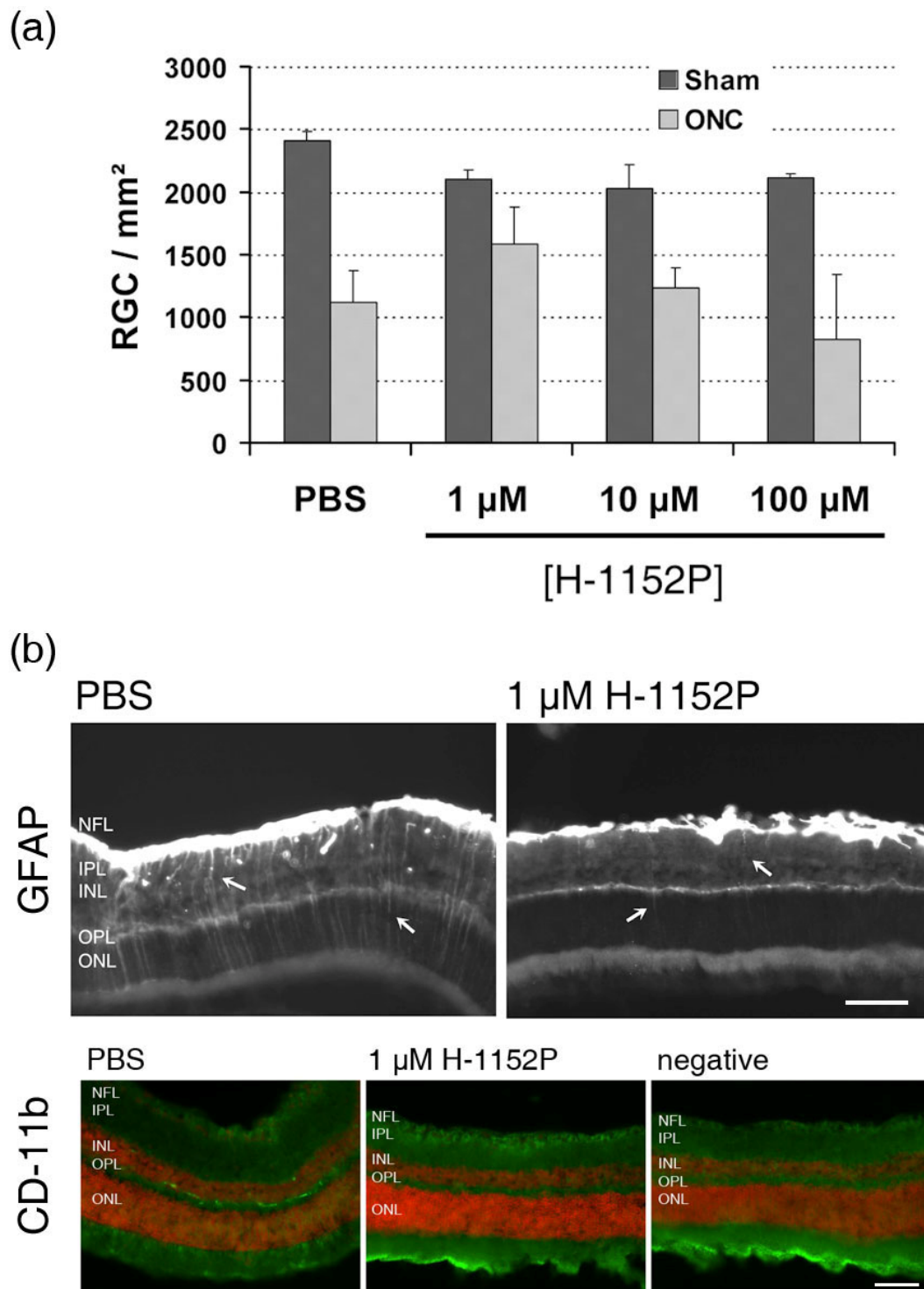


**Figure 41.** H-1152P promotes the survival of RGCs in a dose-dependent manner and reduces the glial cell reactivity after optic nerve crush (ONC). **(a)** Density of RGCs 7 days after ONC. The error bars represent the standard deviation of the RGC density determined in two rats for each group. **(b)** Immunostainings for GFAP and CD11b on transverse sections of retinæ 7 days following ONC, demonstrating the H-1152P associated decrease in the reactivity of GFAP<sup>+</sup> astrocytes in the nerve fiber layer and in Müller cells (arrows) as well as the CD11b<sup>+</sup> microglia in the inner and outer plexiform layers compared to the retina of a rat injected with PBS prior to ONC. “Negative” denotes a section from the H-1152P treated retina incubated without the CD11b antibody. Bar= 50  $\mu$ m.

## 4. DISCUSSION

### **4.1. Influence of ROCK-signaling on the wound healing activities of human Tenon's capsule fibroblasts**

The postoperative wound healing activities executed by Tenon's capsule fibroblasts result in the occlusion of the aqueous humor drainage channel created by glaucoma filtration surgery and account for the failure in lowering IOP. The present study provides further insight into the role of ROCK-mediated signaling in the regulation of the wound healing activities of human Tenon's capsule fibroblasts in vitro. Incubation of these cells with H-1152P, a highly potent inhibitor of ROCK, resulted in a dose-dependent reduction in the assembly of stress fibers, the contractile bundles of actin and myosin II which generate the tension within the cytoskeleton required for the dynamic events. This inhibitor also significantly impaired the proliferation, migration, and contractility of Tenon's capsule fibroblasts without inducing toxic effects.

The antiproliferative effect of H-1152P on Tenon's capsule fibroblasts was demonstrated by measuring BrdU incorporation and analyzing Ki-67 expression, which both showed an 80-90% decrease after 4 days of incubation with 10  $\mu$ M of this inhibitor. Owing to the absence of significant toxic effects in any of the groups, the H-1152P associated decrease in the cleavage of MTT, as determined by the MTT test, can also be interpreted as a reduction of the mitotic activity in these cells. However, the maximal decrease under these conditions was estimated to be 60% by the latter method. This discrepancy might have arisen from the parameters quantified by each procedure. The first two methods measure the extent of events which are hallmarks of cell proliferation<sup>158, 177</sup> whereas the MTT test allows for the estimation of viable cell amount based on the activity of mitochondrial dehydrogenases.<sup>154</sup> However, the mitochondrial activity may not proceed at the same level in all phases of the cell



cycle, as suggested by a study showing the decrease in adenosine triphosphatase function in HeLa cells during the S-phase and mitosis particularly within the endoplasmic reticulum and mitochondria.<sup>178</sup> A possible reduction in the activity of mitochondrial dehydrogenases during the proliferative stages might therefore have obscured the real amount of fibroblasts undergoing these phases in our assays. The MTT test nevertheless allowed for efficiently screening large amount of samples for the overall trend in cell proliferation or survival.

Regardless of the detection method used, the decrease in cell proliferation after continuous exposure to H-1152P for 4 days gained more significance in cells plated at lower densities (Figures 10 and 11), possibly due to contact-inhibition at high seeding densities, which might have withdrawn the cells from further division and accounted for a less prominent difference between the treated and untreated groups. However, a one-day exposure to this inhibitor was not as effective in suppressing the proliferation occurring on the following 3 days (Figure 13), especially under low density-seeding conditions that favoured cell division, indicating that the continuous exposure to H-1152P is necessary to cause a stronger inhibitory effect on proliferation. These findings also suggest that H-1152P present in the medium for 4 days is still able to exert an anti-proliferative effect. The significant reduction in BrdU incorporation between days 3 and 4 in cells incubated with H-1152P without replenishing this inhibitor provides further support for this view. The half-life of H-1152P under different cell-culture conditions or in vivo is to our knowledge not determined yet. However, the findings on Tenon's capsule fibroblasts reported in this study provide evidence for the stability of H-1152P even though it was not possible to predict the exact amount of the inhibitor that remained active after 4 days in culture.

Administration of H-1152P also suppressed the migration of Tenon's capsule fibroblasts on a restrained collagen matrix and into a wound area created in cell monolayers. Though it was not possible to exclude the contribution of cell proliferation from the outcomes, the majority of the cells treated with the ROCK inhibitor exhibited features suggestive of an impairment in motility, such as the absence of a distinct leading or trailing edge. The ROCK-pathway indeed plays an essential role in the protrusion of the leading edge in fibroblasts via clustering integrins, the receptors for ECM components like collagen and fibronectin, to the end

of stress fibers, and forming focal adhesions enabling the cells to adhere to the substratum.<sup>138, 179, 180</sup> Furthermore, ROCK activity coordinates the retraction of the cell rear by localizing integrin to the leading edge of migrating monocytes and promoting actomyosin-based contractility.<sup>181</sup> The H-1152P induced decrease in the amount of fibronectin deposited into ECM was another remarkable event detected in these migration assays. Fibronectin fibrils constitute a considerable portion of the wound matrix, promoting cell adhesion and providing a substrate for migration.<sup>182</sup> Assembly of the fibronectin network requires the interactions between this protein and integrin receptors as well as an intact actin cytoskeleton,<sup>183</sup> which is mediated by RhoA in a variety of cell types.<sup>184</sup> The findings obtained using H-1152P suggest the involvement of ROCK-signaling in the assembly of a fibronectin network by human Tenon's capsule fibroblasts, the impairment of which might have contributed to the reduction in the motility of these cells.

Fibroblasts cultured in collagen matrices have served as useful models to study wound contraction *in vitro*. The contraction of these gels appears to rely on the tractional forces generated by motile cells as the cells try to migrate through the matrix by drawing the proximal collagen fibers<sup>185, 186</sup> as well as on the adhesive interactions between cells and matrix.<sup>187, 188</sup> Untreated Tenon's capsule fibroblasts within a floating 3D-matrix extended rigid protrusions in contrast to the H-1152P treated cells. The distortion of these processes in the latter group of fibroblasts, possibly due to cytoskeletal instability, might have hindered the establishment of strong connections with the matrix and accounted for the H-1152P dependent reduction in lattice contraction. H-1152P also induced a less dense cellular organization and impaired the assembly of the fibronectin network within the gels. Fibronectin was indeed reported to be one of the factors promoting collagen matrix contraction.<sup>189</sup> However, cellular fibronectin, rather than the serum isoform was found to be required for this process.<sup>190, 191</sup> The H-1152P induced decrease in the assembly of a fibronectin matrix may suggest an association between the expression of this protein and ROCK activity in Tenon's capsule fibroblasts, which remains to be investigated.

H-1152P is a very potent and specific ROCK inhibitor with a K(i) value of 1.6 nM for Rho-kinase, 630 nM for protein kinase A, 9.270  $\mu$ M for protein kinase C, and

10.1  $\mu\text{M}$  for myosin light chain kinase in cell-free assays. However, higher concentrations of this inhibitor ranging between 0.1-10  $\mu\text{M}$  were required for the suppression of ROCK in NT-2 cells,<sup>163</sup> possibly due to competition with intracellular ATP present at the micromolar range.<sup>192</sup> The observations on Tenon's capsule fibroblasts support these findings and underscore the need for high doses of this molecule for ROCK-inhibition in cell-based assays. However, this increases the risk of unintentionally targeting other kinases, with PKA being the most likely candidate owing to the relatively lower  $K_i$  value of H-1152P for this kinase. PKA is a ubiquitously expressed intracellular signaling molecule that regulates ion channel conductivity, gene transcription, cell metabolism, actin cytoskeletal dynamics, and migration.<sup>193</sup> PKA can also directly phosphorylate and inactivate RhoA.<sup>194, 195</sup> This broad spectrum of functions, some of which antagonizing the activity of ROCK, may therefore give rise to complications or weaken the effects when an inhibitor showing differential affinity for both kinases is applied at high concentrations. To ascertain that the PKA pathway was not influenced by H-1152P in Tenon's capsule fibroblasts, the phosphorylation level of adducin isoforms at S726/S662 was analyzed as an indicator of PKA activity. The PKA mediated phosphorylation of adducin mainly at S726 causes its dissociation from the F-actin cytoskeleton in vitro. The supernatants of the cell lysates collected after centrifugation at 12000 rcf in this study are expected to contain both the cytoskeleton bound and the dissociated forms of adducin.<sup>196</sup> Immunoblots performed using these extracts revealed no significant change in the levels of  $p$ -alpha-adducin and only a slight decrease in the level of  $p$ -gamma-adducin that did not become more pronounced at increasing concentrations of H-1152P. Though the reason of this decrease remains to be elucidated, these findings favour the view that H-1152P exerted its effects on Tenon's capsule fibroblasts without considerably interfering with PKA activity at the concentrations tested.

Taken together, these data demonstrate that ROCK is involved in the execution of essential dynamic events in human Tenon's capsule fibroblasts and H-1152P specifically inhibits this multifunctional kinase without inducing toxic effects. This, in turn, highlights the potential of H-1152P as an effective and safe means of suppressing the undesirable wound healing activities of these cells for improving the success rate of glaucoma filtration surgery.

## **4.2. Influence of ROCK-signaling on retinal cell survival**

The rearrangements in the actin cytoskeleton which underly the morphological changes in apoptosis and axon retraction are regulated mainly by the activation of RhoA and its downstream effector ROCK. Inhibition of the ROCK-mediated signaling therefore emerges as an effective therapeutic strategy for promoting not only neuronal survival but also axon regeneration and deserves further investigation. Here, we aimed to analyze the influence of this signaling pathway on retinal cell survival and to characterize certain intra- and extracellular changes associated with it by using the ROCK inhibitor H-1152P in mouse retinal explant cultures as well as on a transformed retinal ganglion cell line and prior to optic nerve crush. These analyses were also necessary for evaluating the safety of H-1152P on retinal cells before considering the pharmacological use of this inhibitor for suppressing the wound healing activities of Tenon's capsule fibroblasts.

### **4.2.1. Effect of ROCK inhibition on retinal cell survival in isolated mouse retinae under serum deprivation**

The axotomy of the ganglion cells in the retinal explant culture model deprives the cells of their efferent synapses and trophic support, and results in the retrograde death of the ganglion cell bodies. However, the preservation of the multilayered retinal cell architecture to a greater extent in this model<sup>197</sup> allowed for studying the response of the various cell types to treatment. The extent of cell damage under these stringent conditions, as determined by the ethidium homodimer-1 staining reached 57% in the ganglion cell layer of untreated retinae after 24 hours. The severity of cell damage might be even higher than this estimation, as suggested by the cleaved-caspase 3 immunostaining demonstrating 75% of the cells in the ganglion cell layer to be positive for this apoptosis executor. However, the intensity of the cleaved-caspase 3 immunostaining was not of equal strength in all the cells, as reflected by the standard deviations. This in turn points to the possibility that the cells in a certain retinal layer might be undergoing different phases of apoptosis. Since the cell membrane permeability is not dramatically altered in the early phases of

apoptosis, cells at this stage are likely to have little or no ethidium homodimer-1 uptake, accounting for the relatively low value for the extent of cell damage determined by this staining.

The high rate of cell damage, possibly due to the combination of serum deprivation with axotomy, is very likely to be alleviated by improving the culture conditions. Supplying the medium with serum or growth factors would allow for a higher rate of cell survival and is indeed indispensable when longer incubations are considered. However, even under these unfavorable conditions, administration of H-1152P at 1  $\mu$ M resulted in a significant reduction by 40% in the extent of cells stained with ethidium homodimer-1 and 27% in the amount of cleaved-caspase 3 positive cells in the ganglion cell layer after 24 hours. This protective effect on axotomized ganglion cells and presumably the displaced amacrine cells prompted us to concentrate our work on the characterization of the intra- and extracellular changes induced by 1  $\mu$ M of this inhibitor.

Being very critical determinants of neuronal homeostasis as well as the degree of secondary injury after a primary damage or stress in the CNS, reactive astrocytes play fundamental roles in neuronal survival.<sup>96</sup> Astrocyte reactivity after CNS injury is characterized by an increase in astrocyte proliferation and the upregulation of the intermediate filament GFAP.<sup>60</sup> Immunostainings performed using anti-GFAP antibodies on serum-deprived mouse retinae demonstrated increased astrocyte reactivity particularly around the retinal vasculature in untreated controls, similar to the case observed in glaucomatous human eyes.<sup>62</sup> This increase might bear pathological significance, since reactive astrocytes are known to produce extracellular matrix molecules like elastin and tenascin as well as the mitogen/vasoconstrictor endothelin, the accumulation of which around the blood vessels might impair retinal perfusion.<sup>45, 198</sup> On the other hand, incubating retinal explants with H-1152P allowed for the maintenance of the GFAP levels closer to the basal values and led to a reduction in the reactivity of both the astrocytes particularly around the retinal blood vessels and the Müller cells.

The suppression of GFAP upregulation in the presence of H-1152P suggests that ROCK signaling may be involved in the regulation of GFAP expression. Among the various modulators of GFAP expression, epidermal growth factor, transforming growth factor-beta, and fibroblast growth factor are known to activate the RhoA pathway to regulate diverse cellular events.<sup>199-202</sup> The decrease in the number of GFAP+ astrocytes after H-1152P treatment might also be attributed to the impairment of astrocyte proliferation, considering that the ROCK mediated phosphorylation of GFAP is necessary for the cytokinetic segregation of glial filaments.<sup>203</sup> To investigate the outcomes of H-1152P treatment on astrocyte/Müller cell proliferation, we are planning to incubate the retinae with BrdU in the absence or presence of H-1152P, and detect the proliferating cells that have incorporated BrdU into their DNA by performing double-immunohistochemistry using antibodies recognizing BrdU and cell-specific antigens.

The Western blot analysis suggests that the upregulation of GFAP in isolated retinae under serum deprivation is confined particularly to the lower molecular weight isoforms. Such isoform specific differences, arising presumably from post-translational modifications of GFAP, have been related to the course of various neurodegenerative disorders. For instance, the increase in the levels of the smaller molecular weight GFAP isoforms in the spinal cord of motor neuron degeneration (*Mnd*) mice correlates with the degenerative loss of motor neurons and the onset of behavioral paralytic gait in these animals. These lower molecular weight isoforms are likely to be generated by the phosphorylation of GFAP at the head domain via unknown factors and the subsequent cleavage of the full length protein.<sup>204</sup> The hyperphosphorylation of GFAP was indeed observed in rat hippocampus after transient global cerebral ischemia,<sup>205</sup> and a 60% increase in the amount of more acidic GFAP isoforms, which were both phosphorylated and N-glycosylated, was detected in the post-mortem brains of Alzheimer's disease patients.<sup>173</sup> The ROCK-inhibition dependent decrease in the levels of not only the full-length 49 kDa protein, but also the lower molecular weight GFAP isoforms might therefore suggest a possible interference with the post-translational modifications of GFAP, such as its phosphorylation at the head domain, which is also worthy of investigation.

Interestingly, inhibition of the ROCK pathway in astrocytes leads to cytoskeletal rearrangements characterized by the loss of actin stress fibers and focal adhesions, which promote astrocyte stellation.<sup>206</sup> Though this finding may sound contradictory to our results at first, it may accentuate the therapeutic potential of ROCK inhibition on promoting neuronal survival. By favoring astrocyte stellation, ROCK inhibition may help to preserve the basal astrocyte network that allows for the interaction of astrocytes with neurons and endothelial cells, which is critical for the maintenance of normal neuronal activity and blood-brain barrier. On the other hand, ROCK-inhibition reduces the extent of astrocyte and Müller cell reactivity by interfering with GFAP upregulation and/or possibly cell proliferation. This may in turn decrease the amount of reactive oxygen species, matrix metalloproteinases, and proinflammatory cytokines released by reactive glial cells and help to limit the spread of secondary damage after CNS injury.

The hypothesis suggesting that ROCK-inhibition protects the retinal cells indirectly by suppressing the reactivity of glial cells and the possibly associated release of certain proteins/molecules is further supported by the findings demonstrating the H-1152P associated decrease in the release of various proteins into the culture media of retinae and optic nerve, and the reduction in the toxicity of these conditioned media. The 24-hour incubation of freshly prepared retinae with the conditioned medium of untreated retinae gave rise to a significant increase in the extent of cell damage from 57% to 72% ( $p < 0.05$ , Figure 30). This considerable increase in cell damage could not be solely attributed to the molecules released from the untreated retinae, since the 24-hour incubation period of the retinae was expected to result in the uptake of nutrients, and the release of metabolic wastes, both of which decreasing the quality of the medium. However, the culture medium of the retinae incubated with 1  $\mu$ M of H-1152P resulted in a significantly lower damage of approximately 43%, suggesting the presence of other factors apart from the quality of the medium, which could be altered in the presence of H-1152P. Addition of the ROCK-inhibitor later into the conditioned medium from untreated retinae appeared less effective in promoting recovery, with 58% cell damage in the ganglion cell layer. The incubations with the conditioned media of optic nerve pieces also yielded similar results, favoring the view that H-1152P might be exerting its protective effect mainly

by reducing the amount of certain secreted molecules, and probably to a less extent by directly inhibiting their activity.

The further analysis of these conditioned media by both a membrane-based and a flow-cytometric cytokine array demonstrated the release of various cytokines into the culture medium after 24 hours of serum deprivation. Despite some differences in the detection range of these assays, possibly due to the antibodies used in each procedure, the majority of the cytokines were found to be present at higher concentrations in untreated controls compared to the H-1152P treated retinae. Among the cytokines which underwent a significant reduction in response to H-1152P, TNF-alpha is a major proinflammatory molecule upregulated in glaucomatous retinae and optic nerve heads, and a key inducer of the retinal ganglion and lamina cribrosa cell death.<sup>71, 83, 207</sup> TNF-alpha, IL-1beta, and IFN-gamma also activate the inducible nitric oxide synthase in glia,<sup>208</sup> causing massive NO production which destroys the neighbouring cells. Furthermore, IFN-gamma regulates the synthesis of various cytokines and increases the immunogenic capacity of human brain and lamina cribrosa astrocytes which might be responsible for an autoimmune response.<sup>92</sup> Likewise, overexpression of IL-3 in transgenic mice causes an autoimmune reaction to motor neurons with several features of amyotrophic lateral sclerosis and progressive muscular atrophy.<sup>209</sup> IL-4 was reported to aggravate experimental autoimmune uveitis in rats<sup>210</sup> whereas IL-10 had increased serum levels in glaucoma patients compared to age-matched controls, and like IFN-gamma, it increased the immunogenic capacity of human brain and lamina cribrosa astrocytes.<sup>92</sup> However, conflicting results supporting a neuroprotective role for IL-4 and IL-10 in axotomized retinal ganglion cells or cell lines were also reported.<sup>211-212</sup>

A similar controversy exists regarding the role of the proinflammatory cytokine IL-6, which underwent a 30% reduction in the incubation medium of H-1152P treated retinae, on retinal ganglion cell survival. An earlier study with IL-6 knockout (-/-) mice reports an increase in the number of retinal ganglion cells in these animals after optic nerve crush or glutamate toxicity compared to their wild-type counterparts, suggesting the involvement of IL-6 in neurodegenerative events.<sup>213</sup> However, in another in vivo study, the intravitreal injection of IL-6 immediately following ischemia-



reperfusion injury in rats led to an increase in the number of fluorochrome labeled retinal ganglion cells.<sup>214</sup> Likewise, incubation of isolated retinal ganglion cells with recombinant IL-6 under elevated pressure was reported to have reduced the percentage of TUNEL+ (apoptotic) cells by almost 60% and doubled the cell density.<sup>215</sup> IL-6 might indeed be exerting a protective effect when applied directly on retinal ganglion cells. However, the outcomes of IL-6 treatment might vary depending on the levels of this cytokine, which in some cases may support ganglion cell survival whereas in other cases may give rise to cell death possibly by favouring an excessive immune response. The type of injury and the cellular and molecular factors activated in turn are likely to be the further critical factors shaping the outcomes of IL-6 activity. The balance between the levels of various immunomodulators, rather than the individual molecules themselves is indeed the currently considered decisive factor that may be regulating the conversion of an initially neuroprotective immune response to a neurodegenerative inflammatory or autoimmune reaction.<sup>216</sup>

Soluble cytokine receptors constitute a noteworthy class of immunomodulators owing to the agonistic or antagonistic effects they exert on cytokine activity. These receptors can be generated via several mechanisms, such as the proteolytic cleavage of receptor ectodomains, alternative splicing of membrane receptor transcripts, transcription of genes encoding soluble receptors, release of full-length receptors in exosome-like vesicles, or the cleavage of GPI-anchored receptors.<sup>176</sup> To analyze whether these proteins are also released into the retinal culture medium under serum deprivation, we would like to perform Western blot analysis using monoclonal antibodies recognizing sequences present only in individual soluble/solubilized receptors. We are also planning to subject the unknown bands of ~50 kDa size detected by several anti-cytokine antibodies on the Western blots (Figure 31) to protein sequence analysis, in order to identify these proteins, the levels of which exhibit a considerable decrease upon H-1152P treatment.

H-1152P is the most specific and effective ROCK-inhibitor that is currently available.<sup>151</sup> This inhibitor reduced the extent of cell damage on the ganglion cell layer by 40% without interfering with the PKA-pathway when applied at 1  $\mu$ M to isolated retinae incubated without serum. However, increasing the concentration to

20 and 100  $\mu\text{M}$  decreased its protective effect. A noteworthy feature detected on retinae treated with 20  $\mu\text{M}$  H-1152P was the further decrease in glial cell reactivity, with only a few GFAP-positive astrocytes on the nerve fiber layer and almost no activated Müller cells. Interestingly, the level of total glutathione in these retinae was also considerably lower as compared to untreated controls or retinae incubated with 1  $\mu\text{M}$  H-1152P. Glutathione, a thiol tripeptide composed of glutamate, cysteine, and glycine, is the most abundant intracellular reducing agent in animal cells.<sup>217</sup> Owing to the cysteine residue, glutathione can be non-enzymatically oxidized to glutathione disulfide by electrophilic substances such as free radicals and reactive oxygen/nitrogen species, allowing for the detoxification of these molecules.<sup>217, 218</sup> The synthesis of glutathione is sequentially catalyzed by the cytosolic enzymes  $\gamma$ -glutamylcysteine synthetase and GSH synthetase.<sup>219</sup> Though this pathway occurs in virtually all cell types including neurons, the astrocytes and Müller cells constitute the major source of glutathione in the retina due to the abundance of the enzymes involved in GSH metabolism in these cells.<sup>217, 220-222</sup> The synthesis and regeneration of glutathione as well as the expression of various antioxidant enzymes undergo a further increase in astrocytes and possibly the Müller cells following gliosis,<sup>223-225</sup> accentuating the neuroprotective potential of a certain degree of glial cell reactivity for maintaining the integrity and survival of retinal neurons under stress conditions. The observations regarding the further decrease in reactive gliosis and the possibly associated reduction in the levels of total glutathione in retinae treated with increased concentrations of H-1152P might therefore provide an explanation to the decline in the protective effect of H-1152P when applied at higher concentrations. It remains to be determined whether the reduction in glutathione levels at elevated concentrations of H-1152P arises secondarily to the dramatic decrease in glial cell reactivity or due to a direct interference with the synthesis or activity of the enzymes involved in GSH metabolism upon the inhibition of ROCK or possibly the PKA. Nevertheless, the preliminary data demonstrating the improvement in the protective effect of 20  $\mu\text{M}$  H-1152P when coadministered with glutathione and the significant reduction in cell damage compared to the retinae treated with glutathione alone points to additional mechanisms regulating retinal cell survival under stress, the H-1152P dependent inhibition of which providing beneficial outcomes.

Altogether, these *in vitro* data on isolated retinae demonstrate the neuroprotective potential of H-1152P on retinal cells particularly in the ganglion cell layer. The H-1152P mediated ROCK inhibition was associated with a decrease in the reactivity of astrocytes and Müller cells, caused presumably by an interference with the upregulation or post-translational modification of GFAP. The preliminary data on the response of microglia also demonstrated an H-1152P dependent reduction in the activation of these cells. The impairment of glial cell reactivity by H-1152P might be indirectly protecting retinal cells from the spread of secondary injury by reducing the amount of immunomodulatory cytokines and possibly other diffusible factors like nitric oxide, which remain to be characterized in more detail. The adverse effects which may arise from a further reduction in glial cell reactivity and the possibly associated decrease in the antioxidant levels at higher concentrations of H-1152P are likely to be overcome by coadministering glutathione, which improves the protective potential of this inhibitor. These findings not only indicate the beneficial effects of H-1152P on retinal cells under stress, but also provide more insight into the role of ROCK-signaling in glial cell reactivity and the impact of this process on the survival of retinal cells under stress conditions.

### **4.2.2. The concentration dependent effects of H-1152P on the survival of RGC-5 cells**

Characterizing the direct response of the retinal ganglion cells to ROCK-inhibition constituted an essential part of this study, since the ganglion cells encounter the primary damage in optic neuropathies like glaucoma. However, the isolation of adult retinal ganglion cells is a labor-intensive process yielding a low amount of homogenous cell population. Being very easy to cultivate and maintain in culture, the immortalized rat ganglion cell line RGC-5 offers a practical alternative for studying the response of retinal ganglion cells *in vitro*. Therefore, the RGC-5 cells cultivated without serum were utilized to estimate the direct outcomes of H-1152P treatment on retinal ganglion cells.

Interestingly, the incubation of RGC-5 cells without serum failed to induce a massive cell death in untreated controls (23% cell damage after 5 days estimated by the EthD-1 and DAPI stainings, Figure 37) in contrast to the cells in the ganglion cell layer of serum-deprived retinal explants (57% and 72% cell damage after 1 and 2 days, respectively; Figures 20 and 21). The extent of apoptosis in RGC-5 cells also appeared to be considerably lower, with only ~9% of the untreated cells being positive for cleaved-caspase 3 as opposed to the 75% positive staining on the ganglion cell layer of retinal whole mounts (Figures 38 and 28, respectively). These findings demonstrating the stability of RGC-5 cells in turn raise the question of how well this transformed cell line represents the characteristics of a mature, primary retinal ganglion cell.

The RGC-5 cell line was generated by transforming retinal cells isolated from postnatal day 1 rats with the early region 1A of the adenovirus type 12 genome, which leads to the immortalization of nonpermissive primary rodent cells *in vitro* and *in vivo*. The single cell clones from the transformed cells were then screened randomly for the expression of various cell-specific markers. The RGC-5 cell line was reported to be retaining many features of retinal ganglion cells including the expression of the marker protein Thy-1 and NMDA receptors as well as the sensitivity to excessive glutamate levels and neurotrophin withdrawal.<sup>153</sup> However, the electrophysiologic properties of the undifferentiated RGC-5 cells were found to be differing considerably from that of the primary retinal ganglion cells, possibly due to the diversity of the ion channel repertoire of both cell types.<sup>226</sup> Recently, treating the RGC-5 cells with the broad-spectrum kinase inhibitor staurosporine for as little as 60 seconds was reported to result in nondividing cells with multiple branched neurites characteristic of a neuronal morphology. Interestingly, treatment with 1  $\mu$ M of H-1152P or the less specific inhibitor H-89 which primarily inhibits PKA also induced a mild increase in the neurite counts of RGC-5 cells in the same study. However, despite these features suggestive of a more differentiated phenotype, no evidence of functional synapses could be detected.<sup>227</sup> These observations therefore underscore the need for more cautious evaluation before considering the results obtained with the RGC-5 cell line as evidence for the mechanisms operating in primary retinal ganglion cells.

The protective effect of H-1152P administration at 0.1-1  $\mu$ M on serum-deprived RGC-5 cells and the specificity of this inhibitor analyzed for the latter concentration nevertheless provide further support for the hypothesis concerning the anti-apoptotic outcomes of ROCK-inhibition. Though the extent of apoptosis was mainly determined by performing immunostainings for cleaved caspase-3, the nuclear morphology, which exhibited a more condensed phenotype in the majority of the cells stained strongly for EthD-1 and cleaved caspase-3 provided further evidence for apoptosis. Interestingly, the cells displaying a very strong cytoplasmic staining for *p*-(S726)adducin also possessed condensed nuclei characteristic of apoptotic cells. The phosphorylation of adducin at S726 was, as mentioned previously, reported to be reducing its affinity for F-actin and causing its dissociation from the actin-spectrin complex, accounting for a more cytoplasmic rather than a cortical staining pattern.<sup>165, 196</sup> This phosphorylation event is also implicated in the loss of cell-cell interactions, which eventually activates the apoptotic machinery, indicating the involvement of the PKA-pathway in the execution of apoptosis as well.<sup>170</sup> Yet, this staining pattern was strongly diminished after 3 and 5 days in both treatment groups, suggesting that the PKA-activity is likely to be functioning in the earlier phases of apoptosis. However, there is also evidence for the caspase-3 mediated cleavage of *p*-(S726)adducin in RPTE cells, yielding fragments of 74 and 12 kDa which lack or contain the S726 residue recognized by the *p*-(S726)adducin antibodies, respectively (Figure 24).<sup>170</sup> This in turn raises the possibility that the increase in caspase-3 activation after 2 days might have resulted in the cleavage of the *p*-(S726)adducin in RGC-5 cells. It would be therefore interesting to determine whether adducin undergoes proteolytic cleavage in serum-deprived RGC-5 cells and whether the *p*-(S726)adducin antibody can recognize the hypothetical 12 kDa fragment, to find out whether the decrease in the intensity of *p*-(S726)adducin immunostaining arises due to the inability of the antibodies to bind to the 12 kDa fragment. Nevertheless, the similarities of the staining patterns in the treated and untreated groups and the presence of some stained cells in the H-1152P-treated group even after 5 days weaken the possibility of unspecific PKA-inhibition via 1  $\mu$ M H-1152P in RGC-5 cells.

The specificity of H-1152P administered at 1  $\mu$ M was also confirmed by the immunostainings for *p*-(T445)adducin performed on RGC-5 cells after 1 to 5 days of incubation. The ROCK-mediated phosphorylation of adducin at T445 was found to be confined exclusively to the cells having condensed or fragmented nuclei in the untreated group. The number of stained cells also exhibited a considerable increase after 3 and 5 days together with the rise in the extent of damage in the untreated cells. In contrast, only a few positive cells could be detected among the group incubated with 1  $\mu$ M of H-1152P at each time point analyzed, demonstrating the effective inhibition of the ROCK-pathway via H-1152P and the possible association of this event with the increase in the survival rate of RGC-5 cells. As opposed to the phosphorylation at S726, the phosphorylation of adducin at T445 enhances the adducin-actin interactions.<sup>228</sup> Though this ROCK-dependent phosphorylation was found to be crucial for the ruffling of the plasma membrane at the leading edge of migrating cells,<sup>169</sup> no report concerning the significance of this event during apoptosis exists to our knowledge. However, the ruffling of the plasma membrane is also required for the cell budding, which facilitates the packaging of the cellular content into membrane-bound apoptotic bodies.<sup>229</sup> Therefore, the ROCK-mediated signaling might not only be involved in the cellular contraction, but may also account for the membrane ruffling and cellular budding observed in apoptotic cells. The considerable increase in the intensity of the *p*-(T445)adducin staining in untreated cells after 3 to 5 days and the H-1152P dependent decrease in the phosphorylation of adducin at T445 might therefore provide further evidence for the mechanisms underlying the anti-apoptotic effect of ROCK-inhibition in RGC-5 cells.

Interestingly, the anti-apoptotic effect of H-1152P achieved at 1  $\mu$ M was replaced by a significant toxicity when this inhibitor was administered at 10-20  $\mu$ M. A similar reduction in the protective effect of this inhibitor at higher concentrations was also observed in isolated mouse retinae in this study, possibly due to an interference with glutathione synthesis secondary to the dramatic decrease in glial cell reactivity. However, there was no increase in toxicity even in the presence of 100  $\mu$ M H-1152P on the ganglion cell layer of these retinae (Figure 20). The unexpected observations on RGC-5 cells cultured in isolation with high concentrations of H-1152P therefore appear to contradict the hypothesis concerning the anti-apoptotic effects of ROCK-

inhibition at the first glance. However, the striking alterations in the morphology of the RGC-5 cells treated with 10-20  $\mu\text{M}$  H-1152P provide clues about the prevailing of another cell death program in these cells matching the features of oncosis.

Oncosis, as opposed to apoptosis, defines a programmed cell death mechanism characterized by a marked cell swelling. Though the term oncosis, derived from the Greek word for swelling, was introduced almost a century ago, it has found increased acceptance only recently to designate the events which were formerly ascribed to necrosis. Currently, apoptosis and oncosis are considered as pre-mortal processes executed by different “programs” whereas the term necrosis refers to the features appearing after a cell has died. The oncotic pathway can be activated mainly by prolonged energy depletion and hyperoxia.<sup>229-231</sup> The major morphological changes in the cells undergoing oncosis include the disruption of the actin cytoskeleton, cytoplasmic blebbing, dilatation of the endoplasmic reticulum, swelling of the cytosol and nuclei, normal or condensed mitochondria, and an increase in membrane permeability without any detectable caspase-3 activity. However, oncotic cells can also share some common features with the apoptotic cells, like the exposure of the phosphatidylserine residues on the outer leaflet of the plasma membrane, as well as DNA fragmentation and chromatin condensation in some instances.<sup>229, 232</sup> Though the molecular mechanisms of oncosis are not elucidated in detail yet, the excessive  $\text{Na}^+$  influx due to the dysregulation of the ionic channels on the plasma membrane appears to play a significant role by allowing  $\text{Ca}^{2+}$  entry into the cells.  $\text{Ca}^{2+}$  then activates calpains, a family of  $\text{Ca}^{2+}$  activated neutral cysteine proteases, which cleave various proteins of the cytoskeleton and plasma membrane, accounting for the proteolytic degradation in various cells types undergoing oncosis.<sup>233, 234</sup>

In neurons, the influx of  $\text{Na}^+$  is mediated by the voltage gated  $\text{Na}^+$  channels distributed along the axons.<sup>235</sup> However, the channel subtype expressed exhibits diversity depending on the myelination level of the axon. In the mammalian CNS, the  $\text{Na}_v1.2$  subtype is mainly present on unmyelinated axons whereas the  $\text{Na}_v1.6$  subtype is localized to the initial segments and the nodes of Ranvier on myelinated axons.<sup>236-238</sup> The  $\text{Na}^+$  gradients experience a particularly tight regulation in neurons,

since the inward current of this ion causes the membrane depolarization which underlies the generation of action potentials.<sup>235</sup> However, the maintenance of the ionic gradients can be impaired under pathological conditions. For instance, the depletion of ATP during ischemia results in the failure of the Na<sup>+</sup>-K<sup>+</sup> ATPase. The Na<sup>+</sup> ions can then leak into the axoplasmic space through incompletely activated Na<sup>+</sup> channels. This influx of Na<sup>+</sup> causes the operation of the Na<sup>+</sup>/Ca<sup>2+</sup> exchanger in the reverse fashion, and gives rise to the accumulation of Ca<sup>2+</sup> at damaging levels in the neurons, producing irreversible injury.<sup>239</sup> The expression pattern of the Na<sup>+</sup> channels can also be altered under pathological conditions, as demonstrated by the expression of both the Na<sub>v</sub>1.2 and Na<sub>v</sub>1.6 subtypes along demyelinated axons in the white matter from mice with experimental autoimmune encephalomyelitis (EAE) and in human white matter from acute multiple sclerosis (MS) plaques. Interestingly, the Na<sub>v</sub>1.6 channel was colocalized with the Na<sup>+</sup>/Ca<sup>2+</sup> exchanger in injured axons in both EAE and MS whereas the Na<sub>v</sub>1.2 was expressed often together with the Na<sup>+</sup>/Ca<sup>2+</sup> exchanger along demyelinated axons without signs of injury.<sup>240, 241</sup> Since the Na<sub>v</sub>1.6 subtype can produce a persistent Na<sup>+</sup> current, it is also likely to revert the Na<sup>+</sup>/Ca<sup>2+</sup> exchanger and account for an increase in axonal degeneration.<sup>242</sup> Consistent with this, blocking the Na<sup>+</sup>/Ca<sup>2+</sup> exchanger or the Na<sup>+</sup> channels alone exerted protective effects on rat retinal ganglion cells or in an experimental model of glaucoma, respectively.<sup>243, 244</sup> This in turn suggests that the diversity of the ion channel repertoire on primary retinal ganglion cells and the RGC-5 cells might be one reason accounting for the susceptibility of the latter cell type to oncosis. Though not analyzed in this study, the unmyelinated axons of the ganglion cells on the nerve fiber layer of isolated mouse retinae are likely to be expressing the Na<sub>v</sub>1.2 subtype. The RGC-5 cells, on the other hand, are reported to be expressing not the full repertoire of ion channels present on primary ganglion cells, while the exact ion channel profile of these cells is to our knowledge not determined yet.<sup>227</sup> Interestingly, the RGC-5 cells were found to be having a more positive resting membrane potential ( $-34 \pm 0.5$  mV)<sup>227</sup> compared to the primary ganglion cells isolated from early postnatal (P0-P7;  $-43.64 \pm 8.35$  mV) or adult rats (P23-P32;  $-58.20 \pm 6.52$  mV),<sup>245</sup> supporting the hypothesis of higher Na<sup>+</sup> influx occurring in RGC-5 cells. It would be therefore of particular interest to characterize the Na<sup>+</sup> channel subtypes in both the RGC-5 cells and the ganglion cells of isolated mouse retinae with emphasis on the expression of the Na<sub>v</sub>1.2 and Na<sub>v</sub>1.6 subtypes, to determine whether the differences in the Na<sup>+</sup>



channel repertoire render the RGC-5 cells more sensitive to oncosis when exposed to high concentrations of a molecule altering cytoskeletal organization, particularly under unfavorable conditions like energy depletion.

Hyperoxia, similar to energy depletion, is indicated as another major trigger for oncotic cell death.<sup>246</sup> The anti-oxidant capacity of a cell may therefore play a decisive role in the resistance to oncotic stimuli, as suggested by the rescue of a cardiac cell line overexpressing the detoxification enzyme glutathione-S-transferase from oncosis.<sup>247</sup> The RGC-5 cell line also appears to be sensitive to oxidative stress particularly under serum deprivation, since this treatment was reported to be resulting in a 50% decrease in the levels of GSH after 2 days.<sup>248</sup> It would be therefore interesting to determine whether the treatment with H-1152P at higher concentrations causes a further decrease in the GSH levels as observed in the isolated mouse retinae in this study, and reverses the protective effect of the inhibitor achieved at lower concentrations. Analyzing the specificity of H-1152P at 10-20  $\mu$ M would also allow for elucidating whether the adverse effects at these concentrations arise due to interference with other signaling pathways.

While investigating the causes underlying the susceptibility of the RGC-5 cells to oncosis, it should not be neglected that these cells are transformed and are likely to differ from the primary retinal ganglion cells in additional aspects that are not characterized yet. Though the alterations in transformed cells usually render them insensitive to apoptotic stimuli, they may not always be contributing to the resistance of the cells to oncosis, as suggested by the effects of the uncoupling protein-2 (UCP-2) on HeLa cells. The UCP-2 belongs to a family of mitochondrial transporters located in the inner membrane of mitochondria and appears to be involved in the limitation of free radical generation, exerting neuroprotective effects in experimental stroke and brain trauma. Interestingly, modest increases in the levels of UCP-2 in HeLa cells, but not in normal diploid fibroblasts, was reported to cause a reduction in intracellular ATP and induce a cell death mechanism conforming with oncosis.<sup>249-252</sup> UCP-2 therefore emanates as a candidate molecule shaping the response of transformed vs. untransformed cells to stress stimuli. Considering this, it would be also interesting to analyze the expression of UCP-2 in RGC-5 cells to determine

whether the oncotic effect of H-1152P at higher concentrations arises due to alterations in the levels of this protein. The inhibition of ROCK was indeed shown to exert toxic effects in a variety of transformed cells including the glioma cell line C6.<sup>253</sup> Unfortunately, it was not possible to distinguish the type of cell death in these studies, since the toxicity was determined by measuring parameters like LDH release and propidium iodide uptake, which are expected to occur not only in apoptotic but also in oncotic cells with increased membrane permeability. Nevertheless, these findings also favor the view that despite its anti-apoptotic potential in untransformed cells, ROCK-inhibition is likely to exert adverse effects on transformed cells, possibly by activating an oncotic program.

Taken together, the findings on RGC-5 cells obtained with the lower doses of H-1152P demonstrate the direct anti-apoptotic effects of ROCK-inhibition on a ganglion cell line. The activation of an oncotic death program at higher concentrations of H-1152P is likely to arise from the molecular differences between the RGC-5 and primary retinal ganglion cells, the characterization of which would not only provide more insight into the properties of both cell types, but also aid in elucidating the function of the ROCK-signaling pathway in the execution of oncosis in transformed cells. Though not belonging to the initial aims of this study, the latter aspect is also likely to contribute to the understanding of the anti-tumorigenic actions executed by various RhoA/ROCK inhibitors.<sup>139</sup>

### **4.2.3. Effect of ROCK inhibition on retinal ganglion cell survival after optic nerve crush**

The promising results demonstrating the neuroprotective effect of H-1152P-mediated ROCK-inhibition on retinal ganglion cells *in vitro* prompted us to analyze the outcomes of this treatment on retinal cells experiencing stress *in vivo*. The optic nerve crush, an acute injury triggering the propagation of secondary damage over

time, offers a relatively simple and reproducible model to simulate the neurodegenerative events associated with glaucoma in vivo.<sup>254</sup> This model was therefore chosen to determine the response of not only the damaged retinal ganglion cells, but also the retinal glia to H-1152P in a degenerating environment.

Similar to the observations on isolated mouse retinae in vitro, the injury of the ganglion cell axons at the optic nerve head resulted in the loss of more than 50% of the ganglion cells in PBS-treated rats, whereas the intraocular injection of 1  $\mu$ M H-1152P led to a significant rescue, with a 1.6-fold increase in the number of Fluorogold-labeled neurons. H-1152P treatment at this concentration also induced a notable decrease in the reactivity of the glial cells, particularly the Müller cells and microglia. These findings provide further support to the in vitro findings detected in isolated retinae in this study and suggest that the suppression of the glial cell reactivity to a certain extent after axonal injury may indeed be rescuing the remaining ganglion cells from the spread of secondary damage. However, increasing the concentration of H-1152P to 10 and 100  $\mu$ M resulted in a gradual decrease in the protective effect under these in vivo conditions as well. Interestingly, this concentration-dependent effect of H-1152P was observed only in rats that underwent optic nerve crush whereas the amount of Fluorogold-labeled retinal ganglion cells was not significantly altered in sham operated animals that received H-1152P injections at 1-100  $\mu$ M or PBS. This suggests that the H-1152P molecule does not exert toxic effects to retinal ganglion cells under normal conditions even when applied at high concentrations, but may be interfering with certain defense mechanisms activated upon injury in a dose-dependent way, which would counteract the beneficial outcomes obtained with the lower concentrations and result in the weakening of the protective effect. The in vitro evidence from serum-deprived mouse retinae place the reactive glial cells as likely candidates involved in these defense mechanisms. Characterizing the response of the glial cells to higher concentrations of H-1152P and the possible changes in the levels of the antioxidants like glutathione is therefore believed to provide further insight into the causes underlying the dose-dependent reduction in the protective effect of this inhibitor.

---

In conclusion, the preliminary *in vivo* findings obtained in the optic nerve crush model provide further support to the *in vitro* observations and accentuate the beneficial outcomes of H-1152P administration in promoting the survival of retinal ganglion cells after a primary injury. This protective effect is likely to be attained by a reduction in glial cell reactivity as evidenced by the *in vitro* and *in vivo* findings on retinæ as well as the possible anti-apoptotic effects exerted directly on the ganglion cells, as suggested by the dose-dependent outcomes of H-1152P on the RGC-5 cell line. However, the reasons underlying the gradual decrease in cell survival to control levels in response to higher concentrations of H-1152P need to be clarified, for identifying possible manageable targets like the amount of various antioxidants, which can be modified to minimize adverse effects. Determining the outcomes of H-1152P on the cellular events in retina after topical administration preferably in an animal model in which the ganglion cells are exposed to stress would also be informative in finding out whether this inhibitor is indeed able to reach the posterior segment of the eye at concentrations high enough to interfere with its possible beneficial effects on the retinal ganglion cells. Nevertheless, the findings on not only the retinal cells but also on Tenon's capsule fibroblasts demonstrate the fundamental role of the ROCK-signaling pathway in the regulation of various cellular activities critical for the onset or progress of glaucoma. These findings also highlight the potential of H-1152P administration as a promising approach to simultaneously interfere with diverse cellular events defining the course of glaucoma, offering new hopes for improving the success rate of glaucoma filtration surgery as well as maintaining the remaining retinal ganglion cells alive and functional.

## 5. SUMMARY

Glaucomatous optic neuropathy is characterized by the progressive loss of retinal ganglion cells and their axons, giving rise to irreversible visual field defects leading to blindness when left untreated. Though the activation of an apoptotic cell death program by various molecules implicated in the course of glaucoma accounts for the demise of the retinal ganglion cells, the current methods of glaucoma treatment all aim at reducing the intraocular pressure, the major risk factor for glaucoma arising from an imbalance between the production and outflow of aqueous humor. Glaucoma filtration surgery, which entails the creation of a scleral fistula that enables the drainage of aqueous humor from the anterior chamber to the subconjunctival space, remains to be the most effective method for lowering the intraocular pressure in glaucoma patients. However, the wound healing activities of the Tenon's capsule fibroblasts following this operation eventually result in the occlusion of the artificial drainage channel and account for the surgical failure.

The wound healing activities of Tenon's capsule fibroblasts involve dynamic events like proliferation, migration into the wound area, deposition of extracellular matrix molecules, and acquisition of contractile properties, which facilitate the closure of the drainage channel. Being a key intracellular convergence point for the signals initiating the cytoskeletal alterations underlying such dynamic events, the Rho-kinase/ROCK signaling pathway emerges as a potential pharmacological target for modulating the postoperative fibrotic response. The first part of this study therefore focused on characterizing the functions of the ROCK signaling pathway in human Tenon's capsule fibroblasts *in vitro*. With this purpose, the fibroblasts stimulated with serum were treated with H-1152P, a potent ROCK-inhibitor which already yielded promising results in promoting aqueous humor outflow by relieving the trabecular meshwork and ciliary muscle cell contraction in other studies.<sup>144</sup>

Incubation of the human Tenon's capsule fibroblasts with 10  $\mu$ M H-1152P resulted in an 80-90% reduction in cell proliferation as determined from the levels of BrdU incorporation and Ki-67 upregulation. H-1152P also caused the disassembly of stress fibers in a dose-dependent manner without exerting toxic effects and without a significant interference with the protein kinase A pathway. Migration of fibroblasts on collagen gels and into a wound area created in cell monolayers as well as the contraction of fibroblast populated floating collagen lattices were also suppressed by H-1152P together with an impairment in the assembly of the fibronectin network. These findings provide further evidence for the role of the ROCK-signaling pathway in the wound healing activities of human Tenon's capsule fibroblasts and underline the potential of H-1152P as a safe and specific means to suppress these events.

The RhoA effector ROCK also functions as the convergence point of numerous extracellular signals that induce the cytoskeletal changes underlying axon retraction and apoptosis. This places ROCK as a strategic target for not only suppressing the wound healing response after glaucoma filtration surgery, but also for promoting the survival of retinal ganglion cells and their axons in glaucoma. Considering this, the outcomes of the H-1152P mediated ROCK inhibition on retinal cells under stress were also analyzed in this study, initially on isolated mouse retinae incubated without serum. This stringent in vitro model combining axotomy with serum deprivation severely impaired the survival of the cells in the ganglion cell layer after 1 day, as demonstrated by the high levels of ethidium homodimer-1 uptake and caspase-3 activation. In contrast, the treatment with 1  $\mu$ M H-1152P considerably reduced the extent of apoptosis in all the retinal layers without interfering with the protein kinase A pathway. However, increasing the concentration of this inhibitor weakened its protective effects. The extent of astrocyte, Müller cell, and microglia cell reactivity was also significantly suppressed in retinae treated with 1  $\mu$ M H-1152P. In addition, multiple cytokine arrays demonstrated the reduction in the levels of various proinflammatory cytokines like interleukin (IL)-1 $\beta$ , IL-3, IL-4, IL-6, IL-10, interferon- $\gamma$ , and tumor necrosis factor alpha released into the culture medium in response to H-1152P treatment, which probably underlied the decrease in the toxicity of the conditioned media obtained from retinae incubated with this inhibitor. Interestingly, increasing the concentration of H-1152P to 20  $\mu$ M, which resulted in a further decrease in the reactivity of Müller cells and astrocytes, was found to have

---

reduced the levels of total glutathione, whereas the coadministration of this antioxidant with 20  $\mu\text{M}$  H-1152P improved the cell survival rate in the ganglion cell layer. These results demonstrate that the neuroprotective effect of H-1152P mediated ROCK inhibition on retinal cells may be due to the suppression of glial cell reactivity to a certain extent, leading to the diminishing of cytokine release and to the suppression of secondary damage. The adverse effects at higher concentrations of H-1152P, possibly arising from a further reduction in glial cell reactivity and the associated decrease in the antioxidant levels, are likely to be alleviated by coadministering glutathione, which improves the neuroprotective potential of this inhibitor.

To analyze the direct effects of H-1152P on retinal ganglion cells *in vitro*, the transformed rat retinal ganglion cell line RGC-5 cultivated without serum was also utilised in this study. Despite the stability of this cell line compared to the cells in isolated retinae under serum deprivation, administration of H-1152P at 1  $\mu\text{M}$  exerted direct anti-apoptotic effects by specifically interfering with ROCK-dependent phosphorylation events. However, increasing the concentration of the inhibitor to 10-20  $\mu\text{M}$  resulted in a dramatic increase in the amount of cells undergoing an oncotic cell death, characterized by a marked cellular swelling. These highly contrasting effects of H-1152P are likely to have arisen from the molecular differences of the transformed cell line RGC-5 from primary retinal ganglion cells, the further characterization of which are believed to be useful in providing more insight into the properties of both cell types as well as the mechanisms of oncosis.

To analyze the neuroprotective potential of H-1152P on retinal cells encountering stress *in vivo*, we studied the outcomes of the intravitreal injections of H-1152P on the survival of ganglion cells after optic nerve crush in collaboration with Dr. Frank Schüttauf from the University Eye Hospital in Tübingen. H-1152P administered at 1  $\mu\text{M}$  led to a 1.6 fold increase in the number of Fluorogold-labeled retinal ganglion cells together with a decrease in the extent of glial cell reactivity 7 days after the injury at the optic nerve head. These preliminary findings provide further support for the *in vitro* observations on isolated retinae, and suggest that the suppression of reactive gliosis to a certain degree after axonal injury may indeed be

beneficial in reducing the spread of secondary damage and rescuing the remaining ganglion cells. These data demonstrating the central role of the ROCK-signaling pathway in various cells implicated in the course of glaucoma also highlight the potential of the H-1152P-mediated targeting of this pathway as a promising anti-glaucoma therapy approach not only for suppressing the undesirable wound healing activities of Tenon's capsule fibroblasts after glaucoma filtration surgery, but also for preventing further ganglion cell loss.



## 6. ABBREVIATIONS

<b>(-/-)</b>	double knockout
<b>µl</b>	microliter
<b>µM</b>	micrometer
<b>3D</b>	3-dimensional
<b>A</b>	absorbance
<b>ATP</b>	adenosine triphosphate
<b>ATPase</b>	adenosine triphosphatase
<b>BCA</b>	bichinchoninic acid
<b>BCIP</b>	5-bromo-4-chloro-3 indolyl phosphate
<b>BDNF</b>	brain derived neurotrophic factor
<b>BrdU</b>	bromodeoxyuridine
<b>BSA</b>	bovine serum albumin
<b>CD11b</b>	cluster of differentiation 11b
<b>CM</b>	conditioned medium
<b>CM (H)</b>	CM obtained from retinae / optic nerve incubated with 1 µM H-1152P
<b>CM + H</b>	1 µM H-1152P added into the conditioned medium of retinae/optic nerve
<b>CNS</b>	central nervous system
<b>CPI-17</b>	protein kinase C (PKC)-potentiated inhibitory protein for heterotrimeric myosin light chain phosphatase (MLCP) of 17kDa
<b>Cy3</b>	cyanine-3
<b>DAPI</b>	4',6-diamidino-2-phenylindol
<b>dH<sub>2</sub>O</b>	distilled water
<b>DMEM</b>	Dulbecco's modified Eagle's medium

---

<b>DMSO</b>	dimethylsulfoxide
<b>DNA</b>	deoxyribonucleic acid
<b>DTNB</b>	5,5'-dithiobis(2-nitrobenzoic acid)
<b>EAE</b>	experimental autoimmune encephalomyelitis
<b>ECL</b>	enhanced chemiluminescence
<b>ECM</b>	extracellular matrix
<b>EDTA</b>	ethylene diamine tetraacetic acid
<b>EGF</b>	epidermal growth factor
<b>ERM</b>	ezrin-radixin-moesin
<b>EthD-1</b>	ethidium homodimer-1
<b>F-actin</b>	filamentous actin
<b>FasL</b>	Fas ligand
<b>FBS</b>	fetal bovine serum
<b>FGF</b>	fibroblast growth factor
<b>g</b>	gram
<b>GAP</b>	GTPase activating protein
<b>GCL</b>	ganglion cell layer
<b>GCSF</b>	granulocyte-colony stimulating factor
<b>GDI</b>	guanine nucleotide dissociation inhibitor
<b>GDP</b>	guanine diphosphate
<b>GEF</b>	guanine nucleotide exchange factor
<b>GFAP</b>	glial fibrillary acidic protein
<b>GM-CSF</b>	granulocyte-macrophage colony stimulating factor
<b>GPI</b>	glycosylphosphatidylinositol
<b>GSH</b>	reduced glutathione
<b>GSSG</b>	gluathione disulfide (oxidized glutathione)
<b>GTP</b>	guanosine triphosphate
<b>GTPase</b>	guanosine triphosphatase
<b>Hepes</b>	4-(2-hydroxyethyl)-1-piperazineethanesulfonic acid
<b>hrs</b>	hours
<b>IFN</b>	interferon

---

<b>IFN-g</b>	interferon-gamma
<b>IgG</b>	immunoglobulin
<b>IgG (H+L)</b>	IgG heavy and light chains
<b>IHC</b>	immunohistochemistry
<b>IL</b>	interleukin
<b>IL6-m</b>	mouse IL-6
<b>INL</b>	inner nuclear layer
<b>IOP</b>	intraocular pressure
<b>IPL</b>	inner plexiform layer
<b>KC</b>	keratinocyte-derived chemokine
<b>kDa</b>	kilodaltons
<b>Ki</b>	inhibitory constant
<b>LDH</b>	lactate dehydrogenase
<b>M</b>	mole
<b>m_IFNg_rec</b>	mouse IFN-gamma receptor
<b>MARCKS</b>	myristoylated alanine rich kinase
<b>MCP</b>	monocyte chemoattractant protein
<b>MEM</b>	modified Eagle's medium
<b>mg</b>	milligram
<b>MIP-1<math>\alpha</math></b>	macrophage inflammatory protein-1 alpha
<b>ml</b>	milliliter
<b>MLC</b>	myosin light chain
<b>mM</b>	millimolar
<i>Mnd</i>	motor neuron degeneration
<b>Mr</b>	molecular mass
<b>mRNA</b>	messenger RNA
<b>MS</b>	multiple sclerosis
<b>MTT</b>	3-(4, 5-dimethylthiazolyl)-2, 5 diphenyl tetrazolium bromide
<b>mV</b>	millivolt
<b>MW</b>	molecular weight
<b>NADPH</b>	nicotinamide adenine dinucleotide phosphate

---

<b>Na<sub>v</sub>1.2</b>	voltage gated Na <sup>+</sup> channel, subtype 1.2
<b>Na<sub>v</sub>1.6</b>	voltage gated Na <sup>+</sup> channel, subtype 1.6
<b>NBT</b>	nitroblue tetrazolium chloride
<b>NFL</b>	nerve fiber layer
<b>NF-κB</b>	nuclear factor κB
<b>nM</b>	nanomolar
<b>NMDA</b>	N-methyl-D-aspartate
<b>NMRI</b>	Naval Medical Research Institute
<b>NO</b>	nitric oxide
<b>NOS</b>	nitric oxide synthase
<b>NP-40</b>	Nonidet® P 40
<b>NT-2 cells</b>	Ntera 2/D1 (neuronally committed human teratocarcinoma cell) line
<b>OCT</b>	optimal cutting temperature
<b>ON</b>	optic nerve
<b>ONC</b>	optic nerve crush
<b>ONH</b>	optic nerve head
<b>ONL</b>	outer nuclear layer
<b>OPL</b>	outer plexiform layer
<b>P</b>	postnatal
<b>p-adducin</b>	phospho-adducin
<b>PAGE</b>	polyacrylamide gel electrophoresis
<b>PBS</b>	phosphate buffered saline
<b>PBST</b>	phosphate buffered saline – TritonX-100
<b>PDGF</b>	platelet derived growth factor
<b>PFA</b>	paraformaldehyde
<b>PKA</b>	protein kinase A
<b>p-value</b>	probability of obtaining a result at least as extreme as a given data point, assuming the data point was the result of chance alone
<b>RANTES</b>	regulated upon activation normal T-cell expressed and secreted

---

<b>rcf</b>	relative centrifugal force (x gravity)
<b>RGC</b>	retinal ganglion cell
<b>Rho</b>	ras-homology
<b>RNA</b>	ribonucleic acid
<b>ROCK</b>	Rho-associated coiled-coil kinase
<b>ROS</b>	reactive oxygen species
<b>RPTE</b>	renal proximal tubular epithelium
<b>S</b>	serine
<b>SCF</b>	stem cell factor
<b>SDS</b>	sodium dodecyl sulphate
<b>sIL6Rm</b>	mouse soluble IL-6 receptor
<b>SMA</b>	smooth muscle actin
<b>S-phase</b>	synthesis phase
<b>STNFR</b>	soluble TNF-alpha receptor
<b>T</b>	threonine
<b>T0</b>	time point 0
<b>TBS</b>	Tris buffered saline
<b>TBST</b>	TBS-Tween
<b>Temed</b>	N, N, N', N',-Tetramethylethylenediamine
<b>TGF-β</b>	transforming growth factor beta
<b>Thy-1</b>	T-cell antigen / Theta antigen
<b>TNF</b>	tumor necrosis factor
<b>Tris</b>	Tris-(hydroxymethyl)-aminomethane
<b>TUNEL</b>	terminal deoxynucleotidyl transferase biotin-dUTP nick end labeling
<b>UCP-2</b>	uncoupling factor-2
<b>UV</b>	ultraviolet
<b>v/v</b>	volume / volume
<b>VEGF</b>	vascular endothelial growth factor
<b>w/v</b>	weight / volume

## 7. REFERENCES

1. **Kaushik S, Pandav SS, Ram J.**  
Neuroprotection in glaucoma.  
*J Postgrad Med.* 2003;49(1):90-95.
2. **Osborne NN, Schmidt KG.**  
[Neuroprotection against glaucoma remains a concept]  
*Ophthalmologe* 2004;101(11):1087-1092.
3. **Tsai JC, Kanner EM.**  
Current and emerging medical therapies for glaucoma.  
*Expert Opin Emerg Drugs* 2005;10(1):109-118.
4. **World Health Organization.**  
Blindness and visual disability: Part 2: Major causes worldwide.  
*WHO* 1997; Geneva.
5. **Lee DA, Higginbotham EJ.**  
Glaucoma and its treatment: a review.  
*Am J Health Syst Pharm.* 2005;62(7):691-699.
6. **Schwartz M.**  
Lessons for glaucoma from other neurodegenerative diseases: Can one treatment suit them all?  
*J Glaucoma* 2005;14(4):321-323.
7. **Chen PP.**  
Risk and risk factors for blindness from glaucoma.  
*Curr Opin Ophthalmol.* 2004;15(2):107-111.
8. **Ofri R.**  
Intraocular pressure and glaucoma.  
*Vet Clin North Am Exot Anim Pract.* 2002;5(2):391-406, vii-viii.
9. **Quigley HA.**  
Ganglion cell death in glaucoma: pathology recapitulates ontogeny.  
*Aust N Z J Ophthalmol.* 1995;23(2):85-91.
10. **Piette SD, Sergott RC.**  
Pathological optic-disc cupping.  
*Curr Opin Ophthalmol.* 2006;17(1):1-6.
11. **Liesegang TJ.**  
Glaucoma: changing concepts and future directions.  
*Mayo Clin Proc.* 1996;71(7):689-694.

**12. Marcic TS, Belyea DA, Katz B.**

Neuroprotection in glaucoma: a model for neuroprotection in optic neuropathies.

*Curr Opin Ophthalmol.* 2003;14(6):353-356.

**13. Kuehn MH, Fingert JH, Kwon YH.**

Retinal ganglion cell death in glaucoma: Mechanisms and neuroprotective strategies.

*Ophthalmol Clin North Am.* 2005;18(3):383-395, vi.

**14. Nickells RW.**

Retinal ganglion cell death in glaucoma: the how, the why, and the maybe.

*J Glaucoma* 1996;5(5):345-356.

**15. McKinnon SJ.**

Glaucoma, apoptosis and neuroprotection.

*Curr Opin Ophthalmol.* 1997;8(2):28-37.

**16. Chao MV, Rajagopal R, Lee FS.**

Neurotrophin signalling in health and disease.

*Clin Sci (Lond).* 2006;110(2):167-173.

**17. Johnson JE, Barde YA, Schwab M, Thoenen H.**

Brain-derived neurotrophic factor supports the survival of cultured rat retinal ganglion cells.

*J Neurosci.* 1986;6(10):3031-3038.

**18. Cui Q, Harvey AR.**

At least two mechanisms are involved in the death of retinal ganglion cells following target ablation in neonatal rats.

*J Neurosci.* 1995;15(12):8143-8155.

**19. Anderson DR, Hendrickson A.**

Effect of intraocular pressure on rapid axoplasmic transport in monkey optic nerve.

*Invest Ophthalmol.* 1974;13(10):771-783.

**20. Pease ME, McKinnon SJ, Quigley HA, Kerrigan-Baumrind LA, Zack DJ.**

Obstructed axonal transport of BDNF and its receptor TrkB in experimental glaucoma.

*Invest Ophthalmol Vis Sci.* 2000;41(3):764-774.

**21. Flammer J, Orgul S, Costa VP, Orzalesi N, Kriegelstein GK, Serra LM, Renard JP, Stefansson E.**

The impact of ocular blood flow in glaucoma.

*Prog Retin Eye Res.* 2002;21(4):359-393.

**22. Osborne NN, Ugarte M, Chao M, Chidlow G, Bae JH, Wood JP, Nash MS.**

Neuroprotection in relation to retinal ischemia and relevance to glaucoma.

*Surv Ophthalmol.* 1999;43(Suppl 1):S102-128.

- 
- 23. Harris A, Jonescu-Cuypers C, Martin B, Kagemann L, Zalish M, Garzosi HJ.**  
Simultaneous management of blood flow and IOP in glaucoma.  
*Acta Ophthalmol Scand.* 2001;79(4):336-341.
- 24. Orgul S, Cioffi GA, Bacon DR, Van Buskirk EM.**  
An endothelin-1-induced model of chronic optic nerve ischemia in rhesus monkeys.  
*J Glaucoma* 1996;5(2):135-138.
- 25. Chauhan BC, LeVatte TL, Jollimore CA, Yu PK, Reitsamer HA, Kelly ME, Yu DY, Tremblay F, Archibald ML.**  
Model of endothelin-1-induced chronic optic neuropathy in rat.  
*Invest Ophthalmol Vis Sci.* 2004;45(1):144-152.
- 26. Casson RJ.**  
Possible role of excitotoxicity in the pathogenesis of glaucoma.  
*Clin Experiment Ophthalmol.* 2006;34(1):54-63.
- 27. Yang XL.**  
Characterization of receptors for glutamate and GABA in retinal neurons.  
*Prog Neurobiol.* 2004;73(2):127-150.
- 28. Lucas DR, Newhouse JP.**  
The toxic effect of sodium L-glutamate on the inner layers of the retina.  
*AMA Arch Ophthalmol.* 1957;58(2):193-201.
- 29. Caprioli J, Kitano S, Morgan JE.**  
Hyperthermia and hypoxia increase tolerance of retinal ganglion cells to anoxia and excitotoxicity.  
*Invest Ophthalmol Vis Sci.* 1996;37(12):2376-2381.
- 30. Azuma N, Kawamura M, Kohsaka S.**  
[Morphological and immunohistochemical studies on degenerative changes of the retina and the optic nerve in neonatal rats injected with monosodium-L-glutamate]  
*Nippon Ganka Gakkai Zasshi* 1989;93(1):72-79.
- 31. Dreyer EB, Zurakowski D, Schumer RA, Podos SM, Lipton SA.**  
Elevated glutamate levels in the vitreous body of humans and monkeys with glaucoma.  
*Arch Ophthalmol.* 1996;114(3):299-305.
- 32. Honkanen RA, Baruah S, Zimmerman MB, Khanna CL, Weaver YK, Narkiewicz J, Waziri R, Gehrs KM, Weingeist TA, Boldt HC, Folk JC, Russell SR, Kwon YH.**  
Vitreous amino acid concentrations in patients with glaucoma undergoing vitrectomy.  
*Arch Ophthalmol.* 2003;121(2):183-188.



- 
- 33. Carter-Dawson L, Crawford ML, Harwerth RS, Smith EL 3rd, Feldman R, Shen FF, Mitchell CK, Whitree A.**  
Vitreous glutamate concentration in monkeys with experimental glaucoma.  
*Invest Ophthalmol Vis Sci.* 2002;43(8):2633-2637.
- 34. Lotery AJ.**  
Glutamate excitotoxicity in glaucoma: truth or fiction?  
*Eye* 2005;19(4):369-370.
- 35. Tezel G.**  
Oxidative stress in glaucomatous neurodegeneration: Mechanisms and consequences.  
*Prog Retin Eye Res.* 2006;25(5):490-513.
- 36. Andersen JK.**  
Oxidative stress in neurodegeneration: cause or consequence?  
*Nat Med.* 2004;10(Suppl):S18-25.
- 37. Veach J.**  
Functional dichotomy: glutathione and vitamin E in homeostasis relevant to primary open-angle glaucoma.  
*Br J Nutr.* 2004;91(6):809-829.
- 38. Halliwell B.**  
Oxidative stress and neurodegeneration: where are we now?  
*J Neurochem.* 2006;97(6):1634-1658.
- 39. Muller A, Pietri S, Villain M, Frejaville C, Bonne C, Culcas M.**  
Free radicals in rabbit retina under ocular hyperpressure and functional consequences.  
*Exp Eye Res.* 1997;64(4):637-643.
- 40. Bonne C, Muller A, Villain M.**  
Free radicals in retinal ischemia.  
*Gen Pharmacol.* 1998;30(3):275-280.
- 41. Moreno MC, Campanelli J, Sande P, Sanz DA, Keller Sarmiento MI, Rosenstein RE.**  
Retinal oxidative stress induced by high intraocular pressure.  
*Free Radic Biol Med.* 2004;37(6):803-812.
- 42. Ko ML, Peng PH, Ma MC, Ritch R, Chen CF.**  
Dynamic changes in reactive oxygen species and antioxidant levels in retinas in experimental glaucoma.  
*Free Radic Biol Med.* 2005;39(3):365-373.
- 43. Tezel G, Yang X, Cai J.**  
Proteomic identification of oxidatively modified retinal proteins in a chronic pressure-induced rat model of glaucoma.  
*Invest Ophthalmol Vis Sci.* 2005;46(9):3177-3187.

- 
- 44. Osborne NN, Lascaratos G, Bron AJ, Chidlow G, Wood JP.**  
A hypothesis to suggest that light is a risk factor in glaucoma and the mitochondrial optic neuropathies.  
*Br J Ophthalmol.* 2006;90(2):237-241.
- 45. Neufeld AH, Liu B.**  
Glaucomatous optic neuropathy: when glia misbehave.  
*Neuroscientist* 2003;9(6):485-495.
- 46. Carelli V, Ross-Cisneros FN, Sadun AA.**  
Mitochondrial dysfunction as a cause of optic neuropathies.  
*Prog Retin Eye Res.* 2004;23(1):53-89.
- 47. Andrews RM, Griffiths PG, Johnson MA, Turnbull DM.**  
Histochemical localisation of mitochondrial enzyme activity in human optic nerve and retina.  
*Br J Ophthalmol.* 1999;83(2):231-235.
- 48. Bristow EA, Griffiths PG, Andrews RM, Johnson MA, Turnbull DM.**  
The distribution of mitochondrial activity in relation to optic nerve structure.  
*Arch Ophthalmol.* 2002;120(6):791-796.
- 49. Wang L, Dong J, Cull G, Fortune B, Cioffi GA.**  
Varicosities of intraretinal ganglion cell axons in human and nonhuman primates.  
*Invest Ophthalmol Vis Sci.* 2003;44(1):2-9.
- 50. Barron MJ, Griffiths P, Turnbull DM, Bates D, Nichols P.**  
The distributions of mitochondria and sodium channels reflect the specific energy requirements and conduction properties of the human optic nerve head.  
*Br J Ophthalmol.* 2004;88(2):286-290.
- 51. Ye H, Hernandez MR.**  
Heterogeneity of astrocytes in human optic nerve head.  
*J Comp Neurol.* 1995;362(4):441-452.
- 52. Neufeld AH.**  
Microglia in the optic nerve head and the region of parapapillary chorioretinal atrophy in glaucoma.  
*Arch Ophthalmol.* 1999;117(8):1050-1056.
- 53. Bringmann A, Pannicke T, Grosche J, Francke M, Wiedemann P, Skatchkov SN, Osborne NN, Reichenbach A.**  
Muller cells in the healthy and diseased retina.  
*Prog Retin Eye Res.* 2006;25(4):397-424.
- 54. Hollander H, Makarov F, Dreher Z, van Driel D, Chan-Ling TL, Stone J.**  
Structure of the macroglia of the retina: sharing and division of labour between astrocytes and Muller cells.  
*J Comp Neurol.* 1991;313(4):587-603.

- 
- 55. Provis JM, Penfold PL, Edwards AJ, van Driel D.**  
Human retinal microglia: expression of immune markers and relationship to the glia limitans.  
*Glia* 1995;14(4):243-256.
- 56. Tezel G, Wax MB.**  
Glial modulation of retinal ganglion cell death in glaucoma.  
*J Glaucoma* 2003;12(1):63-68.
- 57. Hatten ME, Liem RK, Shelanski ML, Mason CA.**  
Astroglia in CNS injury.  
*Glia* 1991;4(2):233-243.
- 58. Eddleston M, Mucke L.**  
Molecular profile of reactive astrocytes: implications for their role in neurologic disease.  
*Neuroscience* 1993;54(1):15-36.
- 59. Aschner M.**  
Astrocytic functions and physiological reactions to injury: the potential to induce and/or exacerbate neuronal dysfunction – a forum position paper.  
*Neurotoxicology* 1998;19(1):7-17, discussion 37-38.
- 60. Lewis GP, Fisher SK.**  
Up-regulation of glial fibrillary acidic protein in response to retinal injury: its potential role in glial remodeling and a comparison to vimentin expression.  
*Int Rev Cytol.* 2003;230:263-290.
- 61. Hernandez MR, Pena JD.**  
The optic nerve head in glaucomatous optic neuropathy.  
*Arch Ophthalmol.* 1997;115(3):389-395.
- 62. Wang L, Cioffi GA, Cull G, Dong J, Fortune B.**  
Immunohistologic evidence for retinal glial cell changes in human glaucoma.  
*Invest Ophthalmol Vis Sci.* 2002;43(4):1088-1094.
- 63. Osborne NN, Block F, Sontag KH.**  
Reduction of ocular blood flow results in glial fibrillary acidic protein (GFAP) expression in rat retinal Muller cells.  
*Vis Neurosci.* 1991;7(6):637-639.
- 64. Tanihara H, Hangai M, Sawaguchi S, Abe H, Kageyama M, Nakazawa F, Shirasawa E, Honda Y.**  
Up-regulation of glial fibrillary acidic protein in the retina of primate eyes with experimental glaucoma.  
*Arch Ophthalmol.* 1997;115(6):752-756.
- 65. Honjo M, Tanihara H, Kido N, Inatani M, Okazaki K, Honda Y.**  
Expression of ciliary neurotrophic factor activated by retinal Muller cells in eyes with NMDA- and kainic acid-induced neuronal death.  
*Invest Ophthalmol Vis Sci.* 2000;41(2):552-560.

- 66. Hernandez MR, Andrzejewska WM, Neufeld AH.**  
Changes in the extracellular matrix of the human optic nerve head in primary open-angle glaucoma.  
*Am J Ophthalmol.* 1990;109(2):180-188.
- 67. Morrison JC, Dorman-Pease ME, Dunkelberger GR, Quigley HA.**  
Optic nerve head extracellular matrix in primary optic atrophy and experimental glaucoma.  
*Arch Ophthalmol.* 1990;108(7):1020-1024.
- 68. Quigley HA, Dorman-Pease ME, Brown AE.**  
Quantitative study of collagen and elastin of the optic nerve head and sclera in human and experimental monkey glaucoma.  
*Curr Eye Res.* 1991;10(9):877-888.
- 69. Hernandez MR.**  
Ultrastructural immunocytochemical analysis of elastin in the human lamina cribrosa. Changes in elastic fibers in primary open-angle glaucoma.  
*Invest Ophthalmol Vis Sci.* 1992;33(10):2891-2903.
- 70. Varela HJ, Hernandez MR.**  
Astrocyte responses in human optic nerve head with primary open-angle glaucoma.  
*J Glaucoma* 1997;6(5):303-313.
- 71. Yan X, Tezel G, Wax MB, Edward DP.**  
Matrix metalloproteinases and tumor necrosis factor alpha in glaucomatous optic nerve head.  
*Arch Ophthalmol.* 2000;118(5):666-673.
- 72. Agapova OA, Ricard CS, Salvador-Silva M, Hernandez MR.**  
Expression of matrix metalloproteinases and tissue inhibitors of metalloproteinases in human optic nerve head astrocytes.  
*Glia* 2001;33(3):205-216.
- 73. Morgan JE.**  
Optic nerve head structure in glaucoma: astrocytes as mediators of axonal damage.  
*Eye* 2000;14(Pt 3B):437-444.
- 74. Liu B, Neufeld AH.**  
Nitric oxide synthase-2 in human optic nerve head astrocytes induced by elevated pressure in vitro.  
*Arch Ophthalmol.* 2001;119(2):240-245.
- 75. Shareef S, Sawada A, Neufeld AH.**  
Isoforms of nitric oxide synthase in the optic nerves of rat eyes with chronic moderately elevated intraocular pressure.  
*Invest Ophthalmol Vis Sci.* 1999;40(12):2884-2891.

**76. Tezel G, Wax MB.**

Increased production of tumor necrosis factor-alpha by glial cells exposed to simulated ischemia or elevated hydrostatic pressure induces apoptosis in cocultured retinal ganglion cells.  
*J Neurosci.* 2000;20(23):8693-8700.

**77. Goureau O, Hicks D, Courtois Y, De Kozak Y.**

Induction and regulation of nitric oxide synthase in retinal Muller glial cells.  
*J Neurochem.* 1994;63(1):310-317.

**78. Kashii S, Mandai M, Kikuchi M, Honda Y, Tamura Y, Kaneda K, Akaike A.**

Dual actions of nitric oxide in N-methyl-D-aspartate receptor-mediated neurotoxicity in cultured retinal neurons.  
*Brain Res.* 1996;711(1-2):93-101.

**79. Schmetterer L, Polak K.**

Role of nitric oxide in the control of ocular blood flow.  
*Prog Retin Eye Res.* 2001;20(6):823-847.

**80. Farkas RH, Grosskreutz CL.**

Apoptosis, neuroprotection, and retinal ganglion cell death: an overview.  
*Int Ophthalmol Clin.* 2001;41(1):111-130.

**81. Feuerstein GZ, Wang X, Barone FC.**

The role of cytokines in the neuropathology of stroke and neurotrauma.  
*Neuroimmunomodulation* 1998;5(3-4):143-159.

**82. Dong Y, Benveniste EN.**

Immune function of astrocytes.  
*Glia* 2001;36(2):180-190.

**83. Tezel G, Li LY, Patil RV, Wax MB.**

TNF-alpha and TNF-alpha receptor-1 in the retina of normal and glaucomatous eyes.  
*Invest Ophthalmol Vis Sci.* 2001;42(8):1787-1794.

**84. Wax MB.**

Is there a role for the immune system in glaucomatous optic neuropathy?  
*Curr Opin Ophthalmol.* 2000;11(2):145-150.

**85. Wax MB, Yang J, Tezel G.**

Serum autoantibodies in patients with glaucoma.  
*J Glaucoma* 2001;10(5 Suppl 1):S22-S24.

**86. Wax MB, Tezel G, Saito I, Gupta RS, Harley JB, Li Z, Romano C.**

Anti-Ro/SS-A positivity and heat shock protein antibodies in patients with normal-pressure glaucoma.  
*Am J Ophthalmol.* 1998;125(2):145-157.

**87. Tezel G, Seigel GM, Wax MB.**

Autoantibodies to small heat shock proteins in glaucoma.  
*Invest Ophthalmol Vis Sci.* 1998;39(12):2277-2287.

- 
- 88. Liang P, MacRae TH.**  
Molecular chaperones and the cytoskeleton.  
*J Cell Sci.* 1997;110(Pt 13):1431-1440.
- 89. Yang J, Tezel G, Patil RV, Romano C, Wax MB.**  
Serum autoantibody against glutathione S-transferase in patients with glaucoma.  
*Invest Ophthalmol Vis Sci.* 2001;42(6):1273-1276.
- 90. Whalen R, Boyer TD.**  
Human glutathione S-transferases.  
*Semin Liver Dis.* 1998;18(4):345-358.
- 91. Salinas AE, Wong MG.**  
Glutathione S-transferases--a review.  
*Curr Med Chem.* 1999;6(4):279-309.
- 92. Yang J, Yang P, Tezel G, Patil RV, Hernandez MR, Wax MB.**  
Induction of HLA-DR expression in human lamina cribrosa astrocytes by cytokines and simulated ischemia.  
*Invest Ophthalmol Vis Sci.* 2001;42(2):365-371.
- 93. Yuan L, Neufeld AH.**  
Activated microglia in the human glaucomatous optic nerve head.  
*J Neurosci Res.* 2001;64(5):523-532.
- 94. Wax M, Yang J, Tezel G.**  
Autoantibodies in glaucoma.  
*Curr Eye Res.* 2002;25(2):113-116.
- 95. Burke JM, Smith JM.**  
Retinal proliferation in response to vitreous hemoglobin or iron.  
*Invest Ophthalmol Vis Sci.* 1981;20(5):582-592.
- 96. Swanson RA, Ying W, Kauppinen TM.**  
Astrocyte influences on ischemic neuronal death.  
*Curr Mol Med.* 2004;4(2):193-205.
- 97. Fawcett JW, Asher RA.**  
The glial scar and central nervous system repair.  
*Brain Res Bull.* 1999;49(6):377-391.
- 98. MacLaren RE.**  
Development and role of retinal glia in regeneration of ganglion cells following retinal injury.  
*Br J Ophthalmol.* 1996;80(5):458-464.
- 99. Quigley HA, Nickells RW, Kerrigan LA, Pease ME, Thibault DJ, Zack DJ.**  
Retinal ganglion cell death in experimental glaucoma and after axotomy occurs by apoptosis.  
*Invest Ophthalmol Vis Sci.* 1995;36(5):774-786.

- 
- 100. Okisaka S, Murakami A, Mizukawa A, Ito J.**  
Apoptosis in retinal ganglion cell decrease in human glaucomatous eyes.  
*Jpn J Ophthalmol.* 1997;41(2):84-88.
- 101. Quigley HA.**  
Neuronal death in glaucoma.  
*Prog Retin Eye Res.* 1999;18(1):39-57.
- 102. Kerr JF, Wyllie AH, Currie AR.**  
Apoptosis: a basic biological phenomenon with wide-ranging implications in tissue kinetics.  
*Br J Cancer* 1972;26(4):239-257.
- 103. Nickells RW, Zack DJ.**  
Apoptosis in ocular disease: a molecular overview.  
*Ophthalmic Genet.* 1996;17(4):145-165.
- 104. Coleman ML, Olson MF.**  
Rho GTPase signalling pathways in the morphological changes associated with apoptosis.  
*Cell Death Diff.* 2002;9(5):493-504.
- 105. Susin SA, Zamzami N, Kroemer G.**  
Mitochondria as regulators of apoptosis: doubt no more.  
*Biochim Biophys Acta* 1998;1366(1-2):151-165.
- 106. Heidenreich KA.**  
Molecular mechanisms of neuronal cell death.  
*Ann N Y Acad Sci.* 2003;991:237-250.
- 107. Nicholson DW, Thornberry NA.**  
Caspases: killer proteases.  
*Trends Biochem Sci.* 1997;22(8):299-306.
- 108. Marquis RE, Whitson JT.**  
Management of glaucoma: focus on pharmacological therapy.  
*Drugs Aging* 2005;22(1):1-21.
- 109. Resch H, Garhofer G.**  
Topical drug therapy in glaucoma.  
*Wien Med Wochenschr.* 2006;156(17-18):501-507.
- 110. Yoles E, Wheeler LA, Schwartz M.**  
Alpha2-adrenoreceptor agonists are neuroprotective in a rat model of optic nerve degeneration.  
*Invest Ophthalmol Vis Sci.* 1999;40(1):65-73.  
*Erratum in: Invest Ophthalmol Vis Sci.* 1999;40(11):2470.
- 111. Gao H, Qiao X, Cantor LB, WuDunn D.**  
Up-regulation of brain-derived neurotrophic factor expression by brimonidine in rat retinal ganglion cells.  
*Arch Ophthalmol.* 2002;120(6):797-803.

- 
- 112. Wilensky JT.**  
The role of medical therapy in the rank order of glaucoma treatment.  
*Curr Opin Ophthalmol.* 1999;10(2):109-111.
- 113. Detry-Morel M.**  
Side effects of glaucoma medications.  
*Bull Soc Belge Ophthalmol.* 2006;299:27-40.
- 114. Schwartz K, Budenz D.**  
Current management of glaucoma.  
*Curr Opin Ophthalmol.* 2004; 15(2):119-126.
- 115. Medeiros FA, Weinreb RN.**  
Medical backgrounders: glaucoma.  
*Drugs Today (Barc).* 2002;38(8):563-570.
- 116. Lachkar Y, Hamard P.**  
Nonpenetrating filtering surgery.  
*Curr Opin Ophthalmol.* 2002;13(2):110-115.
- 117. Chang MR, Cheng Q, Lee DA.**  
Basic science and clinical aspects of wound healing in glaucoma filtering surgery.  
*J Ocul Pharmacol Ther.* 1998;14(1):75-95.
- 118. Khaw PT, Chang L, Wong TT, Mead A, Daniels JT, Cordeiro MF.**  
Modulation of wound healing after glaucoma surgery.  
*Curr Opin Ophthalmol.* 2001;12(2):143-148.  
*Erratum in: Curr Opin Ophthalmol.* 2001;12(3):235.
- 119. Collignon NJ.**  
Wound healing after glaucoma surgery: how to manage it?  
*Bull Soc Belge Ophthalmol.* 2005;295:55-59.
- 120. Martin P.**  
Wound healing – aiming for perfect skin regeneration.  
*Science* 1997;276(5309):75-81.
- 121. Hosgood G.**  
Wound healing. The role of platelet-derived growth factor and transforming growth factor beta.  
*Vet Surg.* 1993; 22(6):490-495.
- 122. Cunliffe IA, Rees RC, Rennie IG.**  
The effect of TGF-beta 1 and TGF-beta 2 on the proliferation of human Tenon's capsule fibroblasts in tissue culture.  
*Acta Ophthalmol Scand.* 1996;74(1):31-35.
- 123. Knorr M, Volker M, Denk PO, Wunderlich K, Thiel HJ.**  
Proliferative response of cultured human Tenon's capsule fibroblasts to platelet-derived growth factor isoforms.  
*Graefes Arch Clin Exp Ophthalmol.* 1997;235(10):667-671.



- 
- 124. Mullaney P, Curren B, Collum L, Kilfeather S.**  
Fibroblast and endothelial outgrowth from human Tenon's explants: inhibition of fibroblast growth by 5HT receptor antagonism.  
*Res Commun Chem Pathol Pharmacol.* 1991; 74(2):201-213.
- 125. Khaw PT, Occleston NL, Schultz G, Grierson I, Sherwood MB, Larkin G.**  
Activation and suppression of fibroblast function.  
*Eye* 1994;8(Pt 2):188-195.
- 126. Lama PJ, Fechtner RD.**  
Antifibrotics and wound healing in glaucoma surgery.  
*Surv Ophthalmol.* 2003;48(3):314-346.
- 127. Khaw PT, Doyle JW, Sherwood MB, Grierson I, Schultz G, McGorray S.**  
Prolonged localized tissue effects from 5-minute exposures to fluorouracil and mitomycin C.  
*Arch Ophthalmol.* 1993;111(2):263-267.
- 128. Crowston JG, Akbar AN, Constable PH, Occleston NL, Daniels JT, Khaw PT.**  
Antimetabolite-induced apoptosis in Tenon's capsule fibroblasts.  
*Invest Ophthalmol Vis Sci.* 1998;39(2):449-454.
- 129. Jampel HD, Pasquale LR, Dibernardo C.**  
Hypotony maculopathy following trabeculectomy with mitomycin C.  
*Arch Ophthalmol.* 1992;110(8):1049-1050.
- 130. Stamper RL, McMenemy MG, Lieberman MF.**  
Hypotonous maculopathy after trabeculectomy with subconjunctival 5-fluorouracil.  
*Am J Ophthalmol.* 1992;114(5):544-553.
- 131. Cordeiro MF, Gay JA, Khaw PT.**  
Human anti-transforming growth factor-beta2 antibody: a new glaucoma anti-scarring agent.  
*Invest Ophthalmol Vis Sci.* 1999;40(10):2225-2234.
- 132. Grisanti S, Diestelhorst M, Heimann K, Kriegelstein G.**  
Cellular photoablation to control postoperative fibrosis in a rabbit model of filtration surgery.  
*Br J Ophthalmol.* 1999;83(12):1353-1359.
- 133. Grisanti S, Szurman P, Warga M, Kaczmarek R, Ziemssen F, Tatar O, Bartz-Schmidt KU.**  
Decorin modulates wound healing in experimental glaucoma filtration surgery: a pilot study.  
*Invest Ophthalmol Vis Sci.* 2005;46(1):191-196.
- 134. Hall A.**  
Rho GTPases and the actin cytoskeleton.  
*Science.* 1998;279(5350):509-514.

- 
- 135. Seasholtz TM, Majumdar M, Brown JH.**  
Rho as a mediator of G protein-coupled signalling.  
*Mol Pharmacol.* 1999;55(6):949-956.
- 136. Bishop AL, Hall A.**  
Rho GTPases and their effector proteins.  
*Biochem J.* 2000;348(Pt 2):241-255.
- 137. Takai Y, Sasaki T, Matozaki T.**  
Small GTP-binding proteins.  
*Physiol Rev.* 2001;81(1):153-208.
- 138. Riento K, Ridley AJ.**  
Rocks: multifunctional kinases in cell behaviour.  
*Nat Rev Mol Cell Biol.* 2003;4(6):446-456.
- 139. Wettschureck N, Offermanns S.**  
Rho/Rho-kinase mediated signaling in physiology and pathophysiology.  
*J Mol Med.* 2002;80(10):629-638.
- 140. Geneste O, Copeland JW, Treisman R.**  
LIM kinase and Diaphanous cooperate to regulate serum response factor and actin dynamics.  
*J Cell Biol.* 2002;157(5):831-838.
- 141. Miralles F, Posern G, Zaromytidou AI, Treisman R.**  
Actin dynamics control SRF activity by regulation of its coactivator MAL.  
*Cell* 2003;113(3):329-342.
- 142. Honjo M, Inatani M, Kido N, Sawamura T, Yue BY, Honda Y, Tanihara H.**  
Effects of protein kinase inhibitor, HA1077, on intraocular pressure and outflow facility in rabbit eyes.  
*Arch Ophthalmol.* 2001;119(8):1171-1178.
- 143. Honjo M, Tanihara H, Inatani M, Kido N, Sawamura T, Yue BY, Narumiya S, Honda Y.**  
Effects of rho-associated protein kinase inhibitor Y-27632 on intraocular pressure and outflow facility.  
*Invest Ophthalmol Vis Sci.* 2001;42(1):137-144.
- 144. Rao PV, Deng P, Sasaki Y, Epstein DL.**  
Regulation of myosin light chain phosphorylation in the trabecular meshwork: role in aqueous humour outflow facility.  
*Exp Eye Res.* 2005;80(2):197-206.
- 145. Meyer-ter-Vehn T, Sieprath S, Katzenberger B, Gebhardt S, Grehn F, Schlunck G.**  
Contractility as a prerequisite for TGF-beta-induced myofibroblast transdifferentiation in human tenon fibroblasts.  
*Invest Ophthalmol Vis Sci.* 2006;47(11):4895-4904.

- 
- 146. Deckwerth TL, Johnson EM.**  
Temporal analysis of events associated with programmed cell death (apoptosis) of sympathetic neurons deprived of nerve growth factor.  
*J Cell Biol.* 1993;123(5):1207-1222.
- 147. Huber AB, Kolodkin AL, Ginty DD, Cloutier JF.**  
Signaling at the growth cone: ligand-receptor complexes and the control of axon growth and guidance.  
*Annu Rev Neurosci.* 2003;26:509-563.
- 148. Lehmann M, Fournier A, Selles-Navarro I, Dergham P, Sebok A, Leclerc N, Tigyi G, McKerracher L.**  
Inactivation of Rho signaling pathway promotes CNS axon regeneration.  
*J Neurosci.* 1999;19(17):7537-7547.
- 149. Hu Y, Cui Q, Harvey AR.**  
Interactive effects of C3, cyclic AMP and ciliary neurotrophic factor on adult retinal ganglion cell survival and axonal regeneration.  
*Mol Cell Neurosci.* 2007;34(1):88-98.
- 150. Kitaoka Y, Kitaoka Y, Kumai T, Lam TT, Kuribayashi K, Isenoumi K, Munemasa Y, Motoki M, Kobayashi S, Ueno S.**  
Involvement of RhoA and possible neuroprotective effect of fasudil, a Rho kinase inhibitor, in NMDA-induced neurotoxicity in the rat retina.  
*Brain Res.* 2004;1018(1):111-118.
- 151. Jacobs M, Hayakawa K, Swenson L, Bellon S, Fleming M, Taslimi P, Doran J.**  
The structure of dimeric ROCK I reveals the mechanism for ligand selectivity.  
*J Biol Chem.* 2006;281(1):260-268.
- 152. Lambiase A, Tirassa P, Micera A, Aloe L, Bonini S.**  
Pharmacokinetics of conjunctivally applied nerve growth factor in the retina and optic nerve of adult rats.  
*Invest Ophthalmol Vis Sci.* 2005;46(10):3800-3806.
- 153. Krishnamoorthy RR, Agarwal P, Prasanna G, Vopat K, Lambert W, Sheedlo HJ, Pang IH, Shade D, Wordinger RJ, Yorio T, Clark AF, Agarwal N.**  
Characterization of a transformed rat retinal ganglion cell line.  
*Brain Res Mol Brain Res.* 2001;86(1-2):1-12.
- 154. Berg K, Hansen MB, Nielsen SE.**  
A new sensitive bioassay for precise quantification of interferon activity as measured via the mitochondrial dehydrogenase function in cells (MTT-method).  
*APMIS* 1990;98(2):156-162.
- 155. Decker T, Lohmann-Matthes ML.**  
A quick and simple method for the quantitation of lactate dehydrogenase release in measurements of cellular cytotoxicity and tumor necrosis factor (TNF) activity.  
*J Immunol Methods.* 1988;115(1):61-69.

- 
- 156. Altschul SF, Madden TL, Schaffer AA, Zhang J, Zhang Z, Miller W, Lipman DJ.**  
Gapped BLAST and PSI-BLAST: a new generation of protein database search programs.  
*Nucleic Acids Res.* 1997;25(17):3389-3402.
- 157. Myers EW, Miller W.**  
Optimal alignments in linear space.  
*Comput Appl Biosci.* 1988;4(1):11-17.
- 158. Urruticoechea A, Smith IE, Dowsett M.**  
Proliferation marker Ki-67 in early breast cancer.  
*J Clin Oncol.* 2005;23(28):7212-7220.
- 159. Desmouliere A, Chaponnier C, Gabbiani G.**  
Tissue repair, contraction, and the myofibroblast.  
*Wound Repair Regen.* 2005;13(1):7-12.
- 160. Midwood KS, Williams LV, Schwarzbauer JE.**  
Tissue repair and the dynamics of the extracellular matrix.  
*Int J Biochem Cell Biol.* 2004;36(6):1031-1037.
- 161. Welch MP, Odland GF, Clark RA.**  
Temporal relationships of F-actin bundle formation, collagen and fibronectin matrix assembly, and fibronectin receptor expression to wound contraction.  
*J Cell Biol.* 1990;110(1):133-145.
- 162. Breitenlechner C, Gassel M, Hidaka H, Kinzel V, Huber R, Engh RA, Bossemeyer D.**  
Protein kinase A in complex with Rho-kinase inhibitors Y-27632, Fasudil, and H-1152P: structural basis of selectivity.  
*Structure* 2003;11(12):1595-1607.
- 163. Ikenoya M, Hidaka H, Hosoya T, Suzuki M, Yamamoto N, Sasaki Y.**  
Inhibition of rho-kinase-induced myristoylated alanine-rich C kinase substrate (MARCKS) phosphorylation in human neuronal cells by H-1152, a novel and specific Rho-kinase inhibitor.  
*J Neurochem.* 2002;81(1):9-16.
- 164. Sasaki Y, Suzuki M, Hidaka H.**  
The novel and specific Rho-kinase inhibitor (S)-(+)-2-methyl-1-[(4-methyl-5-isoquinoline)sulfonyl]-homopiperazine as a probing molecule for Rho-kinase-involved pathway.  
*Pharmacol Ther.* 2002;93(2-3):225-232.
- 165. Matsuoka Y, Li X, Bennett V.**  
Adducin: structure, function and regulation.  
*Cell Mol Life Sci.* 2000;57(6):884-895.
- 166. Watanabe Y, Morimatsu M, Syuto B.**  
Botulinum C3 enzyme changes the lactate dehydrogenase isozyme pattern of primary culture of neurons.  
*J Vet Med Sci.* 2000;62(3):249-254.

- 
- 167. Kermer P, Bahr M.**  
[Programmed cell death in the retina. Molecular mechanisms and therapeutic strategies]  
*Ophthalmologe* 2005;102(7): 674-678.
- 168. Cellerino A, Bahr M, Isenmann S.**  
Apoptosis in the developing visual system.  
*Cell Tissue Res.* 2000;301(1):53-69.
- 169. Fukata Y, Oshiro N, Kinoshita N, Kawano Y, Matsuoka Y, Bennett V, Matsuura Y, Kaibuchi K.**  
Phosphorylation of adducin by Rho-kinase plays a crucial role in cell motility.  
*J Cell Biol.* 1999;145(2):347-361.
- 170. van de Water B, Tijdens IB, Verbrugge A, Huigsloot M, Dihal AA, Stevens JL, Jaken S, Mulder GJ.**  
Cleavage of the actin-capping protein alpha -adducin at Asp-Asp-Ser-Asp633-Ala by caspase-3 is preceded by its phosphorylation on serine 726 in cisplatin-induced apoptosis of renal epithelial cells.  
*J Biol Chem.* 2000;275(33):25805-25813.
- 171. Hernandez MR.**  
The optic nerve head in glaucoma: role of astrocytes in tissue remodeling.  
*Prog Retin Eye Res.* 2000;19(3):297-321.
- 172. Porchet R, Probst A, Bouras C, Draberova E, Draber P, Riederer BM.**  
Analysis of glial acidic fibrillary protein in the human entorhinal cortex during aging and in Alzheimer's disease.  
*Proteomics.* 2003;3(8):1476-1485.  
*Erratum in: Proteomics.* 2003;3(10):2067.
- 173. Korolainen MA, Auriola S, Nyman TA, Alafuzoff I, Pirttila T.**  
Proteomic analysis of glial fibrillary acidic protein in Alzheimer's disease and aging brain.  
*Neurobiol Dis.* 2005;20(3):858-870.
- 174. Grimsley PG, Quinn KA, Owensby DA.**  
Soluble low-density lipoprotein receptor-related protein.  
*Trends Cardiovasc Med.* 1998;8(8):363-368.
- 175. Birkenmeier G, Grosche J, Reichenbach A.**  
Immunocytochemical demonstration of alpha 2-M-R/LRP on Muller (glial) cells isolated from rabbit and human retina.  
*Neuroreport.* 1996;8(1):149-151.
- 176. Levine SJ.**  
Mechanisms of soluble cytokine receptor generation.  
*J Immunol.* 2004;173(9):5343-5348.

- 
- 177. Leif RC, Stein JH, Zucker RM.**  
A short history of the initial application of anti-5-BrdU to the detection and measurement of S phase.  
*Cytometry A*. 2004;58(1):45-52.
- 178. Mughal S, Al-Bader AA, Cuschieri A, Kharbat B.**  
Ultrastructural localization of adenosine triphosphatase activity in HeLa cells at various stages of the cell cycle.  
*Cell Tissue Res*. 1987;250(2):349-354.
- 179. Raftopoulou M, Hall A.**  
Cell migration: Rho GTPases lead the way.  
*Dev Biol*. 2004;265(1):23-32.
- 180. Friedl P, Brocker EB.**  
The biology of cell locomotion within three-dimensional extracellular matrix.  
*Cell Mol Life Sci*. 2000;57(1):41-64.
- 181. Worthylake RA, Lemoine S, Watson JM, Burridge K.**  
RhoA is required for monocyte tail retraction during transendothelial migration.  
*J Cell Biol*. 2001;154(1):147-160.
- 182. Yamada KM.**  
Fibronectin peptides in cell migration and wound repair.  
*J Clin Invest*. 2000;105(11):1507-1509.
- 183. Wu C, Keivens VM, O'Toole TE, McDonald JA, Ginsberg MH.**  
Integrin activation and cytoskeletal interaction are essential for the assembly of a fibronectin matrix.  
*Cell* 1995;83(5):715-724.
- 184. Wierzbicka-Patynowski I, Schwarzbauer JE.**  
The ins and outs of fibronectin matrix assembly.  
*J Cell Sci*. 2003;116(Pt 16):3269-3276.
- 185. Harris AK, Stopak D, Wild P.**  
Fibroblast traction as a mechanism for collagen morphogenesis.  
*Nature* 1981;290(5803):249-251.
- 186. Porter RA, Brown RA, Eastwood M, Occleston NL, Khaw PT.**  
Ultrastructural changes during contraction of collagen lattices by ocular fibroblasts.  
*Wound Repair Regen*. 1998;6(2):157-166.
- 187. Schiro JA, Chan BM, Roswit WT, Kassner PD, Pentland AP, Hemler ME, Eisen AZ, Kupper TS.**  
Integrin alpha 2 beta 1 (VLA-2) mediates reorganization and contraction of collagen matrices by human cells.  
*Cell* 1991;67(2):403-410.

- 
- 188. Klein CE, Dressel D, Steinmayer T, Mauch C, Eckes B, Krieg T, Bankert RB, Weber L.**  
Integrin alpha 2 beta 1 is upregulated in fibroblasts and highly aggressive melanoma cells in three-dimensional collagen lattices and mediates the reorganization of collagen I fibrils.  
*J Cell Biol.* 1991;115(5):1427-1436.
- 189. Gillery P, Maquart FX, Borel JP.**  
Fibronectin dependence of the contraction of collagen lattices by human skin fibroblasts.  
*Exp Cell Res.* 1986;167(1):29-37.
- 190. Golubkov SP, Belkin VM, Rudneva SV, Terskikh VV.**  
[Blood plasma fibronectin does not influence fibroblast-induced collagen gel contraction]  
*Tsitologija.* 1990;32(5):499-503.
- 191. Asaga H, Kikuchi S, Yoshizato K.**  
Collagen gel contraction by fibroblasts requires cellular fibronectin but not plasma fibronectin.  
*Exp Cell Res.* 1991;193(1):167-174.
- 192. Mueller BK, Mack H, Teusch N.**  
Rho kinase, a promising drug target for neurological disorders.  
*Nat Rev Drug Discov.* 2005;4(5):387-398.
- 193. Howe AK.**  
Regulation of actin-based cell migration by cAMP/PKA.  
*Biochim Biophys Acta.* 2004;1692(2-3):159-174.
- 194. Lang P, Gesbert F, Delespine-Carmagnat M, Stancou R, Pouchelet M, Bertoglio J.**  
Protein kinase A phosphorylation of RhoA mediates the morphological and functional effects of cyclic AMP in cytotoxic lymphocytes.  
*EMBO J.* 1996;15(3):510-519.
- 195. Ellerbroek SM, Wennerberg K, Burridge K.**  
Serine phosphorylation negatively regulates RhoA in vivo.  
*J Biol Chem.* 2003;278(21):19023-19031.
- 196. Barkalow KL, Italiano JE Jr, Chou DE, Matsuoka Y, Bennett V, Hartwig JH.**  
Alpha-adducin dissociates from F-actin and spectrin during platelet activation.  
*J Cell Biol.* 2003;161(3):557-570.
- 197. Seigel GM.**  
The golden age of retinal cell culture.  
*Mol Vis.* 1999;5:4.

- 198. Ripodas A, de Juan JA, Roldan-Pallares M, Bernal R, Moya J, Chao M, Lopez A, Fernandez-Cruz A, Fernandez-Durango R.**  
Localisation of endothelin-1 mRNA expression and immunoreactivity in the retina and optic nerve from human and porcine eye. Evidence for endothelin-1 expression in astrocytes.  
*Brain Res.* 2001;912(2):137-143.
- 199. Perraud F, Labourdette G, Eclancher F, Sensenbrenner M.**  
Primary cultures of astrocytes from different brain areas of newborn rats and effects of basic fibroblast growth factor.  
*Dev Neurosci.* 1990;12(1):11-21.
- 200. Sakai Y, Rawson C, Lindburg K, Barnes D.**  
Serum and transforming growth factor beta regulate glial fibrillary acidic protein in serum-free-derived mouse embryo cells.  
*Proc Natl Acad Sci U S A.* 1990;87(21):8378-8382.
- 201. Hoi Sang U, Espiritu OD, Kelley PY, Klauber MR, Hatton JD.**  
The role of the epidermal growth factor receptor in human gliomas: II. The control of glial process extension and the expression of glial fibrillary acidic protein.  
*J Neurosurg.* 1995; 82(5):847-857.
- 202. Maddala R, Reddy VN, Epstein DL, Rao V.**  
Growth factor induced activation of Rho and Rac GTPases and actin cytoskeletal reorganization in human lens epithelial cells.  
*Mol Vis.* 2003;9:329-336.
- 203. Yasui Y, Amano M, Nagata K, Inagaki N, Nakamura H, Saya H, Kaibuchi K, Inagaki M.**  
Roles of Rho-associated kinase in cytokinesis; mutations in Rho-associated kinase phosphorylation sites impair cytokinetic segregation of glial filaments.  
*J Cell Biol.* 1998;143(5):1249-1258.
- 204. Fujita K, Yamauchi M, Matsui T, Titani K, Takahashi H, Kato T, Isomura G, Ando M, Nagata Y.**  
Increase of glial fibrillary acidic protein fragments in the spinal cord of motor neuron degeneration mutant mouse.  
*Brain Res.* 1998;785(1):31-40.
- 205. Valentim LM, Michalowski CB, Gottardo SP, Pedroso L, Gestrich LG, Netto CA, Salbego CG, Rodnight R.**  
Effects of transient cerebral ischemia on glial fibrillary acidic protein phosphorylation and immunoccontent in rat hippocampus.  
*Neuroscience* 1999;91(4):1291-1297.
- 206. Abe K, Misawa M.**  
Astrocyte stellation induced by Rho kinase inhibitors in culture.  
*Brain Res Dev Brain Res.* 2003;143(1):99-104.



- 207. Yuan L, Neufeld AH.**  
Tumor necrosis factor-alpha: a potentially neurodestructive cytokine produced by glia in the human glaucomatous optic nerve head.  
*Glia*. 2000;32(1):42-50.
- 208. Lee SC, Dickson DW, Liu W, Brosnan CF.**  
Induction of nitric oxide synthase activity in human astrocytes by interleukin-1 beta and interferon-gamma.  
*J Neuroimmunol*. 1993;46(1-2):19-24.
- 209. Chavany C, Vicario-Abejon C, Miller G, Jendoubi M.**  
Transgenic mice for interleukin 3 develop motor neuron degeneration associated with autoimmune reaction against spinal cord motor neurons.  
*Proc Natl Acad Sci U S A*. 1998;95(19):11354-11359.
- 210. Ramanathan S, de Kozak Y, Saoudi A, Goureau O, Van der Meide PH, Druet P, Bellon B.**  
Recombinant IL-4 aggravates experimental autoimmune uveoretinitis in rats.  
*J Immunol*. 1996;157(5):2209-2215.
- 211. Koeberle PD, Gauldie J, Ball AK.**  
Effects of adenoviral-mediated gene transfer of interleukin-10, interleukin-4, and transforming growth factor-beta on the survival of axotomized retinal ganglion cells.  
*Neuroscience* 2004;125(4):903-920.
- 212. Boyd ZS, Kriatchko A, Yang J, Agarwal N, Wax MB, Patil RV.**  
Interleukin-10 receptor signaling through STAT-3 regulates the apoptosis of retinal ganglion cells in response to stress.  
*Invest Ophthalmol Vis Sci*. 2003;44(12):5206-5211.
- 213. Fisher J, Mizrahi T, Schori H, Yoles E, Levkovitch-Verbin H, Haggiag S, Revel M, Schwartz M.**  
Increased post-traumatic survival of neurons in IL-6-knockout mice on a background of EAE susceptibility.  
*J Neuroimmunol*. 2001;119(1):1-9.
- 214. Sanchez RN, Chan CK, Garg S, Kwong JM, Wong MJ, Sadun AA, Lam TT.**  
Interleukin-6 in retinal ischemia reperfusion injury in rats.  
*Invest Ophthalmol Vis Sci*. 2003;44(9):4006-4011.
- 215. Sappington RM, Chan M, Calkins DJ.**  
Interleukin-6 protects retinal ganglion cells from pressure-induced death.  
*Invest Ophthalmol Vis Sci*. 2006;47(7):2932-2942.
- 216. Tezel G, Wax MB.**  
The immune system and glaucoma.  
*Curr Opin Ophthalmol*. 2004;15(2):80-84.
- 217. Wu G, Fang YZ, Yang S, Lupton JR, Turner ND.**  
Glutathione metabolism and its implications for health.  
*J Nutr*. 2004;134(3):489-492.

- 218. Liu H, Wang H, Shenvi S, Hagen TM, Liu RM.**  
Glutathione metabolism during aging and in Alzheimer disease.  
*Ann N Y Acad Sci.* 2004;1019:346-349.
- 219. Rojas E, Shi ZZ, Valverde M, Paules RS, Habib GM, Lieberman MW.**  
Cell survival and changes in gene expression in cells unable to synthesize glutathione.  
*Biofactors* 2003;17(1-4):13-19.
- 220. Slivka A, Mytilineou C, Cohen G.**  
Histochemical evaluation of glutathione in brain.  
*Brain Res.* 1987;409(2):275-284.
- 221. Makar TK, Nedergaard M, Preuss A, Gelbard AS, Perumal AS, Cooper AJ.**  
Vitamin E, ascorbate, glutathione, glutathione disulfide, and enzymes of glutathione metabolism in cultures of chick astrocytes and neurons: evidence that astrocytes play an important role in antioxidative processes in the brain.  
*J Neurochem.* 1994;62(1):45-53.
- 222. Pow DV, Crook DK.**  
Immunocytochemical evidence for the presence of high levels of reduced glutathione in radial glial cells and horizontal cells in the rabbit retina.  
*Neurosci Lett.* 1995;193(1):25-28.
- 223. Wilson JX.**  
Antioxidant defense of the brain: a role for astrocytes.  
*Can J Physiol Pharmacol.* 1997;75(10-11):1149-1163.
- 224. Schutte M, Werner P.**  
Redistribution of glutathione in the ischemic rat retina.  
*Neurosci Lett.* 1998;246(1):53-56.
- 225. Lu SC, Bao Y, Huang ZZ, Sarthy VP, Kannan R.**  
Regulation of gamma-glutamylcysteine synthetase subunit gene expression in retinal Muller cells by oxidative stress.  
*Invest Ophthalmol Vis Sci.* 1999;40(8):1776-1782.
- 226. Moorhouse AJ, Li S, Vickery RM, Hill MA, Morley JW.**  
A patch-clamp investigation of membrane currents in a novel mammalian retinal ganglion cell line.  
*Brain Res.* 2004;1003(1-2):205-208.
- 227. Frassetto LJ, Schlieve CR, Lieven CJ, Utter AA, Jones MV, Agarwal N, Levin LA.**  
Kinase-dependent differentiation of a retinal ganglion cell precursor.  
*Invest Ophthalmol Vis Sci.* 2006;47(1):427-438.
- 228. Kimura K, Fukata Y, Matsuoka Y, Bennett V, Matsuura Y, Okawa K, Iwamatsu A, Kaibuchi K.**  
Regulation of the association of adducin with actin filaments by Rho-associated kinase (Rho-kinase) and myosin phosphatase.  
*J Biol Chem.* 1998;273(10):5542-5548.

- 
- 229. Van Cruchten S, Van Den Broeck W.**  
Morphological and biochemical aspects of apoptosis, oncosis and necrosis.  
*Anat Histol Embryol.* 2002;31(4):214-223.
- 230. Majno G, Joris I.**  
Apoptosis, oncosis, and necrosis. An overview of cell death.  
*Am J Pathol.* 1995;146(1):3-15.
- 231. Park BS, Kim GC, Back SJ, Kim ND, Kim YS, Kim SK, Jeong MH, Lim YJ, Yoo YH.**  
Murine bone marrow-derived mast cells exhibit evidence of both apoptosis and oncosis after IL-3 deprivation.  
*Immunol Invest.* 2000;29(1):51-60.
- 232. Trump BF, Berezsky IK, Chang SH, Phelps PC.**  
The pathways of cell death: oncosis, apoptosis, and necrosis.  
*Toxicol Pathol.* 1997;25(1):82-88.
- 233. Trump BF, Berezsky IK.**  
The role of altered  $[Ca^{2+}]_i$  regulation in apoptosis, oncosis, and necrosis.  
*Biochim Biophys Acta.* 1996;1313(3):173-178.
- 234. Liu X, Van Vleet T, Schnellmann RG.**  
The role of calpain in oncotic cell death.  
*Annu Rev Pharmacol Toxicol.* 2004;44:349-370.
- 235. Rasband MN, Kagawa T, Park EW, Ikenaka K, Trimmer JS.**  
Dysregulation of axonal sodium channel isoforms after adult-onset chronic demyelination.  
*J Neurosci Res.* 2003;73(4):465-470.
- 236. Westenbroek RE, Merrick DK, Catterall WA.**  
Differential subcellular localization of the RI and RII  $Na^+$  channel subtypes in central neurons.  
*Neuron* 1989;3(6):695-704.
- 237. Gong B, Rhodes KJ, Bekele-Arcuri Z, Trimmer JS.**  
Type I and type II  $Na^+$  channel alpha-subunit polypeptides exhibit distinct spatial and temporal patterning, and association with auxiliary subunits in rat brain.  
*J Comp Neurol.* 1999;412(2):342-352.
- 238. Caldwell JH, Schaller KL, Lasher RS, Peles E, Levinson SR.**  
Sodium channel  $Na(v)1.6$  is localized at nodes of ranvier, dendrites, and synapses.  
*Proc Natl Acad Sci U S A.* 2000;97(10):5616-5620.
- 239. Stys PK, Waxman SG, Ransom BR.**  
Ionic mechanisms of anoxic injury in mammalian CNS white matter: role of  $Na^+$  channels and  $Na^+$ - $Ca^{2+}$  exchanger.  
*J Neurosci.* 1992;12(2):430-439.

- 240. Craner MJ, Hains BC, Lo AC, Black JA, Waxman SG.**  
Co-localization of sodium channel Nav1.6 and the sodium-calcium exchanger at sites of axonal injury in the spinal cord in EAE.  
*Brain* 2004;127(Pt 2):294-303.
- 241. Craner MJ, Newcombe J, Black JA, Hartle C, Cuzner ML, Waxman SG.**  
Molecular changes in neurons in multiple sclerosis: altered axonal expression of Nav1.2 and Nav1.6 sodium channels and Na<sup>+</sup>/Ca<sup>2+</sup> exchanger.  
*Proc Natl Acad Sci U S A.* 2004;101(21):8168-8173.
- 242. Rush AM, Dib-Hajj SD, Waxman SG.**  
Electrophysiological properties of two axonal sodium channels, Nav1.2 and Nav1.6, expressed in mouse spinal sensory neurones.  
*J Physiol.* 2005;564(Pt 3):803-815.
- 243. Saito S, Ohashi M, Naito A, Fukaya Y, Suzuki Y, Araie M.**  
Neuroprotective effect of the novel Na<sup>+</sup>/Ca<sup>2+</sup> channel blocker NS-7 on rat retinal ganglion cells.  
*Jpn J Ophthalmol.* 2005;49(5):371-376.
- 244. Hains BC, Waxman SG.**  
Neuroprotection by sodium channel blockade with phenytoin in an experimental model of glaucoma.  
*Invest Ophthalmol Vis Sci.* 2005;46(11):4164-4169.
- 245. Reiff DF, Guenther E.**  
Developmental changes in voltage-activated potassium currents of rat retinal ganglion cells.  
*Neuroscience* 1999;92(3):1103-1117.
- 246. Franek WR, Morrow DM, Zhu H, Vancurova I, Miskolci V, Darley-USmar K, Simms HH, Mantell LL.**  
NF-kappaB protects lung epithelium against hyperoxia-induced nonapoptotic cell death-oncosis.  
*Free Radic Biol Med.* 2004;37(10):1670-1679.
- 247. L'Ecuyer T, Allebban Z, Thomas R, Vander Heide R.**  
Glutathione S-transferase overexpression protects against anthracycline-induced H9C2 cell death.  
*Am J Physiol Heart Circ Physiol.* 2004;286(6):H2057-H2064.
- 248. Charles I, Khalyfa A, Kumar DM, Krishnamoorthy RR, Roque RS, Cooper N, Agarwal N.**  
Serum deprivation induces apoptotic cell death of transformed rat retinal ganglion cells via mitochondrial signaling pathways.  
*Invest Ophthalmol Vis Sci.* 2005;46(4):1330-1338.
- 249. Mills EM, Xu D, Fergusson MM, Combs CA, Xu Y, Finkel T.**  
Regulation of cellular oncosis by uncoupling protein 2.  
*J Biol Chem.* 2002;277(30):27385-27392.

- 
- 250. Rousset S, Alves-Guerra MC, Mozo J, Miroux B, Cassard-Doulier AM, Bouillaud F, Ricquier D.**  
The biology of mitochondrial uncoupling proteins.  
*Diabetes* 2004;53(Suppl 1):S130-S135.
- 251. Lindholm D, Eriksson O, Korhonen L.**  
Mitochondrial proteins in neuronal degeneration.  
*Biochem Biophys Res Commun.* 2004;321(4):753-758.
- 252. Kim-Han JS, Dugan LL.**  
Mitochondrial uncoupling proteins in the central nervous system.  
*Antioxid Redox Signal.* 2005;7(9-10):1173-1181.
- 253. Rattan R, Giri S, Singh AK, Singh I.**  
Rho/ROCK pathway as a target of tumor therapy.  
*J Neurosci Res.* 2006;83(2):243-255.
- 254. Schwartz M.**  
Optic nerve crush: protection and regeneration.  
*Brain Res Bull.* 2004;62(6):467-471.

## PUBLICATIONS

- **Heiduschka P, Blitgen-Heinecke P, Tura A, Kokkinou D, Julien S, Hofmeister S, Bartz-Schmidt KU, Schraermeyer U.**

Melanin precursor 5,6-dihydroxyindol: Protective effects and cytotoxicity on retinal cells *in vitro* and *in vivo*.

*Toxicologic Pathology, in press.*

- **Tura A, Grisanti S, Petermeier K, Henke-Fahle S.**

The Rho-kinase inhibitor H-1152P suppresses the wound-healing activities of human Tenon's capsule fibroblasts *in vitro*.

*Invest Ophthalmol Vis Sci.* 2007;48(5):2152-2161.

- **Tura A, Brechtel K, Abdibzadeh M, Hirsch S, Conrad S, Schwab JM.**

Intrinsic locomotor outcome in dorsal transection of rat spinal cord: predictive value of minimal incision depth.

*Spinal Cord* 2006;44(10):605-613.

# LEBENS LAUF

## Persönliche Daten

<b>Name</b>	Ayşegül Tura
<b>Geburtsdatum</b>	19.11.1977
<b>Geburtsort</b>	Istanbul (Türkei)
<b>Familienstand</b>	ledig

## Schulbildung

<b>1988-1992</b>	Özel Moda Lisesi (Gymnasium), Istanbul
<b>1992-1995</b>	Özel Doğan Lisesi (Gymnasium), Istanbul

## Studium

<b>Sept. 1995 - Juni 1999</b>	Studium (BSc.) der Molekularbiologie und Genetik an der Universität Boğaziçi (Bosporus), Istanbul
<b>Sept. 1999 - Sept. 2001</b>	Magisterarbeit in Molekularbiologie und Genetik an der Universität Boğaziçi, Istanbul (bei Prof. A. Tolun) mit dem Thema: „Analysis of the locus for microhydranencephaly“
<b>Nov. 2001 -</b>	Mitglied der „Graduate School of Neural and Behavioural Sciences, University of Tübingen“
<b>Sept. 2003 -</b>	Promotionsstudium an der Augenklinik des Universitätsklinikums Tübingen unter der Betreuung von Dr. med. S. Henke-Fahle und Prof. Dr. S. Grisanti. Thema der Arbeit: „The Rho-kinase signaling pathway in Tenon’s capsule fibroblasts and retinal ganglion cells: A novel pharmacological target for improving the outcomes of filtration surgery and promoting retinal cell survival“

## Beruflicher Werdegang

<b>Sept. 1999 - Sept. 2001</b>	Wissenschaftliche Hilfskraft an der Universität Boğaziçi, Istanbul
<b>Nov. 2001 - Juni 2003</b>	Wissenschaftliche Mitarbeiterin bei der Migragen AG, Tübingen (bei PD Dr. B. K. Müller) mit dem Thema: „Inhibition of the RhoA-signalling pathway to promote axon regeneration after spinal cord injury“
<b>Sept. 2003 -</b>	Wissenschaftliche Mitarbeiterin an der Augenklinik (Abteilung I) des Universitätsklinikums Tübingen (Ärztl. Direktor: Prof. Dr. K. U. Bartz-Schmidt)

**Stipendien, Preise**

- |                               |  |
|-------------------------------|--|
| <b>Jan. 2000 – Sept. 2001</b> | Stipendiatin des türkischen Beirats für wissenschaftliche und technologische Forschung (TUBITAK)                           |
| <b>Jan. 2005 – März 2006</b>  | Stipendiatin der Herbert Funke-Stiftung, Deutschland   |
| <b>Sept. 2007</b>             | Glaukomforschungspreis der Deutschen Ophthalmologischen Gesellschaft gestiftet von der Firma PharmAllergan GmbH, Ettlingen |